Final Report

NASA GRANT: NGR 09-011-039

THE MOTION AND STABILITY OF A DUAL-SPIN SATELLITE DURING THE MOMENTUM WHEEL SPIN-UP MANEUVER

HOWARD UNIVERSITY

School of Engineering
Department of Mechanical Engineering
Washington, D.C. 20001

Final Report

NASA GRANT: NGR 09-011-039

THE MOTION AND STABILITY OF A DUAL-SPIN SATELLITE DURING THE MOMENTUM WHEEL SPIN-UP MANEUVER

by

Peter M. Bainum
Associate Professor of Aerospace Engineering
Principal Investigator

and

Subhash Sen
Research Assistant

November 1972

ABSTRACT

The stability of a dual-spin satellite system during the momentum wheel spin-up manuever is treated both analytically and numerically. The dual-spin system consists of: a slowly rotating or despun main-body; a momentum wheel (or rotor) which is accelerated by a torque motor to change its initial angular velocity relative to the main part to some high terminal value; and a nutation damper. A closed form solution for the case of a symmetrical satellite indicates that when the nutation damper is physically constrained from movement (i.e. by use of a mechanical clamp) the magnitude of the vector sum of the transverse angular velocity components remains bounded during the wheel spin-up under the influence of a constant motor torque. The analysis is extended to consider such effects as: the motion of the nutation damper during spin-up; a non-uniform motor torque; and the effect of a non-symmetrical mass distribution in the main spacecraft and the rotor. An approximate analytical solution using perturbation techniques is developed for the case of a slightly asymmetric main spacecraft. From the numerical results for the case of small mass asymmetry the system behaves similarly to the case of a symmetrical satellite; whereas for large asymmetry one component of the transverse angular velocity has an amplitude much greater than the initial value. For the case of an asymmetrical spacecraft when the nutation damping

is activated during spin-up, a decay of the amplitude of the transverse angular velocity vector is noted. When the effect of the misalignment of the main spacecraft (spin) principal axis from the geometrical (polar) axis of symmetry is considered, a problem of stability could arise due to the large initial amplification of the system nutation angle.

NOMENCLATURE

A,B,C	= moments of inertia about X,Y,Z axes, respectively, for the main body
A',B',C'	= composite moments of inertia about X,Y,Z axes, respectively, including main body and rotor
$\overline{A},\overline{B},\overline{C}$	= composite moments of inertia about X,Y,Z axes, respectively, including main body, rotor, and damper
a_i	= coefficients occuring in the solution of the differential equations
$C(x,b)$	= Boehmer integral appearing in approximate perturbation solution
f	= spacecraft center of mass offset
F_c	= centrifugal force
F_{cor}	= Coriolis force
$I(1),I(2),I(3)$	= functions appearing in the particular part of the approximate perturbation solution
I_{ij}	= moment of inertia tensor of satellite main body i,j = x,y,z
I_{R_i}	= moment of inertia of rotor about X,Y,Z axes, respectively (i = x,y,z)
I_{d_i}	= moment of inertia of the pendulous damper(s) about X,Y,Z axes, respectively

K = restoring spring constant of the torsion wire support

K_1, K_2 = constants appearing in solution for the case of a symmetrical spacecraft and rotor without damping

k = damping rate constant

ℓ = height of damper plane above X,Z plane

L_i = applied external torque about the quasi-coordinate axes of symmetry

L_{m_y} = the motor torque

L_{R_y} = rotor torque

M = the mass of the main satellite

$\overline{M}$ = the total system mass = $M + \sum_i^n m_i$

m = the pendulum end mass

N_{R_i} = the inertia (applied) torque action on the rotor

$N_{C.F}$ = torque due to centrifugal force about the damper hinge point

N_{cor} = torque due to coriolis force about the damper hinge point

P = $(A'-B') [\omega_y(0) B' + I_{R_y} s(0)] /B'$

Q = $(B'-A') I_{R_y} /B' - I_{R_y}$

Q_i = the generalized forces occuring in the ϕ_i equation

R_i = the reaction of rotor on main body

R_{R_i} = the reaction of main body on rotor

r_o = the distance from the nominal spin (Y) axis to the pendulum hinge point

r_l = the length of the pendulum

$S(x,b)$ = Boehmer integral appearing in approximate perturbation solution

s = spin rate of rotor relative to main body

T_M = kinetic energy of main body and damper

T_R = kinetic energy of rotor

T = kinetic energy of the system

t = time

$v_{M/cm}$ = velocity of main part relative to the center of mass

$v_{m_i/cm}$ = velocity of ith mass relative to the center of mass

V = potential energy associated with restoring torque effect

X,Y,Z = principal axes of main satellite

x = $|Qc/A'|\ (t+a)^2/2$

α = $I_{xy} = I_{yz}$

β = $I_{R_{yz}}$

$\Gamma(b,ix)$ = incomplete Gamma function with complex argument

γ = I_{xz}

ϕ_i = damper displacement angle

ω_i = angular velocities about the X,Y,Z, axes, respectively ($i = x,y,z$)

TABLE OF CONTENTS

LIST OF ILLUSTRATIONS

LIST OF ILLUSTRATIONS

LIST OF ILLUSTRATIONS

LIST OF ILLUSTRATIONS

LIST OF ILLUSTRATIONS

I. INTRODUCTION

Haseltine[1], Likins[2], and Bainum et al[3] have investigated the motion of spinning satellites with nutation damping together with attitude stability criteria. A dual-spin spacecraft may be considered to consist of two parts constrained so that the relative motion between them is restricted to a common direction fixed in both bodies. Such a system can resist the effects of external torques because of the combined resultant momentum of the system, even though one of the parts may be rotating very slowly (or even with zero inertial angular velocity). A basic result of dual-spin attitude stabilization studies is that the inertial attitude of the spin axis of a freely spinning passive dual-spin vehicle may be stable, in the presence of a properly positioned internal damper, regardless of the mass distribution of the spacecraft. This means that a dual-spin system, depending on the spin rate and the amount and location of the dampers, may be stable in spin about an axis of minimum moment of inertia.[3]

Since 1962, when the feasibility of a dual-spin satellite system was demonstrated with the Orbiting Solar Observatory I (OSO-I), the dual-spin concept has been applied to other satellite systems including the Small Astronomy Satellite - A (SAS-A), the TIROS-M Meterological Satellite, the TACSAT Satellite as well as the advanced versions of the OSO-series. The stability theory and design of dual-spin satellites with various types of nutation damping systems was described at a

symposium on the attitude stabilization and control of dual-spin satellites[4]. Considerable attention has also been made in the recent literature to the dynamics and stability of various types of dual-spin systems with and without energy dissipation on both the high spinning part (rotor or momentum wheel) and the despun portion (or main body). The application to dual-spin systems of heuristic or "energy sink" arguments has indicated that, even in the presence of energy dissipation, spacecraft of this type can be stable in spin about a centroidal principal axis of either maximum or minimum moment of inertia.[2]

In the paper of Mingori[5], an alternate procedure for analyzing the motion of dual-spin satellites is presented. This procedure, which involves Floquet theory, furnishes a means of obtaining precise and accurate stability information for a broad class of dual-spin systems, provided that energy dissipating mechanisms and internal moving parts are specifically included in the mathematical model.

In all of these previous analyses of dual-spin systems it was assumed that the rotor spins at a constant relative angular rate with respect to the main part. Of interest in this investigation is to include the effects of a variable rate of relative rotation such as may be encountered during the deliberate spin-up maneuver of the momentum wheel. This can be accomplished by an on-board torque motor which accelerates the wheel until the desired relative spin rate is obtained, at the same time the main part is decelerated as the momentum is transferred between the main part and the wheel.

A dual-spin Small Astronomy Satellite (SAS-A) was designed and developed for NASA Goddard Space Flight Center by the Applied Physics Laboratory and was launched in December 1970. The satellite was designed to scan the entire celestial sphere to determine the location of X-ray emitting sources relative to the fixed position of the stars. No serious attitude stability problems were encountered during the relatively short time required for wheel spin-up.[6] Because of the experience already gained with this operational system, it was selected as a representative dual-spin system model for the present analysis.

II. ANALYSIS

The elements of the SAS-A attitude control system are shown in Fig. 1a. The satellite is comprised of three parts: (1) the primary part of the satellite, assumed to be essentially a right circular cylinder where the nominal spin axis is the body Y axis, (2) the smaller rotor or momentum wheel which is assumed to be connected near the center of mass of the primary part, and whose spin axis is also parallel to the body Y axis, and (3) the pendulous type nutation dampers which are connected to the primary part and are constrained to move in a plane that is perpendicular to the nominal spin axis and at a distance ℓ, above the transverse inertial plane. It is assumed the dampers are hinged or pivoted about a torsion wire support which offers a restoring (spring) torque in addition to the dissipative torque.[7]

A. Equations of Motion for the Case of a Constant Speed Rotor

The system to be studied is shown schematically in Fig. 1b. The orthogonal coordinate axes X,Y (spin axis), Z are fixed in the parent body with the origin at its equilibrium position center of gravity. The main body has mass M, polar moment of inertia B, and transverse moments of inertia A and C. Four small pendulous dampers each having mass, m, are attached to the main body, and are free to move in a plane $y = \ell$, perpendicular to the polar axis. (The position of two of these are shown in Fig. 1b. The other pair would be aligned, in equilibrium,

along the $\pm$ X axes). The angles swept out by the pendulous dampers are ϕ_i. The analysis shall initially be undertaken with all four end masses being able to move, n = 1,2,3 or 4. Later we shall simplify our analysis by assuming n = 1 or $\phi_2 = \phi_3 = \phi_4 = 0$ for the actual case of SAS-A. Labelling the weights with subscripts, 1-4, the coordinates of the end masses can be expressed:

$$z_1 = r_o + r_1 \cos \phi_1,\ z_2 = -(r_o + r_1 \cos \phi_2),\ z_3 = -r_1 \sin \phi_3,$$

$$z_4 = r_1 \sin \phi_4,\ x_1 = r_1 \sin \phi_1,\ x_2 = -r_1 \sin \phi_2,\ x_3 = r_o + r_1 \cos \phi_3$$

$$x_4 = -(r_o + r_1) \cos \phi_4,\ y = \ell \quad \ldots\ldots\ldots\ldots\ldots\ldots \quad (1)$$

All external forces except gravity are neglected and even with that we shall neglect the effects of the inhomogeneity of the earth's field. The motion of the center of gravity of the system and motion about the center of gravity can then be separated.

If ω_x, ω_y, and ω_z are the angular velocities of the main body about the X,Y, Z axes respectively, and r_i is the position vector of the ith weight, the kinetic energy of the main body and the damper can be expressed as:[1,3]

$$T_M = \frac{1}{2} A\omega_x^2 + \frac{1}{2} B\omega_y^2 + \frac{1}{2} C\omega_z^2 + \frac{1}{2} M v_{M/cm}^2 + \frac{1}{2} \sum_{i=1}^{n} m_i v_{m_i/cm}^2 . \quad (2)$$

From the definition of the system center of mass:

$$\bar{r}_{cm/o} = \frac{m \sum_{i=1}^{n} \bar{r}_{i/o}}{M + \sum_{i=1}^{n} m_i} \quad \ldots\ldots\ldots\ldots \quad (3)$$

where point o is the center of the coordinate system. The velocity of the various components relative to the system center of mass may be expanded:

$$\bar{v}_{m_{i/cm}} = \bar{v}_{m_{i/o}} + \bar{v}_{o/cm} \quad \ldots\ldots\ldots\ldots\ldots\ldots \quad (4)$$

$$\bar{v}_{M/cm} = \bar{v}_{M/o} + \bar{v}_{o/cm} \quad \ldots\ldots\ldots\ldots\ldots\ldots \quad (5)$$

The components appearing in Eqs. (4) and (5) can further be expressed as:

$$\bar{v}_{m_{i/o}} = \dot{\bar{r}}_i \quad \ldots\ldots\ldots\ldots\ldots\ldots \quad (6)$$

$$\bar{v}_{o/M} = 0 \quad \ldots\ldots\ldots\ldots\ldots\ldots \quad (7)$$

$$\bar{v}_{o/cm} = -\bar{v}_{cm/o} = -\dot{\bar{r}}_{cm/o} = -\frac{m\,\Sigma\dot{\bar{r}}_i}{M + \Sigma m} \quad \ldots\ldots\ldots\ldots \quad (8)$$

Upon substitution of Eqs. (6) - (8) into Eq. (2), the kinetic energy of the main body may be expressed as:

$$2T_M = A\omega_x^2 + B\omega_y^2 + C\omega_z^2 + m\,(\Sigma\,\dot{\bar{r}}_i \cdot \dot{\bar{r}}_i) - \frac{m^2}{\bar{M}}\,(\Sigma\,\dot{\bar{r}}_i \cdot \Sigma\,\dot{\bar{r}}_i) \quad . \quad (9)$$

where $\bar{M} = M + \sum_i m_i$

The kinetic energy of the rotor is given by:

$$T_{Rotor} = \frac{1}{2}\,[I_{R_x}\,\omega_x^2 + I_{R_y}\,(\omega_y + s)^2 + I_{R_z}\,\omega_z^2\,] \quad \ldots\ldots \quad (10)$$

where I_{R_i}, i = x,y,z are the rotor principal moments of inertia and

the rotor is assumed to be spinning about the Y-axis with a relative angular velocity s, with respect to the main spacecraft.

If it is remembered that, e.g. the X-component of $\dot{\underline{r}}_i$ is $\dot{x}_i + \omega_y z_i - \omega_z y_i$, and use is made of Eqs. (1) and (2), the kinetic energy takes the rather involved form given in Appendix A. The equations of motion for this case can thus be expressed in terms of the quasi-coordinates $(\omega_x, \omega_y, \omega_z)$ and the angle swept out (ϕ_i) by the pendulous dampers according to:[8]

$$\frac{d}{dt}\left(\frac{\partial T}{\partial \omega_x}\right) - \omega_z \frac{\partial T}{\partial \omega_y} + \omega_y \frac{\partial T}{\partial \omega_z} = L_x$$

$$\frac{d}{dt}\left(\frac{\partial T}{\partial \omega_y}\right) - \omega_x \frac{\partial T}{\partial \omega_z} + \omega_z \frac{\partial T}{\partial \omega_x} = L_y \quad \ldots\ldots\ldots \quad (11)$$

$$\frac{d}{dt}\left(\frac{\partial T}{\partial \omega_z}\right) - \omega_y \frac{\partial T}{\partial \omega_x} + \omega_x \frac{\partial T}{\partial \omega_y} = L_z$$

and

$$\frac{d}{dt}\left(\frac{\partial T}{\partial \dot{\phi}_i}\right) - \frac{\partial T}{\partial \phi_i} + \frac{\partial F}{\partial \dot{\phi}_i} = -\frac{\partial V}{\partial \phi_i} = Q_i, \quad i = 1 \rightarrow n$$

where L_i, $i = x,y,z$ are the applied torques and n, represents the total number of the dampers; the viscous forces on the pendulous end masses, which vary linearly with the angular velocity, $\dot{\phi}_i$, can be derived from the Rayleigh dissipation function, F; in this case,[3,9]

$$F = \frac{1}{2} \sum_{i=1}^{n} (k_i \dot{\phi}_i^2) \quad \ldots\ldots\ldots\ldots\ldots\ldots \quad (12)$$

The restoring torque on each damper provided by the torsion wire support is represented by $Q_i = -\frac{\partial V}{\partial \phi_i}$ where the potential energy, V, is proportional to the square of the angular displacement from the equilibrium position,

$$V = \frac{1}{2} \sum_{i=1}^{n} K_i \phi_i^2 \quad \ldots\ldots\ldots\ldots\ldots\ldots \quad (13)$$

Eqs. (11) may be expanded and simplified with small angle assumptions made relative to the magnitudes of the ϕ_i, and with further assumptions that ω_x/ω_y, ω_z/ω_y and $\dot{\phi}_i/\omega_y$ are small in order to obtain first order damping contributions, for the case of n = 2 dampers and for the case of a constant speed rotor:[3]

$$\bar{A}\dot{\omega}_x + (\bar{C} - \bar{B})\,\omega_y\omega_z - \omega_z\, I_{R_y} s - 2mr_1\bar{\ell}\,\omega_y(\dot{\phi}_1 - \dot{\phi}_2) = L_x \quad \ldots \quad (14)$$

$$\bar{B}\dot{\omega}_y + (\bar{A} - \bar{C})\,\omega_z\omega_x + mr_1(r_o + r_1)\,(\ddot{\phi}_1 + \ddot{\phi}_2) = L_y \quad \ldots\ldots \quad (15)$$

$$\bar{C}\dot{\omega}_z + (\bar{B} - \bar{A})\omega_x\omega_y - mr_1\bar{\ell}(\ddot{\phi}_1 - \ddot{\phi}_2) + mr_1\bar{\ell}(\phi_1 - \phi_2)\,\omega_y^2 + I_{R_y}\,\omega_x s = L_z \quad \ldots\ldots\ldots \quad (16)$$

$$mr_1^2\left(1 - \frac{m}{\bar{M}}\right)\ddot{\phi}_1 + \frac{m^2 r_1^2\,\ddot{\phi}_2}{\bar{M}} - mr_1\bar{\ell}\dot{\omega}_z + mr_1(r_o + r_1)\dot{\omega}_y + mr_1\left(r_o + \frac{mr_1}{\bar{M}}\right)\phi_1\,\omega_y^2 - \frac{m^2 r_1^2}{\bar{M}}\phi_2\omega_y^2 + mr_1\bar{\ell}\omega_x\omega_y = -k\dot{\phi}_1 - K\phi_1 \quad \ldots\ldots\ldots \quad (17)$$

$$mr_1^2 \left(1 - \frac{m}{\bar{M}}\right)\ddot{\phi}_2 + \frac{m^2 r_1^2}{\bar{M}}\ddot{\phi}_1 + mr_1\bar{\ell}\dot{\omega}_z + mr_1(r_o + r_1)\dot{\omega}_y$$

$$+ mr_1\left(r_o + \frac{mr_1}{\bar{M}}\right)\phi_2\omega_y^2 - \frac{m^2}{\bar{M}} r_1^2\phi_1\omega_y^2 - mr_1\bar{\ell}\omega_y\omega_x$$

$$= -k\dot{\phi}_2 - K\phi_2 \quad \ldots\ldots\ldots \quad (18)$$

where the total inertia terms have main body, rotor and damper components:

$$\bar{A} = A + I_{R_x} + I_{d_x}$$

$$\bar{B} = B + I_{R_y} + I_{d_y}$$

$$\bar{C} = C + I_{R_z} + I_{d_z}$$

which can be expanded to yield:

$$\bar{A} = A + I_{R_x} + 4m\ell^2 + 2m(r_o + r_1)^2$$

$$\bar{B} = B + I_{R_y} + 4m(r_o + r_1)^2$$

$$\bar{C} = C + I_{R_z} + 4m\ell^2 + 2m(r_o + r_1)^2$$

and $\bar{\ell} = \frac{\ell M}{\bar{M}}$

k is the damping rate constant

K is the restoring spring constant of the torsion wire support

B. Eulerian Approach of the Formulation of the Equations of Motion for Variable Speed Rotor

The Eulerian approach is considered here so that it will be possible to distinguish between reaction torques, applied torques, damping torques and external torques. The angular momentum of the main body can be expressed as:

$$\bar{L}_M = (A + I_{d_x})\,\omega_x \bar{i} + (B + I_{d_y})\,\omega_y \bar{j} + (C + I_{d_z})\,\omega_z \bar{k} \quad \ldots\ldots \quad (19)$$

whereas for the rotor:

$$\bar{L}_R = I_{R_x}\,\omega_{R_x}\,\bar{i} + I_{R_y}\,\omega_{R_y}\,\bar{j} + I_{R_z}\,\omega_{R_z}\,\bar{k} \quad \ldots\ldots\ldots\ldots \quad (20)$$

Using the familiar relationship,

$$\frac{d\bar{L}}{dt}\Big|_{space} = \frac{d\bar{L}}{dt}\Big|_{Body} + \bar{\omega}\bar{X}\bar{L} = \bar{\Sigma N}$$

the main body equations can be developed as:

$$(A + I_{d_x})\,\dot{\omega}_x + \omega_y\omega_z\,(C + I_{d_z}) - \omega_y\omega_z(B + I_{d_y}) = N_{d_x} + R_x \quad (21)$$

$$(B + I_{d_y})\,\dot{\omega}_y + \omega_z\omega_x\,(A + I_{d_x}) - \omega_z\omega_x\,(C + I_{d_z}) = N_{d_y} + R_y + L_{m_y} \quad (22)$$

$$(C + I_{d_z})\,\dot{\omega}_z + \omega_x\omega_y\,(B + I_{d_y}) - \omega_x\omega_y\,(A + I_{d_x}) = N_{d_z} + R_z \quad (23)$$

and the rotor equations, similarly:

$$I_{R_x}\dot{\omega}_{R_x} + \omega_y\omega_{R_z}\,I_{R_z} - I_{R_y}\,\omega_z\omega_{R_y} = N_{R_x} + R_{R_x} \quad \ldots\ldots\ldots\ldots \quad (24)$$

$$I_{R_y}\dot{\omega}_{R_y} + \omega_z\omega_{R_x}I_{R_x} - \omega_x\omega_{R_z}I_{R_z} = N_{R_y} + R_{R_y} \quad \ldots\ldots\ldots \quad (25)$$

$$I_{R_z}\dot{\omega}_{R_z} + \omega_x\omega_{R_y}I_{R_y} - \omega_y\omega_{R_x}I_{R_x} = N_{R_z} + R_{R_z} \quad \ldots\ldots\ldots \quad (26)$$

where I_{R_i}, are the principal moments of inertia of rotor, (i = x,y,z)

I_{d_i}, are the moments of inertia of dampers about X,Y,Z

N_{d_i}, are the damping torques on the main body

R_i, are the reactions (torque) of rotor on main body

N_{R_i}, are the (applied) torques acting on the rotor

R_{R_i}, are the reactions (torque) of main body on rotor

L_{m_y}, is the motor torque

In Eqs. (21) - (26) the effect of all external torques (e.g. aerodynamic, solar pressure, gravity-gradient) have been neglected. Substituting first order expressions for N_{d_i} previously derived, Eqs. (21) - (23) can be written as:

$$(A + I_{d_x})\dot{\omega}_x + \omega_y\omega_z(C + I_{d_z}) - \omega_y\omega_z(B + I_{d_y}) = 2mr_1\bar{\ell}(\dot{\phi}_1 - \dot{\phi}_2)\omega_y$$

$$+ R_x \quad \ldots\ldots\ldots\ldots\ldots\ldots \quad (27)$$

$$(B + I_{d_y})\dot{\omega}_y + \omega_z\omega_x(A + I_{d_x}) - \omega_x\omega_z(C + I_{d_z})$$

$$= - mr_1(r_o + r_1)\ (\ddot{\phi}_1 + \ddot{\phi}_2) + R_y + L_{m_y} \quad . \quad . \quad . \qquad (28)$$

$$(C + I_{d_z})\dot{\omega}_z + \omega_x\omega_y(B + I_{d_y}) - \omega_x\omega_y(A + I_{d_x})$$

$$= mr_1\bar{\ell}(\ddot{\phi}_1 - \ddot{\phi}_2) - mr_1\bar{\ell}(\phi_1 - \phi_2)\omega_y^2 + R_z \quad . \quad . \quad . \qquad (29)$$

The assumptions are, that reaction torques are equal and opposite, $R_i = - R_{R_i}$, and the inertia (motor) torques about axes other than the spin axis are zero, i.e. $N_{R_x} = N_{R_z} = 0$, but ideally, $N_{R_y} = - L_{m_y}$ i.e. the inertia torque about the spin axis is equal and opposite to the motor torque.

Now combining, (24) with (27), (25) with (28) and (26) with (29) and noting that,

$$\omega_{R_y} = \omega_y + s,\ \omega_{R_z} = \omega_z,\ \text{and}\ \ \omega_{R_x} = \omega_x$$

we obtain,

$$\bar{A}\dot{\omega}_x + (\bar{C} - \bar{B})\omega_y\omega_z - \omega_z I_{R_y} s = 2mr_1\bar{\ell}(\dot{\phi}_1 - \dot{\phi}_2)\omega_y \quad . \quad . \quad . \quad . \quad . \quad . \quad . \qquad (30)$$

$$\bar{B}\dot{\omega}_y + (\bar{A} - \bar{C})\omega_z\omega_x + I_{R_y}\dot{s} = - mr_1(r_o + r_1)\ (\ddot{\phi}_1 + \ddot{\phi}_2) \quad . \quad . \quad . \quad . \qquad (31)$$

$$\bar{C}\dot{\omega}_z + (\bar{B} - \bar{A})\omega_x\omega_y + \omega_x I_{R_y} s = mr_1\bar{\ell}(\ddot{\phi}_1 - \ddot{\phi}_2) - mr_1\bar{\ell}(\phi_1 - \phi_2)\omega_y^2 \quad . \qquad (32)$$

where $\bar{A} = A + I_{d_x} + I_{R_x}$, and similarly for $\bar{B}$ and $\bar{C}$.

In addition, the general torque equation for the symmetrical rotor, (i.e. $I_{R_x} = I_{R_z}$) is obtained from Eq. (25),

$$I_{R_y}(\dot{\omega}_y + \dot{s}) \simeq L_{R_y} \quad \ldots \quad (33)$$

where the following approximation has been made:

$$L_{m_y} \approx L_{R_y} >> R_y$$

When $\dot{s} = 0$, then Eqs. (30) - (32) are identical to Eqs. (14) - (16).

C. Stability Analysis for the Special Case of an Undamped Symmetrical Satellite

We will consider the system without damping, and a spacecraft symmetrical about the nominal spin axis, i.e. $I_{d_i} = 0$, $C = A$, and $I_{R_x} = I_{R_z}$. Under these assumptions Eqs. (30) - (32) take the following form:

$$A'\dot{\omega}_x + (A' - B')\omega_y\omega_z - \omega_z I_{R_y} s = 0 \quad \ldots \quad (34)$$

$$B'\dot{\omega}_y + I_{R_y}\dot{s} = 0 \quad \ldots \quad (35)$$

$$A'\dot{\omega}_z + \omega_x\omega_y(B' - A') + \omega_x I_{R_y} s = 0 \quad \ldots \quad (36)$$

The general torque equation, Eq. (33) is again:

$$I_{R_y}(\dot{\omega}_y + \dot{s}) \simeq L_{R_y}$$

It should be noted that Eqs. (34) - (36) are exact with no restrictions

on the magnitudes of ω_x and ω_z.

After multiplying Eq. (34) by ω_x and Eq. (36) by ω_z and adding then a first integral results as:

$$\omega_x^2 + \omega_z^2 = K_1 = \text{Constant} \quad \ldots\ldots\ldots\ldots \quad (37)$$

Eq. (37) indicates that the amplitude of the vector sum of the transverse angular velocity components is bounded during spin-up.

Eq. (35) can be integrated directly, to yield:

$$\omega_y = \frac{-I_{R_y} s + B'\omega_y(0) + I_{R_y} s(0)}{B'} \quad \ldots\ldots\ldots \quad (38)$$

Upon substitution of $\dot{\omega}_y$ from Eq. (35) into Eq. (33),

$$\dot{s} = \frac{I_{R_y}}{I_{R_y}\left[1 - \frac{I_{R_y}}{B'}\right]} = c = \text{constant} \quad \ldots\ldots\ldots \quad (39)$$

Upon integration of (39),

$$s = ct + s(0) \quad \ldots\ldots\ldots\ldots\ldots\ldots \quad (40)$$

which states that the relative angular velocity of the rotor, for the case of a symmetrical satellite increases uniformly during spin-up.

Substituting the values of ω_y and s into Eqs. (34) and (36) we can get,

$$A'\dot{\omega}_x + \frac{(A' - B')\,[\omega_y(0)B' + I_{R_y}\, s(0)]}{B'}\,\omega_z$$

$$+ \left[\frac{(A' - B')\,(-I_{R_y})}{B'} - I_{R_y}\right][ct + s(0)]\omega_z = 0 \quad . (41)$$

$$A'\dot{\omega}_z + \frac{(B' - A')\,[\omega_y(0)B' + I_{R_y}\, s(0)]}{B'}\,\omega_x$$

$$+ \left[\frac{(A' - B')\,(-I_{R_y})}{B'} - I_{R_y}\right][ct + s(0)]\omega_x = 0 \quad . \quad (42)$$

If $P = \dfrac{(A' - B')\,[\omega_y(0)\,B' + I_{R_y}s(0)]}{B'}$

and, $Q = \dfrac{(A' - B')\,(-I_{R_y})}{B'} - I_{R_y}$

then Eqs. (41) and (42) can be written:

$$A'\dot{\omega}_x + \omega_z[P + Q\{ct + s(0)\}] = 0 \quad . \quad . \quad . \quad . \quad . \quad . \quad . \quad . \quad . \quad . \quad . \quad . \quad (43)$$

$$A'\dot{\omega}_z - \omega_x[P + Q\{ct + s(0)\}] = 0 \quad . \quad . \quad . \quad . \quad . \quad . \quad . \quad . \quad . \quad . \quad . \quad . \quad (44)$$

From Eq. (44) and after differentiation with respect to time,

$$\dot{\omega}_x = \frac{A'[P + Q\{ct + s(0)\}]\ddot{\omega}_z - \dot{\omega}_z A'cQ}{[P + Q\{ct + s(0)\}]^2} \quad . \quad . \quad . \quad . \quad . \quad . \quad . \quad . \quad . \quad (45)$$

After substituting Eq. (45) into Eq. (43), there results

$$\ddot{\omega}_z - \frac{cQ}{[P + Q\{ct + s(0)\}]}\dot{\omega}_z + \left[\frac{P + Q\{ct + s(0)\}}{A'}\right]^2 \omega_z = 0 \quad (46)$$

Similarly by expressing $\omega_z = f(\dot{\omega}_x)$ and differentiating,

$$\ddot{\omega}_x - \frac{cQ}{[P + Q\{ct + s(0)\}]}\dot{\omega}_x + \left[\frac{P + Q\{ct + s(0)\}}{A'}\right]^2 \omega_x = 0 \quad (47)$$

Eqs. (46) and (47) are second order differential equations with variable coefficients and have a regular singularity at time $t = t_o$, where $t_o = -a = -\left[\frac{s(0)\,Q + P}{Qc}\right]$. The solution of this type of differential equation can be represented by a power series expanded around the regular singular point.[10] At least one of the solutions to Eq. (47) can be represented as:

$$\omega_x = \sum_{k=0}^{\infty} a_k (t + a)^{r + k} \quad \ldots\ldots\ldots\ldots\ldots\ldots \quad (48)$$

where 'a' is the regular singular point at time,

$$t = -\left[\frac{s(0)\,Q + P}{Qc}\right]$$

Then, $\dot{\omega}_x = \sum_{k=0}^{\infty} a_k (r + k)(t + a)^{r + k - 1} \quad \ldots\ldots\ldots\ldots \quad (49)$

and $\ddot{\omega}_x = \sum_{k=0}^{\infty} a_k (r + k)(r + k - 1)(t + a)^{r + k - 2} \quad \ldots\ldots \quad (50)$

Now Eq. (47) can be written as:

$$\ddot{\omega}_x - \frac{\dot{\omega}_x}{(t + a)} + \frac{Q^2 c^2}{A'^2}(t + a)^2 \omega_x = 0 \quad \ldots\ldots\ldots\ldots \quad (51)$$

Substituting Eqs. (48) - (50) into Eq. (51), there results,

$$\sum_{k=0}^{\infty} a_k (r + k)(r + k - 1)(t + a)^{r + k - 2}$$

$$- \sum_{k=0}^{\infty} a_k (r + k)(t + a)^{r + k - 2}$$

$$+ \frac{Q^2 c^2}{A'^2} \sum_{k=0}^{\infty} a_k (t + a)^{r + k + 2} = 0 \quad \ldots \quad (52)$$

The indicial equation is obtained by equating to zero the coefficiencts of the terms in the smallest power in $(t + a)$ and assuming $a_o \neq 0$. In this case the smallest power of $(t + a)$, obtained by setting $k = 0$ is $(t + a)^{r - 2}$.

Then,

$$a_o[r(r - 1) - r] = 0 \quad \ldots \quad (53)$$

Since it has already been assumed that $a_o \neq 0$, then the roots of the indicial equation are:

$$r = 0, \text{ and } r = 2$$

Equating the coefficient of $(t + a)^{r - 1}$ to zero, we obtain:

$$a_1 (r + 1)r - a_1(r + 1) = 0 \quad \ldots \quad (54)$$

From consideration of Eq. (54) it can be concluded that $a_1 = 0$ for both $r = 0$ and $r = 2$.

By equating the coefficients of $(t + a)^r$ to zero it is seen that a_2 is arbitrary for $r = 0$ and a_2 is zero for $r = 2$. Similarly by equating the coefficients of $(t + a)^{r + 1}$ to zero we get $a_3 = 0$ for both the values $r = 0$ and $r = 2$.

Now by equating the coefficient of $(t + a)^{r + k}$ to zero, the following relation is obtained:

$$a_{k+2}(r + k + 2)(r + k + 1) - a_{k+2}(r + k + 2) + \frac{\varrho^2 c^2}{A'^2} a_{k-2} = 0 \quad \ldots\ldots\ldots\ldots\ldots \quad (55)$$

From Eq. (55), the general recurrence relation between the coefficients can be derived:

$$a_{k+2} = - \frac{\varrho^2 c^2}{A'^2} \frac{a_{k-2}}{(r + k)(r + k + 2)} \quad \ldots\ldots\ldots\ldots \quad (56)$$

For a_o selected arbitrarily ($a_o \neq 0$) and for the root, $r = 0$, the other coefficients may be expressed as follows:

$$a_1 = 0; \quad a_2 = 0; \quad a_3 = 0; \quad a_4 = - \frac{\varrho^2 c^2}{A'^2} \frac{a_o}{2.4}; \quad a_5 = 0;$$

$$a_6 = - \frac{\varrho^2 c^2}{A'^2} \frac{a_2}{4.6}; \quad a_7 = 0; \quad a_8 = \frac{\varrho^4 c^4}{A'^2} \frac{a_o}{2.4.6.8}; \quad a_9 = 0;$$

$$a_{10} = \frac{\varrho^4 c^4}{A'^4} \frac{a_2}{4.6.8.10}; \quad a_{11} = 0; \quad a_{12} = - \frac{\varrho^6 c^6}{A'^6} \frac{a_o}{2.4.6.8.10.12}; \ldots$$

etc.

After substituting a_o, a_1, a_2, ... , a_m into Eq. (48) the solution corresponding to the root, $r = 0$, takes the following form:

$$\omega_{x_1} = a_o + a_2(t + a)^2 - \frac{\varrho^2 c^2}{A'^2} \frac{a_o}{2.4} (t + a)^4 - \frac{\varrho^2 c^2}{A'^2} \frac{a_2}{4.6} (t + a)^6$$

$$+ \frac{\varrho^4 c^4}{A'^4} \frac{a_o}{2.4.6.8} (t + a)^8 - \frac{\varrho^4 c^4}{A'^4} \frac{a_2}{4.6.8.10} (t + a)^{10}$$

$$- \frac{\varrho^6 c^6}{A'^6} \frac{a_o}{2.4.6.8.10.12} (t + a)^{12} - \ldots \quad (57)$$

Similarly, for $r = 2$ and selecting $a_o \neq 0$, with the aid of Eq. (56), the coefficients can be related as:

$$a_1 = 0; \quad a_2 = 0; \quad a_3 = 0; \quad a_4 = - \frac{\varrho^2 c^2}{A'^2} \frac{a_o}{4.6};$$

$$a_5 = 0; \quad a_6 = 0; \quad a_7 = 0; \quad a_8 = \frac{\varrho^4 c^4}{A'^4} \frac{a_o}{4.6.8.10};$$

$$a_9 = 0; \quad a_{10} = 0; \quad a_{11} = 0; \quad a_{12} = - \frac{\varrho^6 c^6}{A'^6} \frac{a_o}{4.6.8.10.12.14}; \ldots$$

etc.

Again after substitution of the above values of a_o, a_1, a_2, ... a_m into Eq. (48), the solution corresponding to $r = 2$, becomes:

$$\omega_{x_2} = a_o (t + a)^2 - \frac{\varrho^2 c^2}{A'^2} \frac{a_o}{4.6} (t + a)^6$$

$$+ \frac{\varrho^4 c^4}{A'^4} \frac{a_o}{4.6.8.10} (t + a)^{10} - \frac{\varrho^6 c^6}{A'^6} \frac{a_o}{4.6.8.10.12.14} (t + a)^{14}$$

$$+ \ldots \quad (58)$$

The complete solution of Eq. (47) is, in general, an arbitrary linear combination of Eqs. (57) and (58):

$$\omega_x = C_1 \omega_{x_1} + C_2 \omega_{x_2} \ldots \ldots \ldots \ldots \ldots \ldots \ldots \quad (59)$$

Eq. (59) can be expressed, using Eqs. (57) and (58), as:

$$\omega_x = C_1[a_o + a_2(t+a)^2 - \frac{Q^2c^2}{A'^2}\frac{a_o}{2.4}(t+a)^4 - \frac{Q^2c^2}{A'^2}\frac{a_2}{4.6}(t+a)^6$$

$$+ \frac{Q^4c^4}{A'^4}\frac{a_o}{2.4.6.8}(t+a)^8 - \frac{Q^4c^4}{A'^4}\frac{a_2}{4.6.8.10}(t+a)^{10}$$

$$- \frac{Q^6c^6}{A'^6}\frac{a_o}{2.4.6.8.10.12}(t+a)^{12} - \ldots.]$$

$$+ C_2[a_o(t+a)^2 - \frac{Q^2c^2}{A'^2}\frac{a_o}{4.6}(t+a)^6 + \frac{Q^4c^4}{A'^4}\frac{a_o}{4.6.8.10}(t+a)^{10}$$

$$- \frac{Q^6c^6}{A'^6}\frac{a_o}{4.6.8.10.12.14}(t+a)^{14} + \ldots] \quad (60)$$

for $-\infty < t < \infty$

It should be noticed that the solution converges for all finite values of time since there is no other singular point of the differential Eq. (47).

Eq. (60) can also be represented as:

$$\omega_x = K_1 \mathrm{Cos}\left[\frac{Qc}{A'}\frac{(t+a)^2}{2} + K_2\right] \quad (61)$$

where

$$K_1 = \frac{C_1 a_o}{\mathrm{Cos}K_2} \quad \text{and} \quad K_2 = \mathrm{Tan}^{-1}\left[\frac{(C_1' + C'_2)}{Qc}\,2A'\right]$$

$$C_1' = \frac{a_2}{a_o} \quad \text{and} \quad C_2' = \frac{C_2}{C_1}$$

It can also be seen that Eq. (61) can also be represented as:

$$\omega_x = K_1 \text{ Cos } \int_o^t M'dt \quad \ldots \ldots \ldots \ldots \ldots \ldots \quad (62)$$

where

$$M' = \frac{P}{A'} + \frac{Q}{A'} [ct + s(0)]$$

Now if we assume that the solution of Eq. (46) has the form:

$$\omega_z = \sum_{k=0}^{\infty} b_k (t + a)^{r+k}$$

then by applying the method of Frobenius as before we obtain the complete solution to Eq. (46) as:

$$\omega_z = K_1 \text{ Sin } [\frac{Qc}{A'} \frac{(t + a)^2}{2} + K_2] \quad \ldots \ldots \ldots \quad (63)$$

where the constants can again be related by:

$$K_1 \text{ Cos } K_2 \frac{Qc}{2A'} = C'_3 + C'_4, \quad \frac{2A'}{Qc} \text{ Tan } K_2 = C_3 b_o$$

where

$$C'_3 = \frac{b_2}{b_o} \quad \text{and} \quad C'_4 = \frac{C_4}{C_3}$$

Eq. (63) can further be reduced as before to the form:

$$\omega_z = K_1 \text{ Sin } \int_o^t M'dt \quad \ldots \ldots \ldots \ldots \ldots \quad (64)$$

From consideration of Eqs. (62) and (64) it is apparent that:

$$\omega_x^2 + \omega_z^2 = K_1^2 \quad \ldots \ldots \ldots \ldots \ldots \ldots \quad (65)$$

which compares directly with the first integral, (37).

When the nutation damper is physically constrained from movement, the magnitude of vector sum of the transverse angular velocity components remain constant during wheel spin up under the influence of a constant motor torque. The stability criteria for this system is based on the magnitude of the transverse components of the angular velocity. If the transverse components of the angular velocity do not exceed the initial values, then it is assumed that no serious stability problems would be encountered. The implication of Eq. (65) is the boundedness of this motion during spin-up.

D. Analysis for Asymmetrical Main Body

Assuming the system is undamped and has a symmetrical rotor, i.e. $I_{d_i} = 0$ and $I_{R_x} = I_{R_z}$, but with $A \neq C$, Eqs. (30) - (32) can be expressed as follows:

$$A'\dot{\omega}_x + (C' - B')\omega_y\omega_z - \omega_z I_{R_y} s = 0 \quad \ldots\ldots\ldots\ldots\ldots \quad (66)$$

$$B'\dot{\omega}_y + (A' - C')\omega_z\omega_x + I_{R_y}\dot{s} = 0 \quad \ldots\ldots\ldots\ldots\ldots \quad (67)$$

$$C'\dot{\omega}_z + (B' - A')\omega_x\omega_y + \omega_x I_{R_y} s = 0 \quad \ldots\ldots\ldots\ldots\ldots \quad (68)$$

and the torque equation for the symmetrical rotor is the same as before:

$$I_{R_y}(\dot{\omega}_y + \dot{s}) = L_{R_y}$$

After multiplying Eq. (66) by ω_x and Eq. (68) by ω_z and adding there results:

$$\omega_x\omega_z(A' - C') = \frac{A'(\omega_x\dot{\omega}_x) + C'(\omega_z\dot{\omega}_z)}{\omega_y} \quad \ldots\ldots\ldots \quad (69)$$

Substituting Eq.(69) into Eq. (67) and after simplifying we obtain the result as:

$$A'(\omega_x\dot{\omega}_x) + B(\dot{\omega}_y\dot{\omega}_y) + C'(\omega_z\dot{\omega}_z) + L_{R_y}\omega_y = 0 \quad \ldots\ldots\ldots \quad (70)$$

If the torque control law during spin-up is as: $B\dot{\omega}_y + L_{R_y} = 0$, then Eq. (70) becomes:

$$A'(\omega_x\dot{\omega}_x) + C'(\omega_z\dot{\omega}_z) = 0 \quad \ldots\ldots\ldots\ldots\ldots\ldots \quad (71)$$

which results in:

$$A'\omega_x^2 + C'\omega_z^2 = c = \text{Constant} \quad \ldots\ldots\ldots\ldots\ldots\ldots \quad (72)$$

and the motion is bounded as in the case of a symmetrical main body. In general, the integration of (70) yields the following first integral:

$$\frac{1}{2}A'\omega_x^2 + \frac{1}{2}B\omega_y^2 + \frac{1}{2}C'\omega_z^2 + \int_o^t L_{R_y}\omega_y(u)du = \text{Constant} \quad \ldots \quad (73)$$

E. Effects of the Nutation Damper

Under the assmumptions of a symmetrical spacecraft and only one damper free to move, the equations of motion, (30) - (32), are as follows:

$$\bar{A}\dot{\omega}_x + (\bar{A} - \bar{B})\omega_y\omega_z - \omega_z I_{R_y} s = 2mr_1\bar{\ell}\dot{\phi}_1\omega_y \quad \ldots\ldots\ldots \quad (74)$$

$$\bar{B}\dot{\omega}_y + I_{R_y}\dot{s} = -mr_1(r_o + r_1)\ddot{\phi}_1 \quad \ldots\ldots\ldots\ldots\ldots \quad (75)$$

$$\bar{A}\dot{\omega}_z + (\bar{B} - \bar{A})\omega_x\omega_y + \omega_x I_{R_y} s = mr_1\bar{\ell}\ddot{\phi}_1 - mr_1\bar{\ell}\phi_1\omega_y^2 \quad \ldots\ldots \quad (76)$$

and from Eq. (33), the torque equation is written:

$$I_{R_y}(\dot{\omega}_y + \dot{s}) \cong L_{R_y} \quad \ldots\ldots\ldots\ldots\ldots\ldots \quad (77)$$

In addition the damper equation, from (17) is:

$$mr_1^2\left(1 - \frac{m}{\bar{M}}\right)\ddot{\phi}_1 + mr_1(r_o + r_1)\dot{\omega}_y - mr_1\bar{\ell}\dot{\omega}_z$$

$$+ mr_1\left(r_o + \frac{mr_1}{\bar{M}}\right)\phi_1\omega_y^2$$

$$+ mr_1\bar{\ell}\omega_x\omega_y = -k\dot{\phi}_1 - K\phi_1 \quad \ldots\ldots \quad (78)$$

Eq. (75) can be integrated directly, to yield:

$$\omega_y = \omega_{y(0)} - \frac{I_{R_y}s}{\bar{B}} - \frac{mr_1(r_o + r_1)}{\bar{B}}\dot{\phi}_1 - \frac{I_{R_y}s(0)}{\bar{B}}$$

$$- \frac{mr_1(r_o + r_1)}{\bar{B}}\dot{\phi}_1(0) \quad \ldots\ldots \quad (79)$$

Upon substitution of $\dot{\omega}_y$ from Eq. (75) into Eq. (77), there results:

$$\dot{s} = \frac{L_{R_y}}{I_{R_y}\left(1 - \frac{I_{R_y}}{\bar{B}}\right)} + \frac{mr_1(r_o + r_1)}{\bar{B}\left(1 - \frac{I_{R_y}}{\bar{B}}\right)}\ddot{\phi}_1 \quad \ldots\ldots \quad (80)$$

The first term on the right hand side is constant, say, c, under the assumption that L_{R_Y} is constant.

Upon integration of Eq. (80)

$$S = ct + \frac{mr_1(r_o + r_1)}{\bar{B}\left(1 - \frac{I_{R_y}}{\bar{B}}\right)} \dot{\phi}_1 + s(0) \quad \ldots\ldots\ldots \quad (81)$$

It is seen from Eq. (80) that compared to the symmetrical case, the relative spin rate of the rotor in this case does not increase uniformly; also that if the damper mass is zero (effect of damping neglected) Eq. (40) would follow directly.

F. Analysis for the Case of a Variable Torque Law

In this section an analysis is made assuming a variable rotor torque instead of a constant torque as described in the previous cases. The rotor torque is assumed to be a linear function of time and reaches twice the value of the constant torque case during spin-up. It is clear that the average torque for the variable torque case is the same as that for the constant torque case previously treated. If we assume a symmetrical satellite without the effect of the damping, the equations of motion can be obtained from Eqs. (34) - (36) as:

$$A'\dot{\omega}_x + (A' - B')\,\omega_y\omega_z - \omega_z I_{R_y} s = 0 \quad \ldots\ldots\ldots\ldots \quad (82)$$

$$B'\dot{\omega}_y + I_{Ry}\,\dot{s} = 0 \quad \ldots\ldots\ldots\ldots\ldots\ldots \quad (83)$$

$$A'\dot{\omega}_z + (B' - A')\,\omega_x\omega_y + \omega_x I_{R_y} s = 0 \quad \ldots\ldots\ldots\ldots \quad (84)$$

and from Eq. (33), the general torque equation:

$$I_{R_y}(\dot{\omega}_y + \dot{s}) \simeq L_{R_y} \quad \ldots\ldots\ldots\ldots\ldots\ldots \quad (85)$$

In addition, for the variable torque law:

$$L_{R_y} = ct \quad \ldots\ldots\ldots\ldots\ldots\ldots\ldots\ldots \quad (86)$$

After multiplying Eq. (81) by ω_x and Eq. (83) by ω_z and adding, there again results the first integral as:

$$\omega_x^2 + \omega_z^2 = \text{Constant} \quad \ldots\ldots\ldots\ldots\ldots \quad (87)$$

Eq. (87) indicates that the amplitude of the vector sum of the transverse angular velocity components is bounded during spin-up, as obtained before. Upon substitution of $\dot{\omega}_y$ from Eq. (83) into Eq. (85) and using Eq. (86),

$$\dot{s} = c't \quad \ldots\ldots\ldots\ldots\ldots\ldots\ldots \quad (88)$$

where c' is a constant equal to $\dfrac{c}{I_{R_y}\left(1 - \dfrac{I_{R_y}}{B'}\right)}$

Upon integration of Eq. (88),

$$s = \frac{c't^2}{2} + s(0) \quad \ldots\ldots\ldots\ldots\ldots\ldots \quad (89)$$

from which it can be concluded that the relative angular velocity of the rotor increases parabolically with time.

G. Effects of the Misalignment of the Principal Axes from the Geometrical Axes

It is noted that the rotor will be displaced from the system center of mass and that the rotor spin axis will nominally be parallel to the desired main body spin axis. In the event that a perfect static mass balance is not achieved, the center of mass of the system will not be at the geometrical center of symmetry when the system is in equilibrium. For this situation there may be a misalignment of the principal main body axes from the geometrical (x,y,z) axes. In addition, if the rotor is not perfectly mass balanced there may also be a misalignment of the rotor principal axes from the geometrical axes.

To consider these possibilities the first order nonlinear equations of motion were developed for both the main body and rotor, as before, but now including all the cross products of inertia terms for both the main body and rotor as referenced to the x,y,z system. The main body and rotor equations may be combined as in Section B and expanded to include first-order small amplitude nutation damping effects. The following first order nonlinear equations result in the coordinates: ω_x, ω_y, ω_z, s, and ϕ_1.

$$[I_{xx} + I_{R_{xx}} + 4m\ell^2 + 2m(r_o + r_1)^2]\dot{\omega}_x - [I_{xy} + I_{R_{xy}} + m\ell r_1\phi_1]\dot{\omega}_y$$

$$- [I_{xz} + I_{R_{xz}}]\dot{\omega}_z - I_{R_{xy}}\dot{s} = [I_{xz} + I_{R_{xz}} + mr_1(r_o+r_1)\phi_1]\omega_x\omega_y$$

$$- [I_{zz} + 4m\ell^2 - I_{R_{yy}} - I_{yy} + I_{R_{zz}} - 2m(r_o+ r_1)^2]\omega_y\omega_z$$

$$+[I_{yz} + I_{R_{yz}}]\omega_y^2 + [I_{R_{yy}}\omega_z + I_{R_{yz}}\omega_y]s - [I_{yz} + I_{R_{yz}}]\omega_z^2$$

$$-[I_{xy} + I_{R_{xy}}]\omega_z\omega_x + m\ell r_1\dot{\phi}_1^2 + 2mr_1\bar{\ell}\dot{\phi}_1\omega_y$$

$$+ 2mr_1(r_o + r_1)\dot{\phi}_1\omega_z \quad \ldots\ldots\ldots\ldots\ldots\ldots (90)$$

$$- [I_{xy} + I_{R_{xy}} + m\ell r_1\phi_1]\dot{\omega}_x + [I_{yy} + I_{R_{yy}} + 4m(r_o+r_1)^2]\dot{\omega}_y$$

$$- [I_{yz} + I_{R_{yz}}]\dot{\omega}_z + I_{R_{yy}}\dot{s} + mr_1(r_o+r_1)\ddot{\phi}_1$$

$$= [I_{xy} + I_{R_{xy}} + m\ell r_1\phi_1]\omega_y\omega_z - [I_{xx} + I_{R_{xx}}$$

$$- I_{zz} - I_{R_{zz}}]\omega_z\omega_x - [I_{yz} + I_{R_{yz}}]\omega_x\omega_y$$

$$-[I_{xz} + I_{R_{xz}}](\omega_x^2 - \omega_z^2) - [I_{R_{yz}}\omega_x - I_{R_{xy}}\omega_z]s$$

$$+ 2mr_or_1\phi_1\dot{\phi}_1\omega_y \quad \ldots\ldots\ldots\ldots\ldots\ldots (91)$$

$$- [I_{xz} + I_{R_{xz}} + mr_1(r_o+r_1)\phi_1]\dot{\omega}_x - [I_{yz} + I_{R_{yz}}]\dot{\omega}_y$$

$$+ [I_{zz} + I_{R_{zz}} + 4m\ell^2 + 2m(r_o+r_1)^2]\dot{\omega}_z - I_{R_{yz}}\dot{s}$$

$$- mr_1\bar{\ell}\ddot{\phi}_1 = [I_{yz} + I_{R_{yz}}]\omega_x\omega_z + [I_{xy} + I_{R_{xy}}]\omega_x^2$$

$$- [I_{yy} + I_{R_{yy}} - I_{xx} - I_{R_{xx}} - 4m\ell^2]\omega_x\omega_y$$

$$- [I_{xz} + I_{R_{xz}} + mr_1(r_o+r_1)\phi_1]\omega_y\omega_z$$

$$- [I_{xy} + I_{R_{xy}} + mr_1\bar{\ell}\phi_1]\omega_y^2 - [I_{R_{xy}}\omega_y + I_{R_{yy}}\omega_x]s$$

$$- 2m\ell r_1\phi_1\dot{\phi}_1\omega_y \quad \ldots\ldots\ldots\ldots\ldots\ldots\ldots\ldots \quad (92)$$

Torque Equation

$$-I_{R_{xy}}\dot{\omega}_x + I_{R_{yy}}\dot{\omega}_y - I_{R_{yz}}\dot{\omega}_z + I_{R_{yy}}\dot{s}$$

$$= L_{R_y} + R_{R_y} - (I_{R_{xx}} - I_{R_{zz}})\omega_z\omega_x + I_{R_{xy}}\omega_y\omega_z$$

$$+ I_{R_{xy}}\omega_z s + I_{R_{xz}}\omega_z^2 - I_{R_{xz}}\omega_x^2 - I_{R_{yz}}\omega_x\omega_y$$

$$- I_{R_{yz}}\omega_x s \quad \ldots\ldots\ldots\ldots\ldots\ldots\ldots\ldots \quad (93)$$

Damper Equation

$$mr_1(r_o+r_1)\dot{\omega}_y - mr_1\bar{\ell}\dot{\omega}_z + mr_1^2\left(1 - \frac{m}{M}\right)\ddot{\phi}_1$$

$$= -mr_1\left(r_o + \frac{mr_1}{\bar{M}}\right)\phi_1\,\omega_y^2 - mr_1\bar{\ell}\omega_x\omega_y - k\dot{\phi}_1 - K\phi_1 \quad . \quad (94)$$

Eqs. (90)-(94) for the general case where all (or most) of the cross product terms appear can not be readily solved analytically and must be evaluated by numerical integration. However, these equations will be considered for three special cases which are representative of numerical cases studied in Part III for the SAS-A and OSO spacecraft.

Case 1

The system will be considered for the case where $I_{xz} = I_{zx} = \gamma$, $I_{xy} = I_{yz} = 0$, $C' = A'$, $I_{R_{zz}} = I_{R_{xx}}$ and all effects of rotor axes misalignment will be neglected. When it is also assumed that $\omega_x/\omega_y << 1$, $\omega_z/\omega_y << 1$, $\gamma << A'$, and $\gamma << B'$, the equations can be written, for the case of no damping, as:

$$A'\dot{\omega}_x + (A'-B')\omega_y\omega_z - \omega_z I_{R_{yy}} s = \gamma(\dot{\omega}_z + \omega_x\omega_y) \quad . \quad . \quad . \quad (95)$$

$$B'\dot{\omega}_y + I_{R_{yy}}\dot{s} = 0 \quad . \quad . \quad . \quad . \quad . \quad . \quad . \quad . \quad . \quad . \quad . \quad . \quad . \quad (96)$$

$$A'\dot{\omega}_z + (B'-A')\omega_x\omega_y + \omega_x I_{R_{yy}} s = \gamma(\dot{\omega}_x - \omega_y\omega_z) \quad . \quad . \quad .(97)$$

$$I_{R_{yy}}(\dot{\omega}_y + \dot{s}) = L_{R_y} \quad . \quad . \quad . \quad . \quad . \quad . \quad . \quad . \quad . \quad . \quad . \quad . \quad . \quad . \quad . \quad . \quad . \quad . \quad . \quad (98)$$

It should be recalled that $A' = A + I_{R_{xx}}$ and similarly for B'. Case 1 is dynamically similar to that of a spacecraft having no misalignment in its principal axes but a small difference between each of its moments of inertia about the two transverse principal axes. (see Case D, p. 22).

Consider the matrix whose elements are the principal and cross products of inertia, for this case,

$$[\,\text{III}\,]_{xyz} = \begin{bmatrix} A' & 0 & \gamma \\ 0 & B' & 0 \\ \gamma & 0 & A' \end{bmatrix}_{xyz}$$

It can be verified that the eigenvalues of this matrix are B', $A' \pm \gamma$ respectively and that the y (or b_2) axis still remains a principal axis but that the new principal axes in the transverse plane are now misaligned from the x,z geometrical axes.

An approximate solution to Eqs. (95)-(98) has been obtained using pertubation techniques and will be developed later in this section.

Case 2

The following are the approximate equations of motion where $I_{xy} = I_{yx} = I_{yz} = I_{zy} = \alpha$, $I_{xz} = 0$, $C'=A'$, $I_{R_{zz}} = I_{R_{xx}}$, no misalignment of rotor principal axes, and no damping as before:

$$A'\dot{\omega}_x + (A'-B')\omega_y\omega_z - \omega_z I_{R_{yy}} s = \alpha[\dot{\omega}_y + \omega_y^2] \quad . \quad . \quad . \quad . \quad (99)$$

$$B'\dot{\omega}_y + I_{R_{yy}} \dot{s} = \alpha[\dot{\omega}_x + \dot{\omega}_z + \omega_y(\omega_z - \omega_x)] \quad . \quad . \quad . \quad . \quad . \quad (100)$$

$$A'\dot{\omega}_z + (B'-A')\omega_x\omega_y + \omega_x I_{R_{yy}} s = \alpha[\dot{\omega}_y - \omega_y^2] \quad . \quad . \quad . \quad (101)$$

$$I_{R_{yy}} (\dot{\omega}_y + \dot{s}) = L_{R_y} \quad . \quad . \quad . \quad . \quad . \quad . \quad . \quad . \quad . \quad . \quad . \quad . \quad . \quad . \quad (102)$$

Case 3

If no misalignment of the main body principal axes from the geometrical axes is assumed, but that $I_{R_{yz}} = \beta$ and also $C'=A'$, $I_{R_{zz}} = I_{R_{xx}}$ and $I_{R_{xy}} = I_{R_{xz}} = 0$, the approximate undamped equations become:

$$A'\dot{\omega}_x + (A'-B')\omega_y\omega_z - \omega_z I_{R_{yy}} s$$

$$= \beta[\omega_y^2 + \omega_y s - \omega_z^2] \quad . \quad . \quad . \quad . \quad . \quad . \quad . \quad . \quad . \quad . \quad . \quad . \quad . \quad . \quad (103)$$

$$B'\dot{\omega}_y + I_{R_{yy}} \dot{s} = \beta[\dot{\omega}_z - \omega_x\omega_y - \omega_x s] \quad . \quad . \quad . \quad . \quad . \quad . \quad . \quad . \quad (104)$$

$$A'\dot{\omega}_z + (B'-A')\omega_x\omega_y + \omega_x I_{R_{yy}} s = \beta[\dot{\omega}_y + \omega_x\omega_z + \dot{s}]. \quad (105)$$

$$I_{R_{yy}} (\dot{\omega}_y + \dot{s}) = L_{R_y} + \beta[\dot{\omega}_z - \omega_x\omega_y - \omega_x s] \quad . \quad . \quad . \quad . \quad . \quad (106)$$

In all three cases above $I_{R_{yy}}$ is the same as I_{R_y} as before

It should be noted that Cases 2 and 3 reflect situations where the polar axis of symmetry for the main body and rotor, respectively, are no longer principal axes. These three cases correspond to cases considered in the next section using numerical integration techniques.

An approximate analytic solution can be developed for Case 1 using pertubation techniques. Eqs. (96) and (98) in the variables ω_y and s correspond to Eqs. (33) and (35) developed in the stability analysis of an undamped symmetrical satellite. The solutions can be represented as before:

$$s = ct + s(0) \quad (107)$$

where $c = L_{R_y} / I_{R_{yy}} [1 - I_{R_{yy}} / B']$

and

$$\omega_y = \omega_y(0) - c_1 t \quad (108)$$

and

$$c_1 = I_{R_{yy}} c/B'$$

After substituting the solutions of Eqs. (107) and (108) into Eqs. (95) and (97) for the case where s(0) = 0, there results:

$$A'\dot{\omega}_x + (P + Qct)\omega_z = \gamma[\dot{\omega}_z + \omega_x(\omega_y(0) - c_1 t)] \quad (109)$$

$$A'\dot{\omega}_z - (P+Qct)\omega_x = \gamma[\dot{\omega}_x - \omega_z(\omega_y(0) - c_1 t)] \quad . \quad . \quad . \quad (110)$$

where P and Q have been previously defined after Eq. (42).

For the case where $\gamma << A'$ and $\gamma << |B'-A'|$ a solution using perturbation techniques may be developed by substituting the zeroth order solutions for ω_x and ω_z, Eqs. (61) and (63), (previously obtained for the homogeneous form of Eqs. (109) and (110) into the right hand side of Eqs. (109) and (110). The zeroth order solutions can be represented by

$$\omega_{x_o} = K_1 \cos(x + K_2) \quad . \quad . \quad . \quad . \quad . \quad . \quad . \quad . \quad . \quad . \quad . \quad . \quad . \quad (111)$$

$$\omega_{z_o} = K_1 \sin(x + K_2) \quad . \quad . \quad . \quad . \quad . \quad . \quad . \quad . \quad . \quad . \quad . \quad . \quad . \quad (112)$$

where $x = x(t) = \left| \frac{Qc}{A'} \right| \frac{(t+a)^2}{2}$

Eq. (109) may be differentiated term by term with respect to time and $\dot{\omega}_z$ appearing on the left side eliminated by using Eq. (110) to yield:

$$A'\ddot{\omega}_x + \left[\frac{P+Qct}{A'}\right]\{\omega_x[P+Qct] + \frac{\gamma}{A'}[\dot{\omega}_{x_o} - \omega_{z_o}(\omega_y(0) - c_1 t)]\}$$

$$+ Qc\omega_z = \gamma\{\ddot{\omega}_{z_o} + [\omega_y(0) - c_1 t]\dot{\omega}_{x_o} - c_1\omega_{x_o}\} \quad . \quad . \quad . \quad . \quad (113)$$

After elimination of ω_z by using Eq. (109) and algebraic simiplification of all terms appearing with the coefficient "γ", noting that:

$$\dot{x} \approx |Qc|(t+a)/A', \quad \dot{\omega}_{x_o} = -\omega_{z_o}\dot{x}, \quad \dot{\omega}_{z_o} = \omega_{x_o}\dot{x}$$

and $a = P/Qc$, there results:

$$\ddot{\omega}_x - \frac{\dot{\omega}_x}{t+a} + \left(\frac{Qc}{A'}\right)^2 (t+a)^2 \omega_x = -\frac{\gamma\omega_{x_o}}{A'}\left[\frac{\omega_y(0) + c_1 a}{t+a}\right] \quad (114)$$

Following the analogous procedure beginning with Eq. (110) and eliminating $\dot{\omega}_x$ and ω_x terms on the left side, a second order differential equation in ω_z may be obtained:

$$\ddot{\omega}_z - \frac{\dot{\omega}_z}{t+a} + \left(\frac{Qc}{A'}\right)^2 (t+a)^2 \omega_z = \frac{\gamma\omega_{z_o}}{A'}\left[\frac{\omega_y(0) + c_1 a}{t+a}\right] \quad (115)$$

Eqs. (114) and (115) are nonhomogeneous differential equations with variable coefficients. It is clear that the solutions to the homogeneous parts of (114) and (115) are the same as developed previously, namely Eqs. (61) and (63). The particular solution can be obtained by using the method of the variation of parameters. It is convenient to write the complementary solutions as

$$\omega_{x_h} = K'_1 \cos x + K'_2 \sin x \quad (116)$$

$$\omega_{z_h} = -K'_2 \cos x + K'_1 \sin x \quad (117)$$

where $K'_1 = K_1 \cos K_2$, $K'_2 = -K_1 \sin K_2$

The particular solution for ω_x is assumed to have the form:

$$\omega_{x_p} = u_1(t)\, K'_1 \cos x + u_2(t)\, K'_2 \sin x \quad \ldots\ldots \quad (118)$$

subject to the constraint that

$$\dot{u}_1\, K'_1 \cos x + \dot{u}_2\, K'_2 \sin x = 0 \quad \ldots\ldots\ldots\ldots \quad (119)$$

After differentiating Eq. (118) term by term with respect to time the two equations may be solved simultaneously for $\dot{u}_1$ and $\dot{u}_2$ with the result:

$$\dot{u}_1 = \frac{K_3 \sin 2x}{4x} + \frac{K_3 K'_2}{2K'_1} \frac{\sin^2 x}{x} \quad \ldots\ldots\ldots \quad (120)$$

$$\dot{u}_2 = -\frac{K_3 K'_1}{2K'_2} \frac{\cos^2 x}{x} - \frac{K_3 \sin 2x}{4x} \quad \ldots\ldots \quad (121)$$

The integration of these equations may be facilitated by noting that,

$$dt = [A'/2|Qc|]^{1/2}\, x^{-1/2}\, dx \quad \ldots\ldots\ldots\ldots\ldots \quad (122)$$

and performing the integration of the right side with respect to x instead of t.

The integration of these functions is accomplished by using relationships in Section 2.632 of Ref. 11 (see Appendix D) which are valid for $x>0$ and $a = P/Qc>0$. These integrals involve products of exponential functions with incomplete

gamma functions. A comprehensive discussion of the incomplete gamma function is given in the text by the Bateman manuscript project[12] where it can be noted that the incomplete gamma function with a complex argument, $\Gamma(b,ix)$, can be related to the Boehmer integrals $C(x,b)$ and $S(x,b)$ according to:

$$\Gamma(b,ix) = e^{i\pi b/2}\,[C(x,b) - iS(x,b)] \quad . \quad . \quad . \quad . \quad . \quad . \quad . \quad . \quad (123)$$

and

$$\Gamma(b,-ix) = e^{-i\pi b/2}[C(x,b) + iS(x,b)] \quad . \quad . \quad . \quad . \quad . \quad . \quad . \quad . \quad (124)$$

where

$$C(x,b) = \int_x^\infty t^{b-1} \cos t \, dt \quad . \quad . \quad . \quad . \quad . \quad . \quad . \quad . \quad . \quad . \quad . \quad . \quad . \quad (125)$$

$$S(x,b) = \int_x^\infty t^{b-1} \sin t \, dt \quad . \quad . \quad . \quad . \quad . \quad . \quad . \quad . \quad . \quad . \quad . \quad . \quad . \quad (126)$$

(for the real part of $b<1$) and the Boehmer integrals may be evaluated by the following series:[12]

$$C(x,b) = \Gamma(b) \cos\left(\frac{b\pi}{2}\right) - \sum_{m=0}^{\infty} \frac{(-1)^m\, x^{2m+b}}{(2m)!\,(2m+b)} \quad . \quad . \quad . \quad . \quad (127)$$

$$S(x,b) = \Gamma(b) \sin\left(\frac{b\pi}{2}\right) - \sum_{m=0}^{\infty} \frac{(-1)^m\, x^{2m+1+b}}{(2m+1)!\,(2m+1+b)} \quad (128)$$

It can be verified that for the integrals appearing in Eqs. (120) and (121), $b = -\frac{1}{2}$ and no imaginary terms will appear in the final answer. After some algebra and simplification, utilizing Ref. 11, Eq. (123) and Eq. (124), it can be shown that:

$$u_1(t) = (K_4/K_1')\{I(1)\cos K_2 + I(2)\sin K_2 - I_3 \sin K_2\} \quad (129)$$

$$u_2(t) = (K_4/K_2')\{I(1)\sin K_2 - I(2)\cos K_2 - I(3)\cos K_2\} \quad (130)$$

where

$$K_4 = K_3K_1\sqrt{A'/2|Qc|}/2;\ K_3 = \gamma[\omega_y(0) + c_1a]/A' \quad (131)$$

$$I(1) = -\frac{1}{\sqrt{2}}\left[S(2x, -\tfrac{1}{2})\Big|_{x_t=0}^{x}\right] \quad (132)$$

$$I(2) = -\frac{1}{\sqrt{2}}\left[C(2x, -\tfrac{1}{2})\Big|_{x_t=0}^{x}\right] \quad (133)$$

$$I(3) = -\frac{1}{4}\,x^{-1/2}\Big|_{x_t=0}^{x} \quad (134)$$

The complete approximate solution for ω_x can then be represented by:

$$\omega_x = K_1\cos(x + K_2) + K_1'\,u_1(t)\cos x + K_2'\,u_2(t)\sin x \quad (135)$$

Following the same procedure as explained above the complete approximate solution for ω_z may be developed as:

$$\omega_z = K_1\sin(x + K_2) - K_2'\,u_3(t)\cos x + K_1'\,u_4(t)\sin x \quad (136)$$

where

$$u_3(t) = -(K_4/K_2')\{-I(1)\sin K_2 + I(2)\cos K_2 - I(3)\cos K_2\} \quad (137)$$

$$u_4(t) = (K_4/K_1')\{I(1) \cos K_2 + I(2) \sin K_2 + I(3) \sin K_2\}$$

The constants K_1 and K_2 can be related to the initial conditions on ω_x, ω_z, $\dot{\omega}_x$, and $\dot{\omega}_z$.

Attempts to obtain complete approximate solutions using perturbation techniques for the equations of Cases 2 and 3 have not been successful. For these cases the form of the "ω_y" equation and/or the torque equations are more complicated than those appearing in Case 1. Approximate solutions for rotor spin rate, s, can be obtained again in terms of the imcomplete gamma functions. When this solution is substituted back into the left side of the ω_x and ω_z equations further integration or differentiation of this complicated form would be implied.

III. NUMERICAL RESULTS

Since the SAS-A dual-spin spacecraft system was used as the basis for the mathematical model in the previous analyses, the following SAS-A spacecraft design parameters were used in the numerical calculations:[13]

Rotor spin rate	s	2000 r.p.m. or 209 rad/sec
Main body spin rate	ω_y	0.5 rad/sec
Satellite mass	M	132.33 kg
Polar moment of inertia of main body	B	28.54 kg-m^2
Transverse moment of inertia of main body	A = C	27.00 kg-m^2
The motor torque[14]	L_{R_y}	0.8 oz-in.

A.1 Calculations of Spin Rate of Rotor During Spin-Up for the Symmetrical Satellite

From Eq. (39),

$$\dot{s} = \frac{L_{R_y}}{I_{R_y}\left(1 - \frac{I_{R_y}}{B'}\right)} = c$$

$$= \frac{8 \times 2.45 \times 9.8066}{16 \times 2.2 \times 11.519\left(1 - \frac{11.55159}{28.55159}\right)}$$

$$= 0.49171863 \text{ rad/sec}^2$$

and the time for spin-up,

$$t = \frac{s - s(0)}{c}$$

$$= \frac{209 - 0}{.49171863} = 425 \text{ sec or } 7.08 \text{ min.}$$

The total time of spin up is 7.08 min. which is compared to an orbital period of approximately 90 minutes.

During spin-up for the symmetrical satellite without damping, Eq. (38) can be used to calculate the change of main body angular velocity about the spin axis,

$$\omega_y - \omega_y(0) = - \frac{I_{R_y}}{B'} [s - s(0)]$$

Substituting the values of I_{R_y}, B', and s we obtain,

$$\omega_y - \omega_y(0) = - \frac{011519}{28.551519} \times 2000$$

$$= 0.8068922 \text{ r.p.m.}$$

In the actual SAS-A Satellite, its spin rate was observed to be 5 r.p.m. immediately after launch. The wheel was then uncaged and accelerated. This resulted in a decrease in satellite spin rate to about 4 r.p.m.[6] This change in observed spin rate during spin-up compares with the 0.8068922 r.p.m. in this calculation.

A.2 Numerical Results for OSO - Spacecraft

In connection with the computer studies discussed later numerical results are calculated using the following OSO spacecraft design parameters:

Rotor spin rate	s	6 r.p.m. or 0.628 rad/sec.
Satellite mass	M	64.25465 lb
The motor torque	L_{Ry}	2 ft - lb.
Polar moment of inertia of main body	B	34 slug - ft^2
Transverse moments of inertia	A	131 slug - ft^2
	C	136 slug - ft^2
Polar moment of inertia of rotor	$I_{R_{yy}}$	378 slug - ft^2

Calculation of Main Body Spin Rate:

If the main body spin rate of OSO is zero after the spin-up, Eq. (38) can be written as:

$$\omega_y(0) = \frac{I_{R_{yy}}}{B'}$$

$$= \frac{378 \times 6 \times 2 \times 3.1416}{412 \times 60} = 0.5761 \text{ rad/sec.}$$

Calculation for Spin Rate of Rotor During Spin-up:

Since the transverse moments of inertia of the OSO spacecraft only differ by 4%, the spin rate equation for the symmetrical satellite

(Eq. 39) can be used for approximating the spin rate of the rotor for this case.

From Eq. (39),

$$\dot{s} = \frac{L_{Ry}}{I_{Ryy}\left(1 - \frac{I_{Ryy}}{B'}\right)} = c$$

$$= \frac{2}{378\left(1 - \frac{378}{412}\right)} = 0.064113 \text{ rad/sec.}^2$$

The time for spin-up,

$$t = \frac{s - s(0)}{c}$$

$$= \frac{0.628}{0.064113} = 9.8 \text{ seconds}$$

B. Results of Numerical Integration

In this section the results of numerical integration of the nonlinear differential equations of motion for the most general case, i.e. the asymmetrical main part and the symmetrical rotor and also the effect of damping are presented. The purposes of the numerical investigation are twofold: first, to verify some of the previous analytic results and, secondly, to compare the motion for different cases considered. The numerical integration was carried out using the IBM 1130 and IBM 360/50 electronic computers. The RKGS and SIMQ subroutines are used to integrate five nonlinear equations, i.e. Eqs. (25), (30)-(32), and (78). It should be noted that Eq. (25) is the more general form of the rotor torque equation. The subroutine RKGS uses the fourth order Runge-Kutta method for the solution of initial value problems. The purpose of the Runge-Kutta method is to obtain an approximate solution of a system of first order differential equations with given initial values. It is a fourth-order integration procedure which is stable and self-starting; that is, only the functional values at a single previous point are required to obtain the functional values ahead. For this reason it is easy to change the step size at any step in the calculations. The entire input of the procedure is: [15](a) lower and upper bound of the integration interval, initial increment of the independent variable, upper bound of the local truncation error; (b) initial values of the dependent variables and weights for the local truncation errors in each

component of the dependent variables; (c) the number of differential equations in the system; (d) as external subroutine subprograms, the computation of the right hand side of the system of differential equations; for the flexibility in output, an output subroutine. The SIMQ subroutine is used to solve the simultaneous system equations, for the accelerations: $\dot{\omega}_x, \dot{\omega}_y, \dot{\omega}_z$, $\ddot{s}$ and $\ddot{\phi}_1$ in terms of the angular velocity and position coordinates. A complete Fortran listing of the computer program is given in Appendix B.

In all numerical results to be presented here, the main body is assumed to spin with an initial component of 0.5 rad/sec. and one of the components of the transverse angular velocity, i.e. $\omega_x(0)$ is chosen initially to be 0.000159 rad/sec. All other initial variables are chosen zero.

In the first case considered, the spin-up for the satellite with symmetrical main part without damping is shown. Fig. 2a shows the linearity of the rotor spin rate with respect to time. It also shows the rotor reaches its nominal spin rate of 209 rad/sec after a time interval of 425 seconds as previously calculated. Fig. 2b illustrates the time history of the transverse components of the main body angular velocity. It is seen that these components have a constant amplitude of 0.000159 rad/sec., the initial value of ω_x. Therefore the first integral expression, Eq. (37) has been verified. It should be noted that the time response of these components is that of a compressed

sine wave with increasing frequency. This is explained from Eqs. (61) and (63), which show that the frequency increases directly with the square of the time. Since the components of the transverse angular velocity never exceed the initial value, from the concept of stability previously explained, no serious stability problem would be encountered here. It should be noted that at the completion of the wheel spin-up manuever, the transverse angular velocity magnitude of 0.000159 rad/sec could be removed by activating the nutation damper as described previously.[3] It can be seen from Fig. 2c that the main body spin rate decreases linearly with respect to time, which verifies Eq. (38).

In the actual orbital configuration of the spacecraft a small asymmetry in the main body exists. Fig. 3 shows the motion of the transverse components of the angular velocity for the case of a small mass asymmetry in the main body without the effect of the damping. The moment of inertia parameters coorespond to SAS-A early design parameters. A small increase in amplitudes of both the transverse components of angular velocity is noted from the figure. No significant nonlinearity of the rotor spin rate nor the main body spin rate is observed from the data obtained by the computer simulation; therefore these graphs are not shown.

The total computer time for running the symmetrical case and for the case of small asymmetry varies from 20 to 25 minutes with the IBM 1130 computer. When large mass asymmetry in the main part was included a significant increase of IBM 1130 computer time was noted

due to the excessive iterations required in the RKGS subroutines to maintain the same accuracy as in the previous two cases. So for better performance the numerical integration for this case was performed using the IBM 360/50 computer instead of the IBM 1130.

Figs. 4 illustrate the effect of large mass asymmetry in the satellite main part without the effect of the damping. From Fig. 4a which shows the time history of the transverse components of the main body angular velocity, during the first 20 seconds, it is seen that one component of the transverse angular velocity has an amplitude almost twice the initial value. Since the stability criteria is based on the boundedness of the transverse components of the angular velocity, a problem of stability could be encountered in this case, especially in the presence of external torques which are continuously acting on the main spacecraft. A significant phase change in the time response of the transverse components of angular velocity when compared to the symmetrical case is also noted for the case of large asymmetry. Along with the phase change a significant increase in the frequency of the transverse components of the main body angular velocity is also noted. For the above two reasons the response is shown only in the intervals from 0 to 20 seconds, and from 400 to 420 seconds (Fig. 4b), compared to the total interval from 0 to 450 seconds for the case of symmetrical satellite. For the rest of the time interval (not shown) the time response does not show any significant change in amplitude variation from that shown.

The effect of the nutation damper for the case of spin-up with a symmetrical main body is shown in Figs. 5. Fig. 5a is the representation of the time history of the transverse components of the main body angular velocity. A small increase in the initial value of the amplitude is noted for both the components. No significant reduction in these initial amplitudes is noted due to the action of the nutation damper. Fig. 5b is the response of the nutation damper during spin-up. The figure shows a bias around the value 0.006 rad. The reason for the bias can be explained by the fact that during the derivation of the equations of motion the lateral center of mass shift due to the damper motion was not included.[16] When one damper is free to move, this shift could be more noticable than when a pair of dampers, diametrically opposed in equilibrium, is used. In the actual SAS-A post-launch performance a small damper bias angle was actually observed.[6,16] One of the causes for this phenomenon was the actual lateral shift in the spacecraft center of mass due to small errors in the final mass balancing prior to launch.[16] It is also seen from Fig. 5b. that the nutation damper reaches a value of 1.0168° at 425 seconds.

Figs. 6 illustrate the damping effect considered for the case of small mass asymmetry in the main body. A small decay in amplitude of one of the transverse angular velocity components (ω_z) is observed from Fig. 6a. If the initial rate of decay were extrapolated linearly the time constant for the decay would have been 31.79 min. (where the

time constant is the time required to reach 1/e of the initial amplitude). When compared with Fig. 5a, a small phase shift is observed. Fig. 6b, which is the damper response for this case, shows a noticable growth of damper angle amplitude during the time of spin-up. It can be concluded that the activation of the nutation damper during spin-up for this case results in an improvement in the system stability.

When the effect of the nutation damper is included for the spacecraft with large asymmetry, it is seen from the Figs. 7a and 7b, that a small average decay of the amplitude of one of the transverse components (ω_x component) of main body angular velocity results. The amplitude of the ω_z component never exceeds the amplitude during the first cycle of ω_z motion. If the initial rate of decay were extrapolated linearly the time constant for the decay would have been 41.06 min. This result could be compared with the time constant of SAS-A during nominal performance, which is 22.3 mins.[17] Comparing the two cases, i.e. cases of large asymmetry with damping and without damping, it is observed from the Figs. 4a and 4b, that the maximum value of ω_z is slightly higher than the value of ω_z in Figs. 7a and 7b. So it can be hypothesized that, for the case of large asymmetry without damping the energy is being transferred into the transverse motion from another mode. It is observed from the Fig. 7c, that the damper reaches a maximum value of 0.713° at 15.6 secs. The results presented in the Figs. 4 and 7 were obtained using the IBM 360

computer, requiring about 130 minutes of running time for each spin-up case.

All the numerical calculations in the above cases are based on the assumption of a constant rotor torque of 0.8 oz-in. Two cases are considered where the torque is assumed to be a linear function of time and reaches a terminal value of twice the average value of the constant torque, (i.e. 1.6 oz-in) during spin-up. Figs. 8 and 9 show the effect of this variable torque law during spin-up. From Fig. 8a, which is the time history of the transverse components of the main body angular velocity for the case of a symmetrical satellite without damping, it could be concluded that the vector sum of the transverse components of the angular velocity maintains the same amplititude throughout the motion as previously shown analytically, i.e. Eq. (87). Fig. 8b shows that the rotor spin rate is a parabolic function of time and reaches the nominal spin rate of 209 rad/sec after a time interval 425 seconds as before. The main body spin rate also exhibits a parabolic variation as seen from the Fig. 8c. Under the consideration of the variable torque law applied for the case of a symmetrical satellite including the effect of the damping, a small decay in amplitude of one of the transverse components (ω_x) of angular velocity is noted from Fig. 9a. The time constant for the decay is calculated to be 27.82 minutes. In addition a phase shift is noted when compared with Fig. 8a. In the case represented by Figs. 9b and 9c a small departure from the parabolic variation shown in Figs. 8b and 8c is noted from

consideration of the printout. Because of the small magnitudes of this departure, differences between Figs. 8b and 9b and also between Figs. 8c and 9c are not apparent within the plotting accuracy. For this case, the nutation damper reaches a maximum value of 1.356° at 425 secs., which is slightly higher than the maximum angle attained by the nutation damper for the case of the symmetrical satellite with damping under the influence of a constant motor torque (Fig. 5b).

B.1. Numerical Integration Results with SAS-A Spacecraft and Principal Axes Misalignment

In all numerical results presented above, the effect of the misalignment of the principal axes from the geometrical axes of symmetry is neglected. A few cases are considered here including the above mentioned effects. All the numerical integration of these cases were performed using the IBM 360/50 electronic computer.

In all of the numerical results to be presented for the SAS-A Satellite with principal axes misalignment the main body is assumed to spin with an initial component of 0.5 rad/sec., and results are obtained varying one of the components of transverse angular velocity i.e. $\omega_x(0)$; also all other initial variables are chosen zero as before. All the moments of inertia (including the cross-products) parameters are based on the Small Astronomy Satellite (SAS-A) orbital configuration. [13]

In the first case considered, $\omega_x(0)$ is chosen 0.000159 rad/sec. Fig. 10a, shows the time history of the transverse components of the main body angular velocity. It is seen from the figure that during the first 100 seconds the amplitude of both the transverse components of main body angular velocity increases to approximately 7 times the initial value. After the first cycle of motion, both the components of transverse angular velocity show a decay in their amplitude. Since the stability criteria is based on the boundedness of the transverse components of angular velocity, a problem of stability could be encountered here, especially in the presence of external torques which are initially and continuously acting on the main spacecraft. From Fig. 10b and 10c which show the time response of the main body and rotor spin rate, respectively, it is seen that no significant nonlinearity of both of these motions is observed within the plotting accuracy.

The effect of the nutation damper for the case of Fig. 10 is shown in Fig. 11. From Fig. 11a, it is observed that during the first cycle of the motion, the amplitudes of both transverse components of main body angular velocity increase much greater than the initial value. After the first cycle of motion of the transverse components, significant reduction in these amplitudes is observed due to the action of the nutation damper. The time constants for the decay are 1.45 and 5.407 minutes for ω_x and ω_z respectively. A small phase change in the time response of the transverse components of angular velocity when compared to the undamped

case is also noted. Fig. 11b is the response of the nutation damper during spin-up. The figure shows a bias around the value 0.02 rad. which is greater than the bias observed when the effect of the inertia cross products are neglected (Fig. 5b). It is also seen that the nutation damper reaches a maximum value of 3.391° at 426 seconds.

Figs. 12 illustrate the motion of the satellite with the initial transverse component increased by a factor of ten. Other input conditions are kept as before. From this figure a small percentage increase in the amplitudes of both the transverse components of angular velocity is noted. After the first cycle of motion a decay in amplitude of both the components is also observed, but the rate of decay is less than that for the case of Fig. 10a. The effect of damping in this case is illustrated in Figs. 13. An increase in amplitude of both the transverse components of main body angular velocity is observed from Fig. 13a similar to that shown in Fig. 12. A decay in amplitude of both the components of the transverse angular velocity vector is noted with a projected time constant of 12.27 and 50.97 minutes for ω_x and ω_y respectively. A phase shift in the time response of the transverse components of angular velocity when compared to the undamped case (Fig. 12) is also observed. It is seen from Fig. 13b that the nutation damper shows a steady growth in amplitude after a few initial cycles of motion and reaches a maximum value of 6.87° at 425 seconds which is about twice the value obtained compared to the case where $\omega_x(0)$ is

chosen to be 1/10 the value for this case.

The initial value of one of the transverse components of main body angular velocity (ω_x) was once again increased, to 100 times the value in Fig. 10a and numerical integration of the equations of motion was again performed. From the time responses (Fig. 14) no significant increase in amplitude nor of the decay in amplitude in either of the transverse components is observed. It is seen from all the time response curves of the transverse components of main body angular velocity, that the frequency of the motion increases as $\omega_x(0)$ increases.

When the effect of the nutation damper is considered in this case, a small decay in amplitude of one of the components of the transverse angular velocity (ω_x) vector is noted from Fig. 15a with a projected time constant of 48 minutes. From Fig. 15b, it is noted that the maximum angular displacement of the nutation damper is 41° which is a physical impossibility since in reality the damper would hit the mechanical stops at $\pm$ 20° amplitude. As expected, the larger value of initial transverse velocity (i.e. system nutation angle) results in a higher amplitude nutation damper motion. Because of the larger amplitude damper motion, the damper bias angle previously referred to is not apparent from the scale used in Fig. 15b.

The average IBM 360/50 running time for the cases shown in Figs. 10-15 was about 15 minutes.

B.2. Numerical Results Using OSO Spacecraft Parameters

All the numerical calculations in the above cases are based on

SAS-A design parameters. The OSO series of dual-spin spacecraft is of current interest to many investigators. The numerical integration of the general equations of motion is carried out with the OSO spacecraft design parameters using theIBM 360/50 electronic computer.

In all numerical results to be presented here for the OSO spacecraft, the main body is assumed to spin with an initial component of 0.5761 rad/sec as calculated previously, and results are obtained varying one of the components of the transverse angular velocity, i.e. $\omega_x(0)$. All other initial variables are chosen zero.

In the first case considered, $\omega_x(0)$ is chosen 0.003170 rad/sec, which corresponds to an initial system nutation angle (the angle between the total angular momentum vector and the nominal spin axis) of 0.1 degree. From the time response curve (Fig. 16a) of the transverse components of main body angular velocity, it is noted that both the transverse components complete about one-half cycle of their motion during the total time of spin-up. A small increase in amplitude of both the components during the first cycle of the motion is also observed. Fig. 16b illustrates the motion of the main body spin rate. It is seen from the figure that the main body is essentially de-spun inertially after the total time of spin-up of 9.8 seconds. It is observed from Fig. 16c that the rotor reaches its nominal spin rate of 0.628 rad/sec after a time interval of 9.8 seconds in an essentially linear manner.

Fig. 17 illustrates the effect of a greater initial nutation angle. In this case the value of $\omega_x(0)$ is increased to 0.03172 rad/sec which corresponds to a nutation angle of 1°. It is observed that Fig. 17 is identically in phase with Fig. 16a except for the scale factor on the ordinate.

When the initial system nutation angle is further increased by a factor of ten (Fig. 18), the phasing of the response of ω_x and ω_z is still identical to that shown in Figs. 16a and 17. The frequency response of the OSO main body components appears to be less sensitive to changes in initial nutation angle than that for the SAS-A system, perhaps because for the OSO system the majority of the momentum as well as inertia contribution is associated with the rotor.

In the previous OSO cases considered (Figs. 16-18) the geometrical axes of the main part and rotor were assumed to be the principal axes. The effect of the misalignment of the principal axes of both the rotor and the main part from the geometrical axes of symmetry is illustrated in Fig. 19. In this case an initial nutation angle is chosen to be the same as in the case of Fig. 17. No significant change in any of the motion is observed as compared to Fig. 17.

Some results are now obtained with an increased initial value of main body spin rate and no misalignment of principal axes. In all cases mentioned below the main body is assumed to spin with an initial component of 6.98543 rad/sec and results are obtained varying one of the components of the transverse angular velocity, i.e. $\omega_x(0)$.

All other initial conditions are chosen zero as before.

In the first case considered, $\omega_x(0)$ is chosen 0.03172 rad/sec., which corresponds to an initial system nutation angle of 0.21°. From Fig. 20a a small increase in amplitude of one of the transverse components of angular velocity (ω_z) is noted. After the first cycle of the motion, a decay in amplitude of ω_z is also observed from the figure. The rotor spin rate curve (Fig. 20c) shows that the rotor reaches its nominal spin rate of 0.628 rad/sec after time interval of 9.8 seconds as previously calculated. No severe nonlinearity of main body spin nor of the rotor spin rate is observed from Figs. 20b and 20c. The above mentioned results could be compared qualitatively with the cases in Fig. 3, where initial amplification is observed for both the transverse components of main body angular velocity.

Fig. 21 illustrates the effect of a greater initial nutation angle. In this case the value of $\omega_x(0)$ is increased by a factor of ten. From Fig. 21 a small decay in amplitude of one of the components (ω_z) is observed after the initial amplification of both the components. It is also observed that the rate of decay is less than for the case in Fig. 20a. Figs. 21 and 20a are identically in-phase except for the scale factor in the ordinate.

The nonlinearity of the main body spin rate and the rotor relative spin rate (Figs. 22b and 22c) is observed when the initial amplitude of ω_x is again increased by a factor of ten. This

nonlinearity (present to some extent in all OSO cases but observable here due to the large initial nutation angle) is attributed to the fact that for the OSO spacecraft the rotor polar (principal) axis is no longer an axis of rotor symmetry. No significant decay in amplitude is observed from the time response curve of the transverse components of main body angular velocity (Fig. 22a), though it differs in phase and amplitude with Figs. 20 and 21.

The effect of the misalignment of the principal axes of the main body as well as the rotor from the geometrical axes of symmetry is illustrated in Fig. 23. The initial nutation angle is the same as in Fig. 20, i.e. 0.21 degree. The amplitude of both the transverse components of main body angular velocity has increased by a factor of almost 2. After the initial amplification a significant decay in the amplitudes of both the transverse components is also noted. The linearity of the main body and rotor spin rate responses (figures not shown) is not significantly affected by the inclusion of inertia cross products terms in the general equations of motion. It appears that the nonlinearity in ω_y and s responses is more sensitive to change in the initial nutation angle than to the presence of small cross products of inertia terms.

B.3 Comparison between the Numerical Integration and Approximate Solution for the Special Case Considered

In this section a comparison is made between the results of the numerical integration and the approximate solution for the case which is dynamically similar to that of a spacecraft having no misalignment in its principal axes, but a small difference between each of its moments of inertia about the two transverse principal axes (Eqs. 95-98). To compare the approximate solutions (Eqs. 135 and 136) with the exact solutions (numerical integration), the numerical evaluation of the approximate solution was carried out using the IBM 360/50 electronic computer. The numerical evaluation of the approximate solution for the SAS-A spacecraft during spin-up was performed for a total time interval of 450 seconds with a time step of one second. Two cases are considered here varying the only inertia cross product considered i.e. I_{xz}.

In the first case considered the value of I_{xz} is chosen 0.1048 kg-m^2. Fig. 24 illustrates the comparison between the approximate solution and the exact solution for this case. The solid line, which is the result of the numerical integration shows a small initial amplification in amplitude of one of the transverse components (ω_x) of main body angular velocity. No initial amplification can be observed from the results of the approximate solution (shown by dotted lines), but a small change in phase compared to the results

of the numerical integration is observed from Fig. 24.

The effect of the increased value of I_{xz} (0.5) is illustrated in Fig. 25. The results of the numerical integration show a significant initial amplification of both the transverse components of main body angular velocity. No decay in amplitude of any of the velocity components is observed within the specified time interval. In this case the phase difference between the results of the approximate solution and the results of the numerical integration is more noticable as compared to the case considered in Fig. 24. A small increase in initial amplification of both the velocity components is also observed from the computer print-out of the approximate solution which is not noticable within the plotting accuracy. It could be concluded at this point that the larger is the difference between the moments of inertia about the two transverse principal axes, the greater is the change in phase between the approximate and the exact solutions. Of course the approximate pertubation solution can no longer be expected to provide reasonable convergence when $\mathcal{O}|I_{xz}| \approx \mathcal{O}|B'-A'|$.

The case considered in Fig. 24 could be compared with the case in Fig. 10a, where an initial amplification in amplitude of a factor of seven is observed for both the transverse components. By observing the cases considered in Figs. 24 and 25, it could be concluded that when the nominal spin axis (polar axis) is no longer a principal axis ($I_{xy} \neq 0$, $I_{yz} \neq 0$) the large amount of initial amplification of the

transverse components of main body angular velocity is the result. The amplification is more sensitive to a small misalignment between the principal axis of spin and the nominal spin (geometrical -yy) axis, than to small differences between the two transverse moments of inertia. The amplification can further be explained as, when the nominal spin axis is no longer the principal axis, the motor torque has a component perpendicular to the nominal spin vector. This perpendicular component could cause an excitation in the motion about the transverse axis due to the altering nature of the torque component, depending on the relative phasing.

The total time of execution of the approximate solution for both the cases is less than the running time of the numerical integration. For example, the total time of execution of the approximate solution for the cases when $I_{xz} = 0.1048$ and $I_{xz} = 0.5$ are 12.33 and 20.19 minutes respectively compared to 32.83 and 26.31 minutes respectively for the numerical integration. By performing the ratio test of the series (Eqs. 127 and 128) associated with the approximate solution, for the numerical case considered, it is observed that a minimum of 16 terms is required for the series to converge. By evaluating the approximate solution considering the number of terms in the series to be 16,20, and 27 respectively, no changes within five decimal places are observed from the computer print-out. It is interesting to mention further that, the computer is unable to evaluate the factorial in the denominator of the series when the number of terms in the series exceeds 27,

because of its sensitivity towards generating a large real constant (maximum magnitude ~ 10^{75}). Stirling's approximation is the best recommended method for evaluating a large factorial, and could be used in cases where series convergence is improved by increasing the number of terms.

IV. CONCLUSIONS

As a result of the present analysis and numerical results the following conclusions can be made:

(1) For the case of a symmetrical satellite with no damping, the magnitude of the vector sum of the transverse angular velocity components remains constant during wheel spin-up under the influence of a constant motor torque.

(2) With a small mass asymmetry in the main body, and without damping, behavior is similar to the symmetrical case, but a small increase in amplitude of one of the transverse components of angular velocity is noted in addition to a phase change.

(3) For the case of large asymmetry in the main body, one component of the transverse angular velocity has an amplitude approximately twice that of the initial value. Stability problems could result for this case in the presence of all the external torques which are continuously acting on the main spacecraft.

(4) The effect of the nutation damper during spin-up is significant only for the case of an asymmetry in the main spacecraft, where a small decay in the amplitude of the transverse angular velocity vector is noted. There appears to be little advantage (or disadvantage) in activating the nutation damper for the case of no asymmetry.

(5) For the case where motor torque is proportional to time and the spacecraft is symmetrical, the activation of the nutation damper during spin-up results in a small decay in the amplitude of the transverse angular velocity vector.

(6) When the effect of the misalignment of the main spacecraft principal axis from the geometrical (polar) axis of symmetry is considered, a problem of stability could arise due to the large initial amplification the system nutation angle.

(7) For the case of a dual-spin spacecraft with a large asymmetrical rotor, a nonlinearity of the main body and rotor spin time responses can result, depending on the initial nutation angle. This could cause an error in reaching the nominal terminal conditions.

REFERENCES

(1) Haseltine, W. R., "Nutation Damping Rates for a Spinning Satellite", Aerospace Engineering, Vol. 21, No. 3, March 1962, pp. 10-17.

(2) Likins, Peter W., "Attitute Stability Criteria for Dual-Spin Spacecraft", Journal of Spacecraft and Rockets, Vol. 4, No. 12, December 1967, pp. 1638-1643.

(3) Bainum, P.M., Fuechsel, P.G., and Mackison, D.L., "Motion and Stability of a Dual-Spin Satellite with Nutation Damping", Journal of Spacecraft and Rockets, Vol. 7, No. 6, June 1970, pp. 690-696.

(4) Proceedings of the Symposium on Attitude Stabilization and Control of Dual-Spin Spacecraft, 1-2 August 1967, Aerospace Corporation Report No. TR-0158, (3-307-01)-16, November 1967.

(5) Mingori, D.L., "Effects of Energy Dissipation on the Attitude Stability of Dual-Spin Satellites", AIAA Journal, Vol. 7, No. 1, January 1969, pp. 20-27.

(6) Fischell, Robert E., and Kershner, Richard B., "Attitude Control System for a Small Astronomy Satellite", 4th IFAC Symposium on Automatic Control in Space, Dubrovnik, Yugoslavia, Sept., 1971.

(7) Tossman, B.E., "Variable Parameter Nutation Damper for SAS-A", AIAA Guidance, Control, and Flight Mechanics Conference, Santa Barbara, California, August 1970, AIAA Paper No. 70-972.

(8) Whittaker, E.T., A Treatise on the Analytical Dynamics of Particles and Rigid Bodies, 4th ed., Cambridge University Press, Cambridge, England, pp. 41-44.

(9) Goldstein, H., Classical Mechanics, Addison-Wesley Publishing Company, Inc., Reading, Mass., pp. 21-22.

(10) Wylie, C.R., Jr., Advanced Engineering Mathematics, 2nd ed., McGraw-Hill Book Company, Inc., New York, N.Y., 1960, p. 407.

(11) Gradshteyn, I.S. and Ryzhik, I.M., Tables of Integrals, Series, and Products, 4th ed., (Translated from the Russian by Scripta Technica, Inc.), Academic Press, New York and London, 1965, p. 183.

(12) Bateman Manuscript Project, Higher Transcendental Functions, Vol. II, McGraw-Hill Book Company, Inc., 1953, pp. 133-151.

(13) Fuechsel, P.G., Bainum, P.M., and Grunberger, P.J., "The Attitude Motion of a Nutationally Damped Dual-Spin Spacecraft in the Presence of Near-Earth Environment", AIAA 9th Aerospace Sciences Meeting, New York, N.Y., January 25-27, 1971, AIAA Paper No. 71-90; also Journal of Spacecraft and Rockets, Vol. 8, No. 9, September 1971, pp. 913-914 (Synoptic).

(14) Fountain, Glen H., and Philips, B.M., "SAS-A Momentum Wheel," the Johns Hopkins University, Applied Physics Laboratory, Report No. APL/JHU CP 012, February 1972.

(15) IBM 1130 Scientific Subroutine Package Programmer's Manual, IBM Technical Publications Department, White Plains, N.Y., pp. 92-94.

(16) Tossman, B.E., "SAS-A Nutation Damper-Flight Observed Bias Angle," The Johns Hopkins University, Applied Physics Laboratory Memo S2P-2-410, January 20, 1971.

(17) Bainum, P.M., Fuechsel, P.G., and Fedor, J.V., "Stability of a Dual-Spin Spacecraft with Energy Dissipation in a Flexible Momentum Wheel," AAS/AIAA Astrodynamics Specialists Conference 1971, Ft. Lauderdale, Fla. August 17-19, 1971, Paper No. AAS 71-347; accepted for publication Journal of Spacecraft and Rockets, 1972.

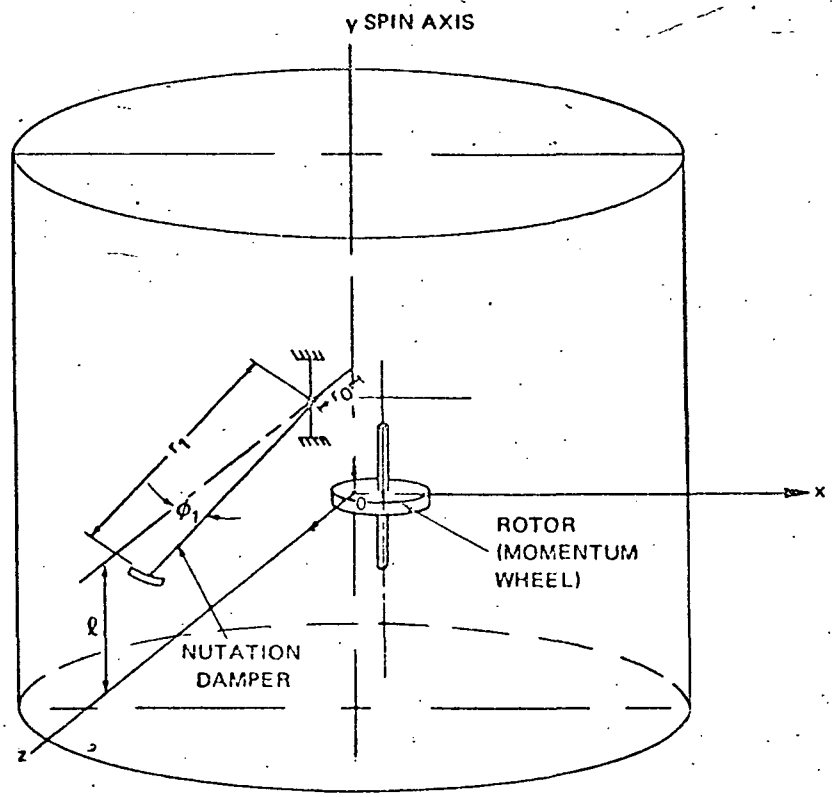

Figure 1a. Elements of SAS-A Attitude Control System

(rotor displaced from spin axis)

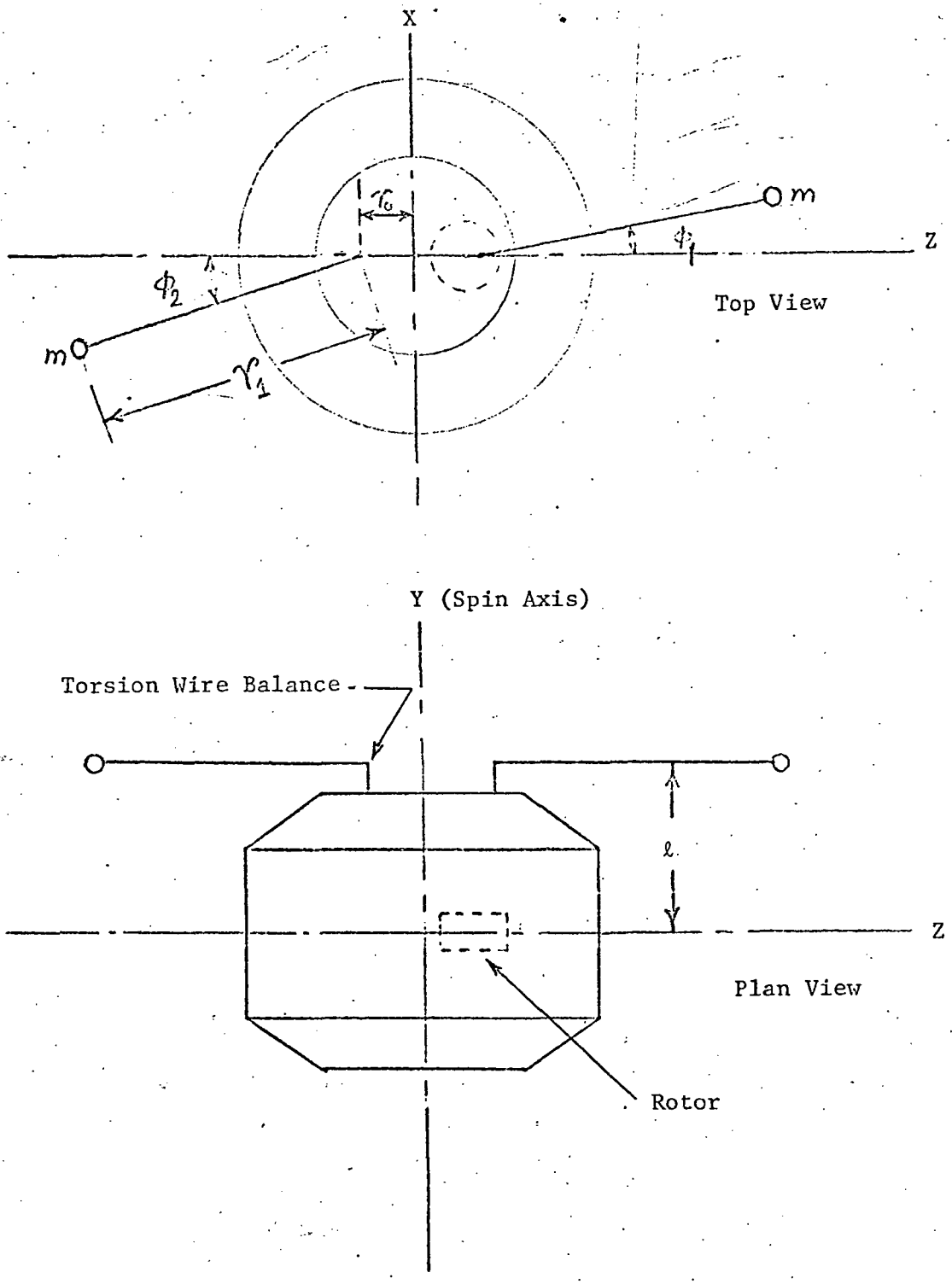

Figure 1b. Schematic of Satellite, Rotor and Damper

Figure 2a. Rotor Spin Rate During Spin-Up
Symmetrical Satellite and No Damping,
$A = C = 27.00$ kg-m^2; $B = 28.54$ kg-m^2

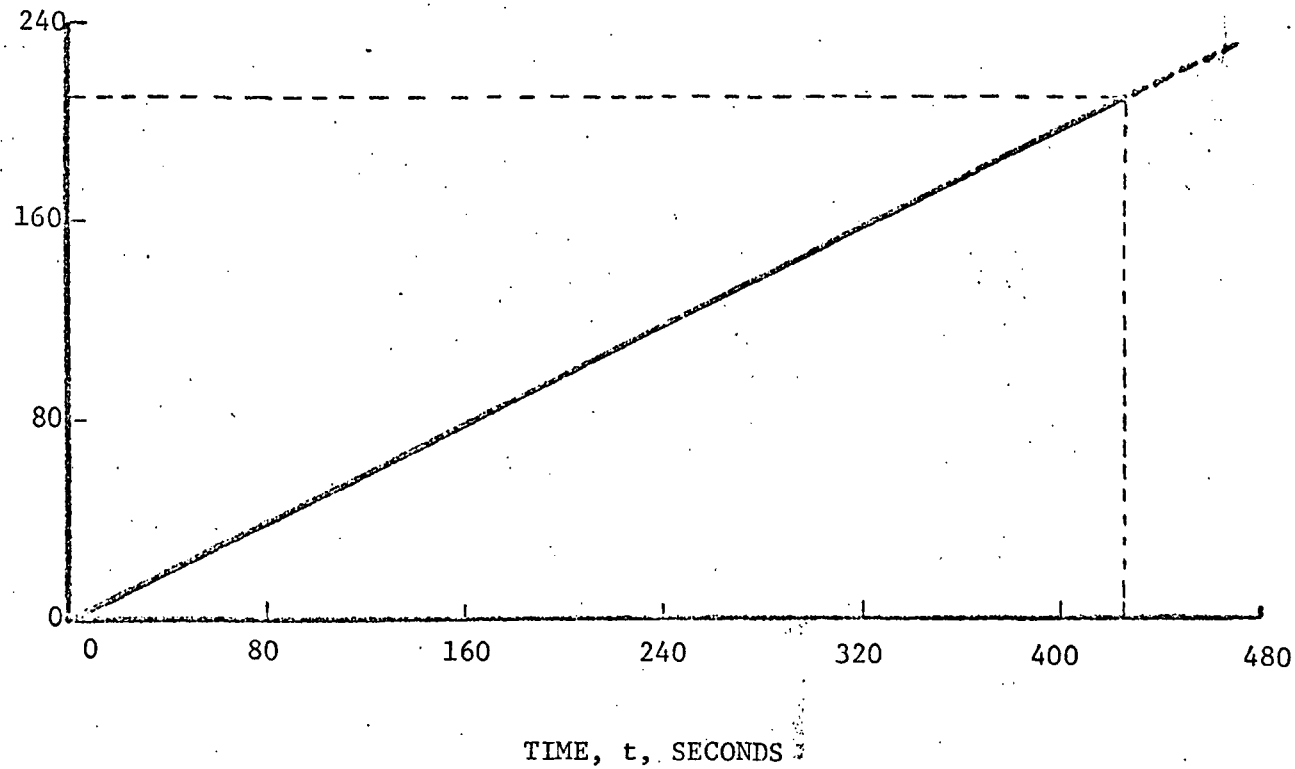

Figure 2b. Time History of the Transverse Components of Main Body Angular Velocity
Symmetrical Satellite and No Damping
$A = C = 27.00$ kg-m^2
$B = 28.54$ kg-m^2

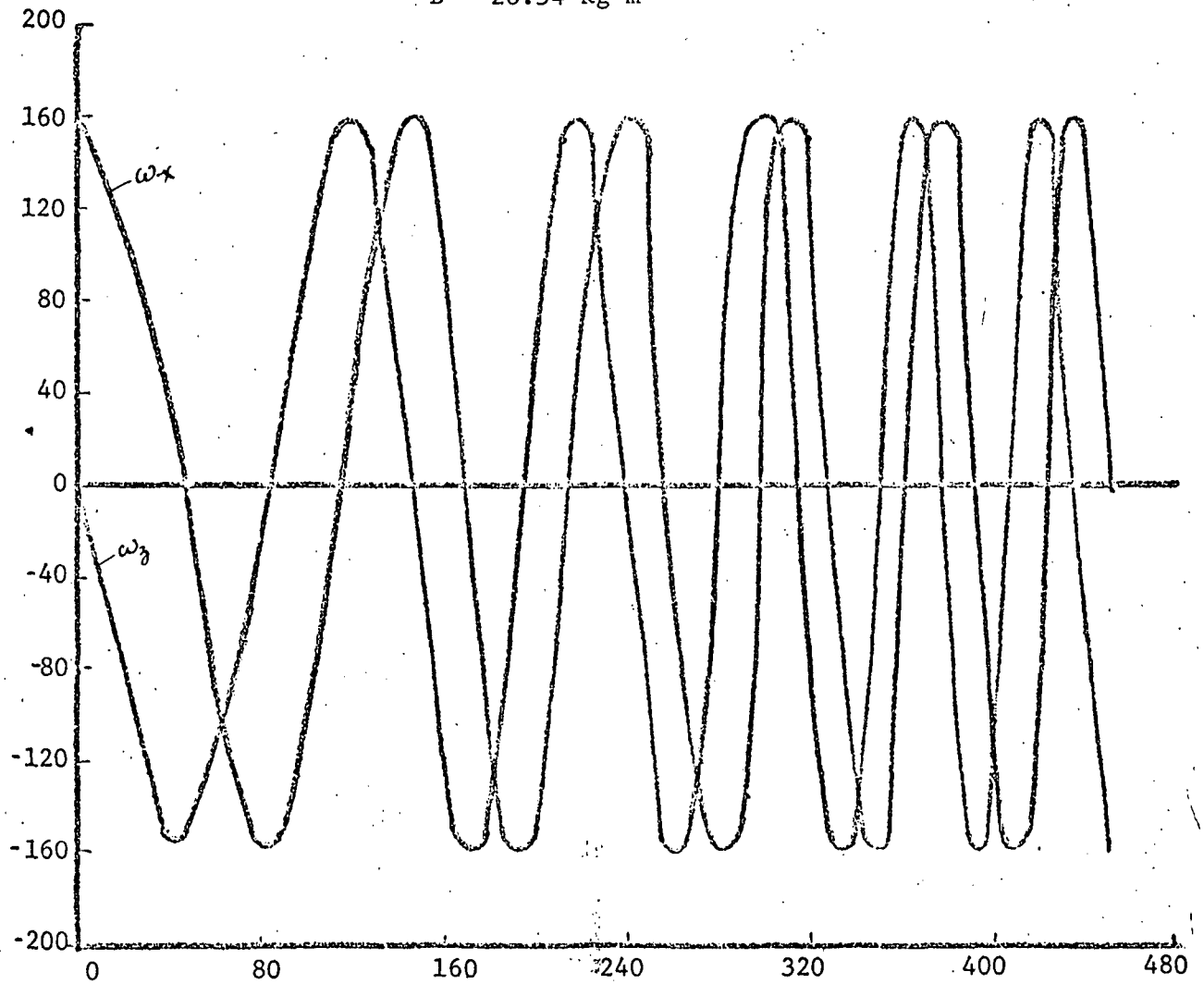

Figure 2c. Main Body Spin Rate During Spin-Up

Symmetrical Satellite and No Damping.
$A = C = 27.00$ kg-m^2
$B = 28.54$ kg-m^2

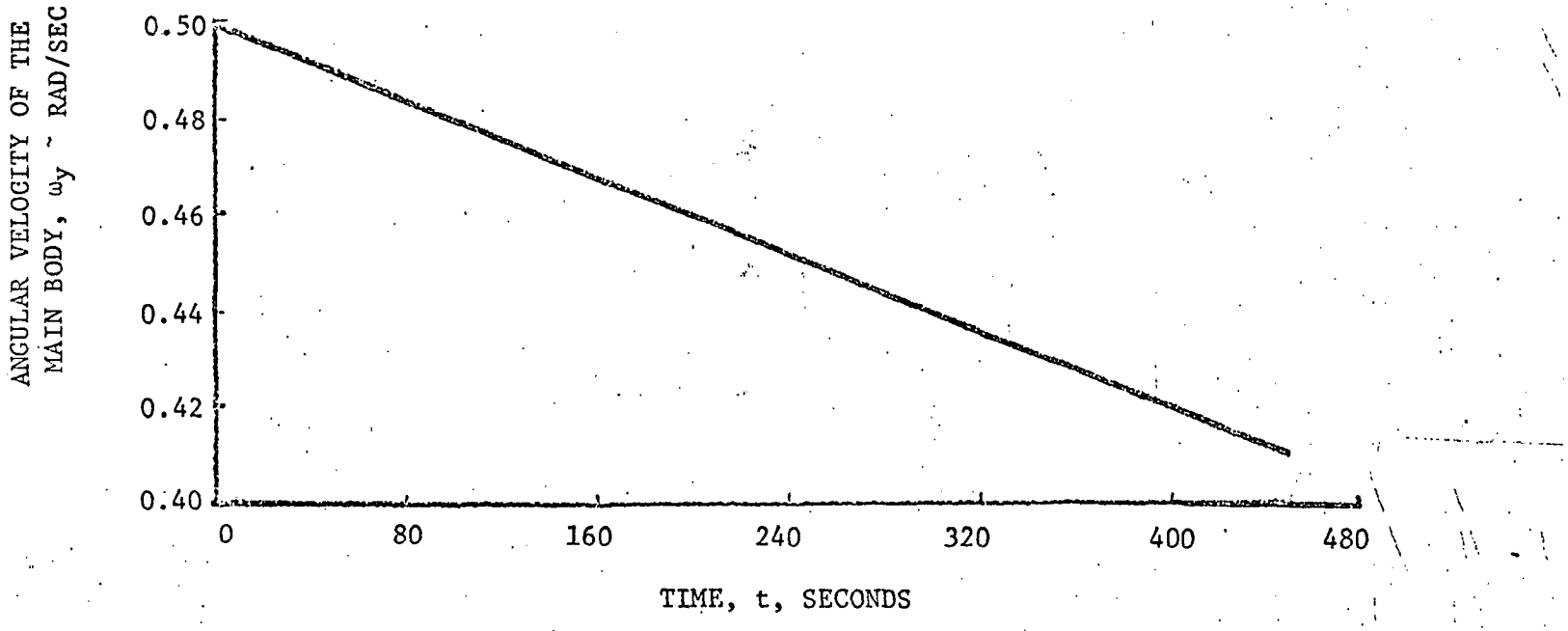

Figure 3. Time History of the Transverse Components of Main Body Angular Velocity Satellite with Small Asymmetry in the Main Body and No Damping

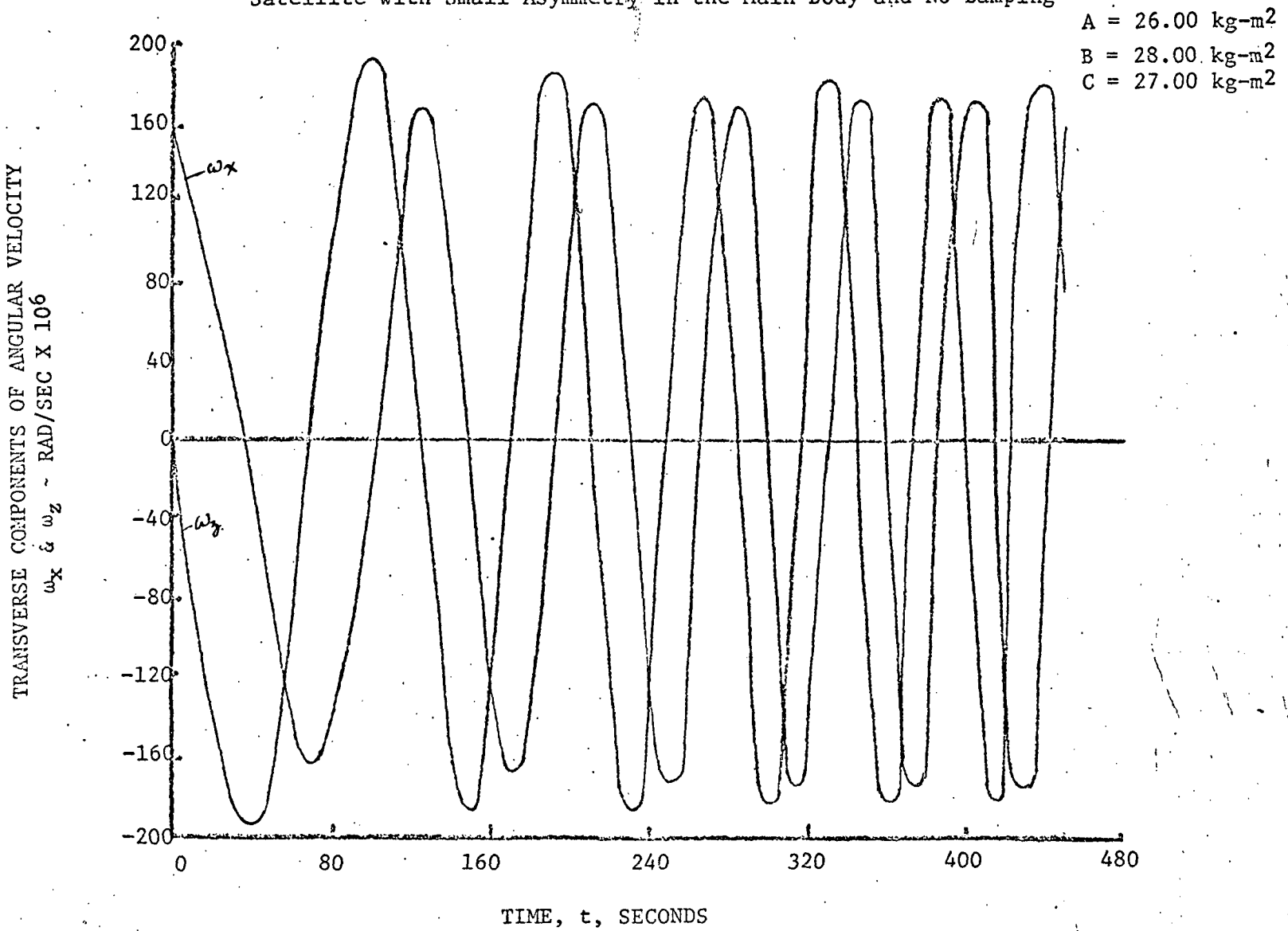

Figure 4a. Time History of the Transverse Components of Main Body Angular Velocity
Satellite with Large Asymmetry in the Main Body and No Damping

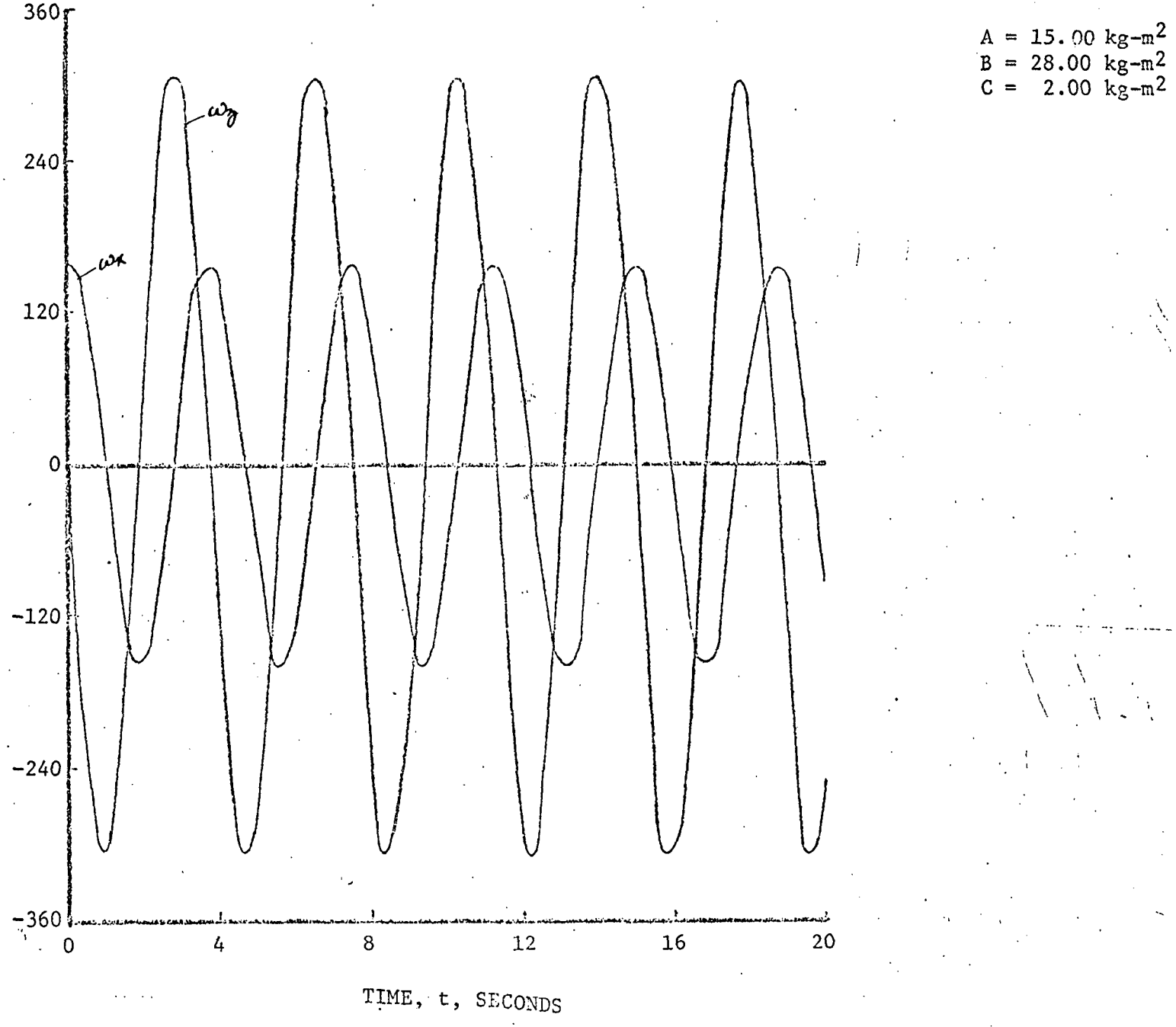

Figure 4b. Time History of the Transverse Components of Main Body Angular Velocity
Satellite with Large Asymmetry in the Main Body and No Damping

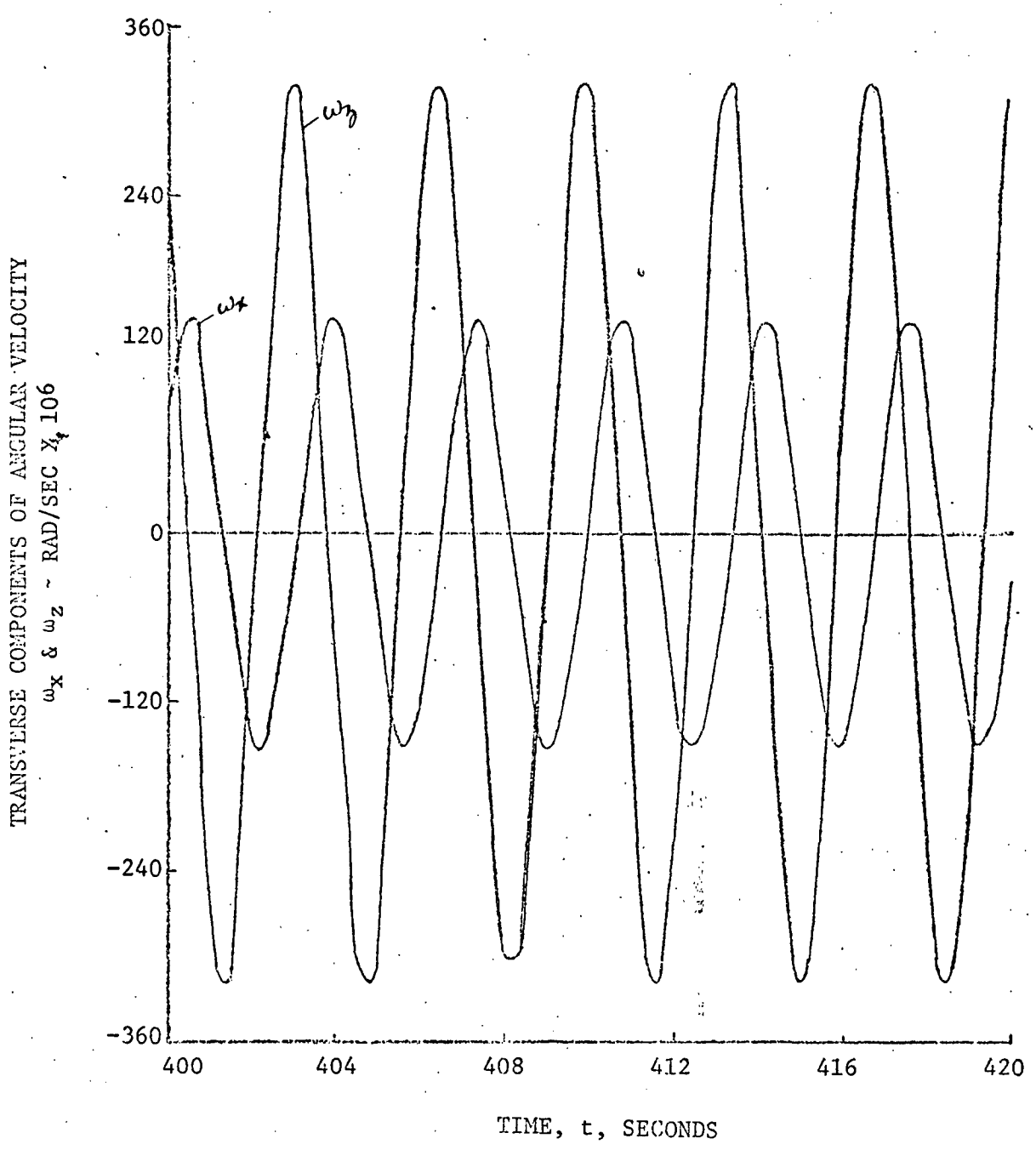

Figure 5a. Time History of the Transverse Components of Main Body Angular Velocity
Symmetrical Satellite with Damping

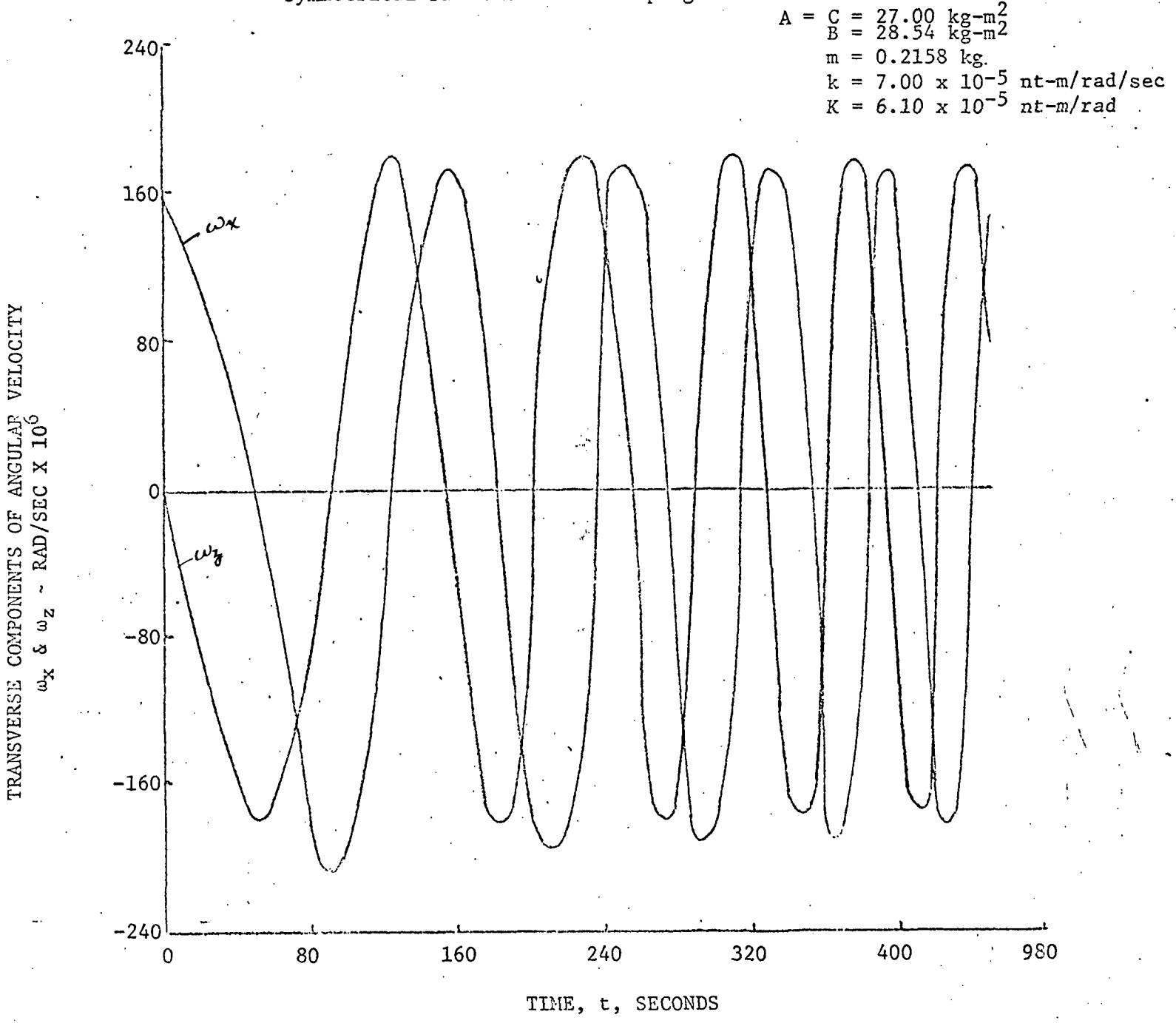

Figure 5b. Nutation Damper Response During Spin-Up
Symmetrical Satellite with Damping

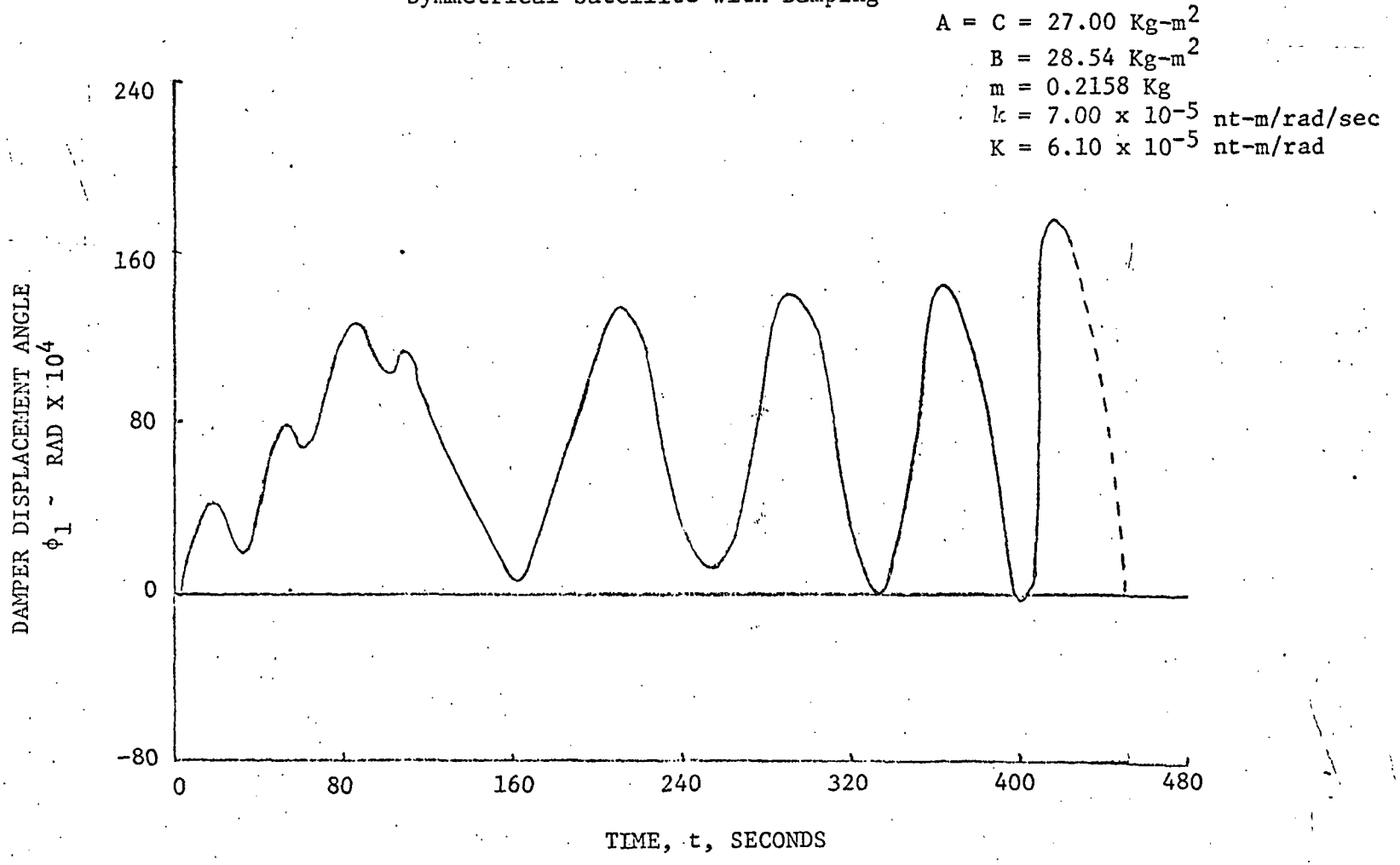

Figure 6a. Time History of the Transverse Components of Main Body Angular Velocity
Satellite with Small Asymmetry in the Main Body and Damping

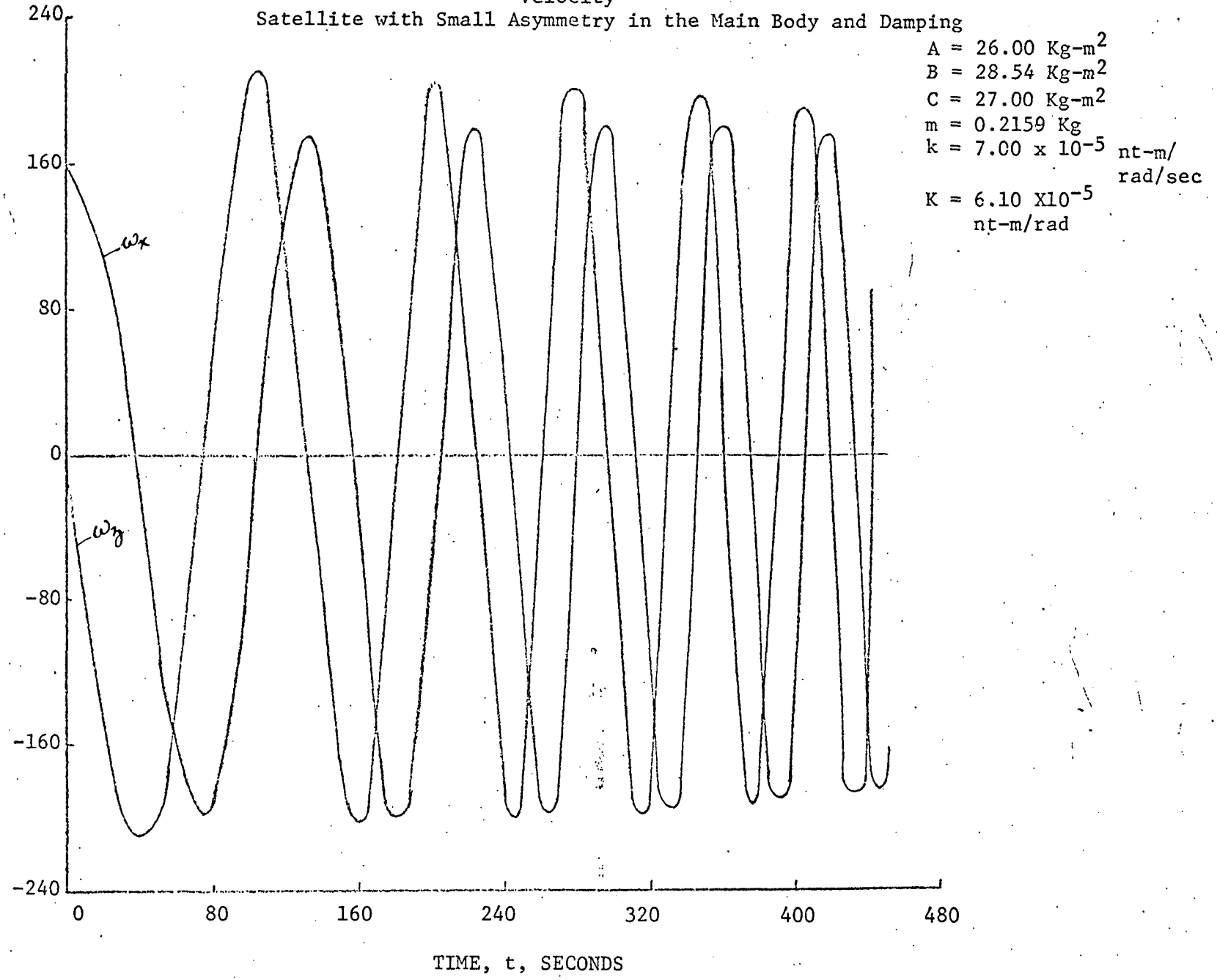

Figure 6b. Nutation Damper Response During Spin-Up
Satellite with Small Asymmetry in the Main Body and Damping

$A = 26.00$ Kg-m^2; $B = 28.54$ Kg-m^2
$C = 27.00$ Kg-m^2; $m = 0.2158$ Kg
$k = 7.00 \times 10^{-5}$; $K = 6.10 \times 10^{-5}$
nt-m/rad/sec nt-m/rad

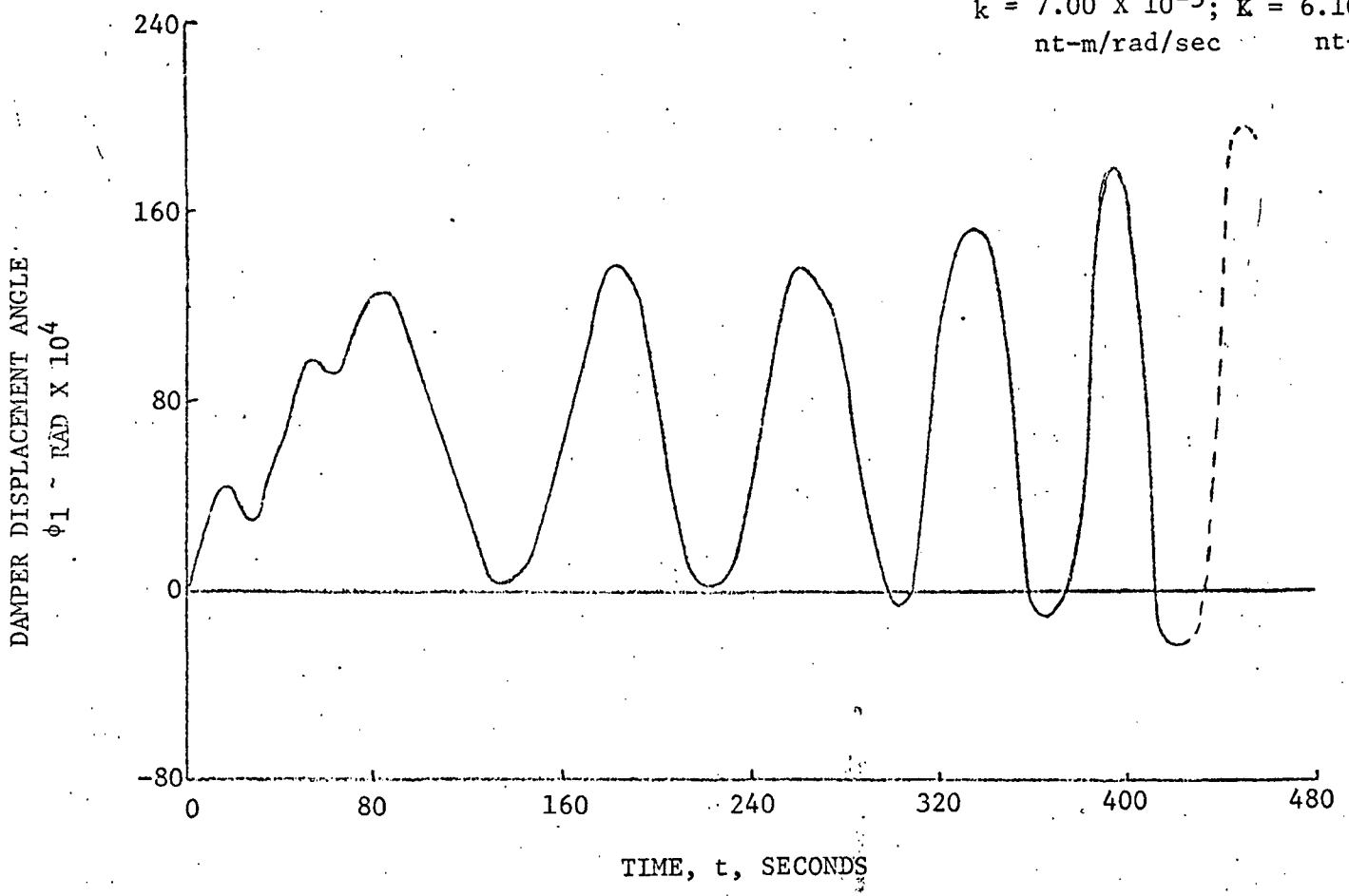

Figure 7a. Time History of the Transverse Components of Main Body Angular Velocity
Satellite with Large Asymmetry in the Main Body and Damping

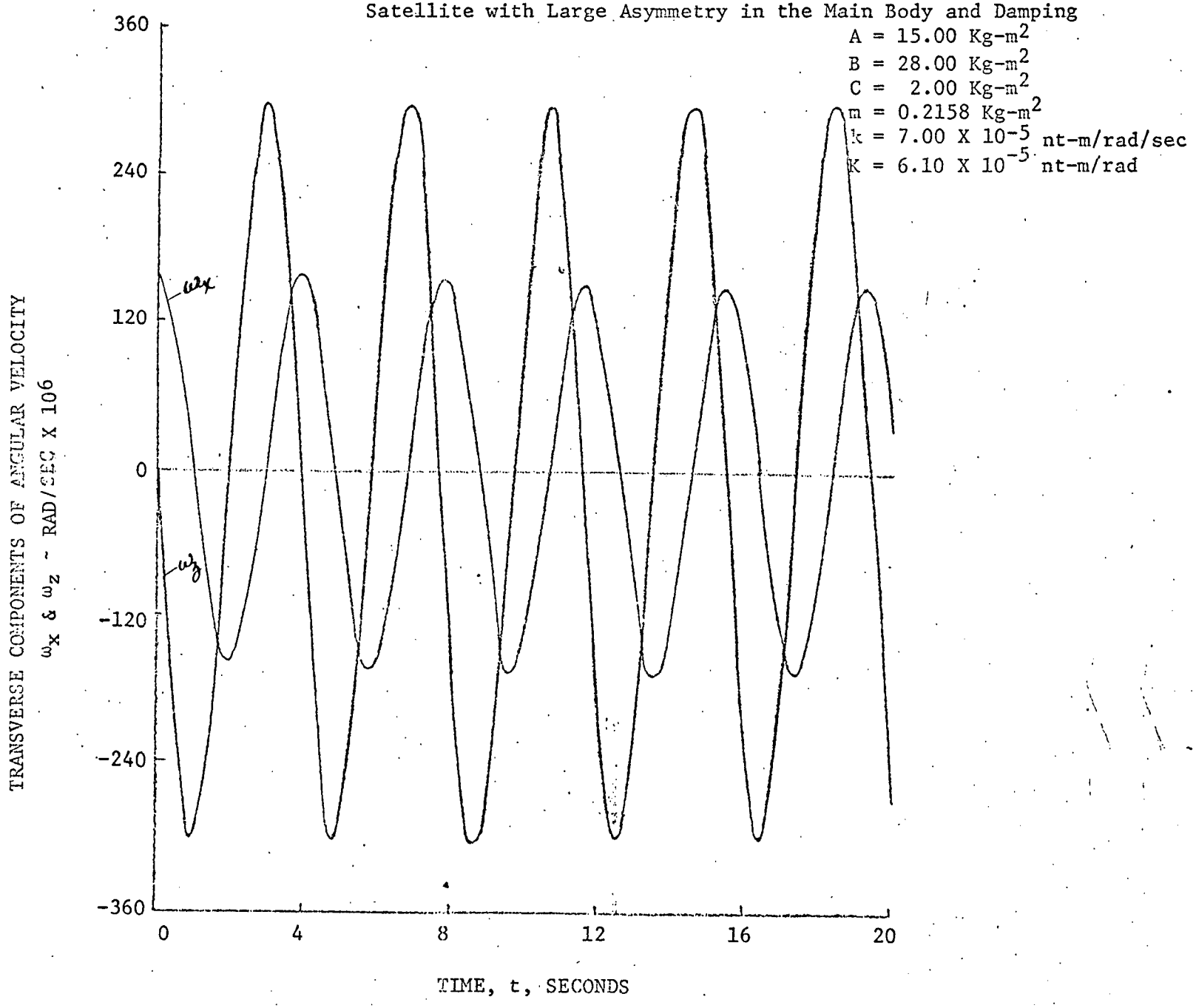

Figure 7b. Time History of the Transverse Components of Main Body Angular Velocity Satellite with Large Asymmetry in the Main Body and Damping

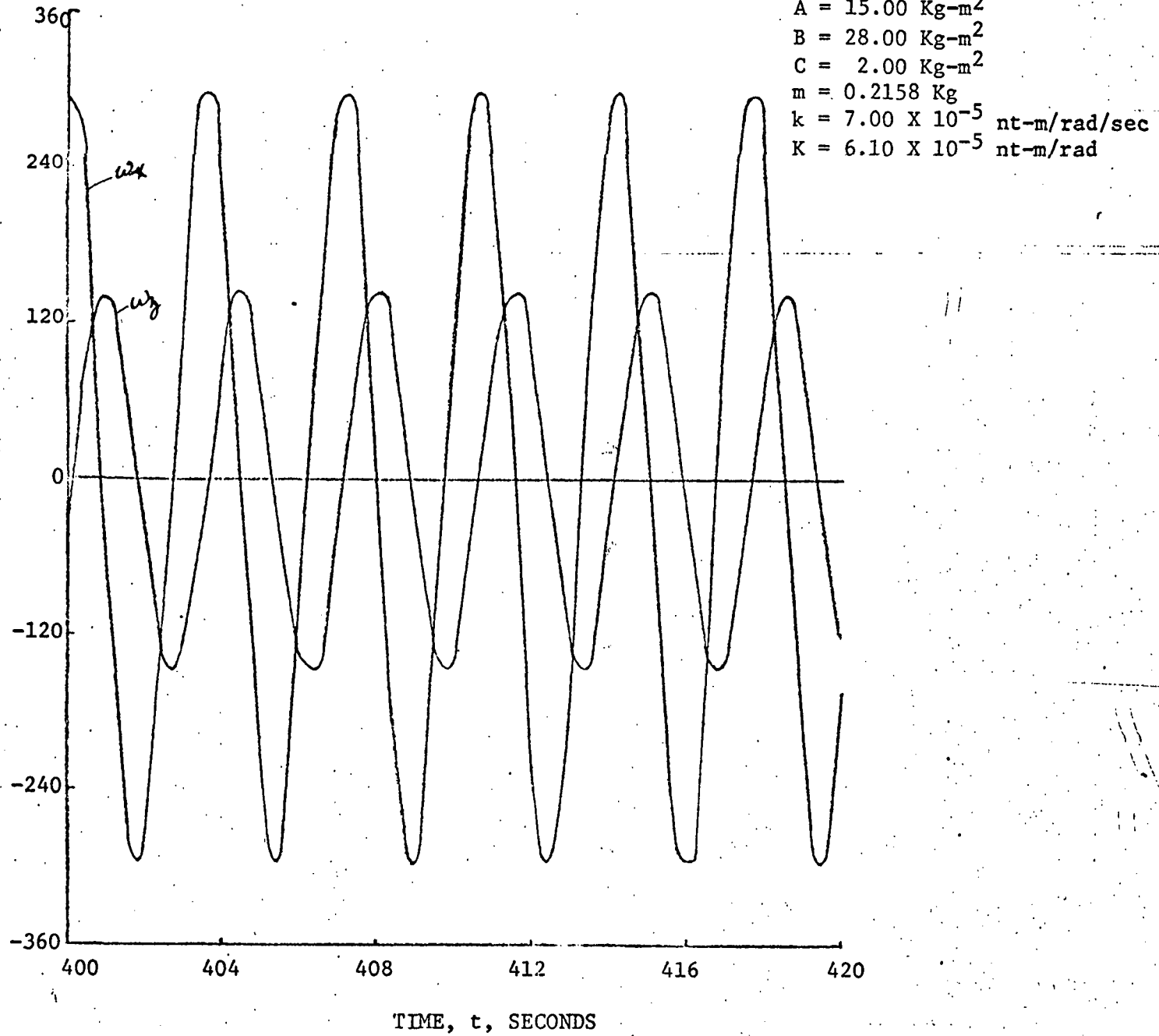

Figure 7c. Nutation Damper Response During Spin-Up
Satellite with Large Asymmetry in the Main Body and Damping

$A = 15.00$ Kg-m^2
$B = 28.00$ Kg-m^2
$C = 2.00$ Kg-m^2
$m = 0.2158$ Kg
$k = 7.00 \times 10^{-5}$ nt-m/rad/sec
$K = 6.10 \times 10^{-5}$ nt-m/rad

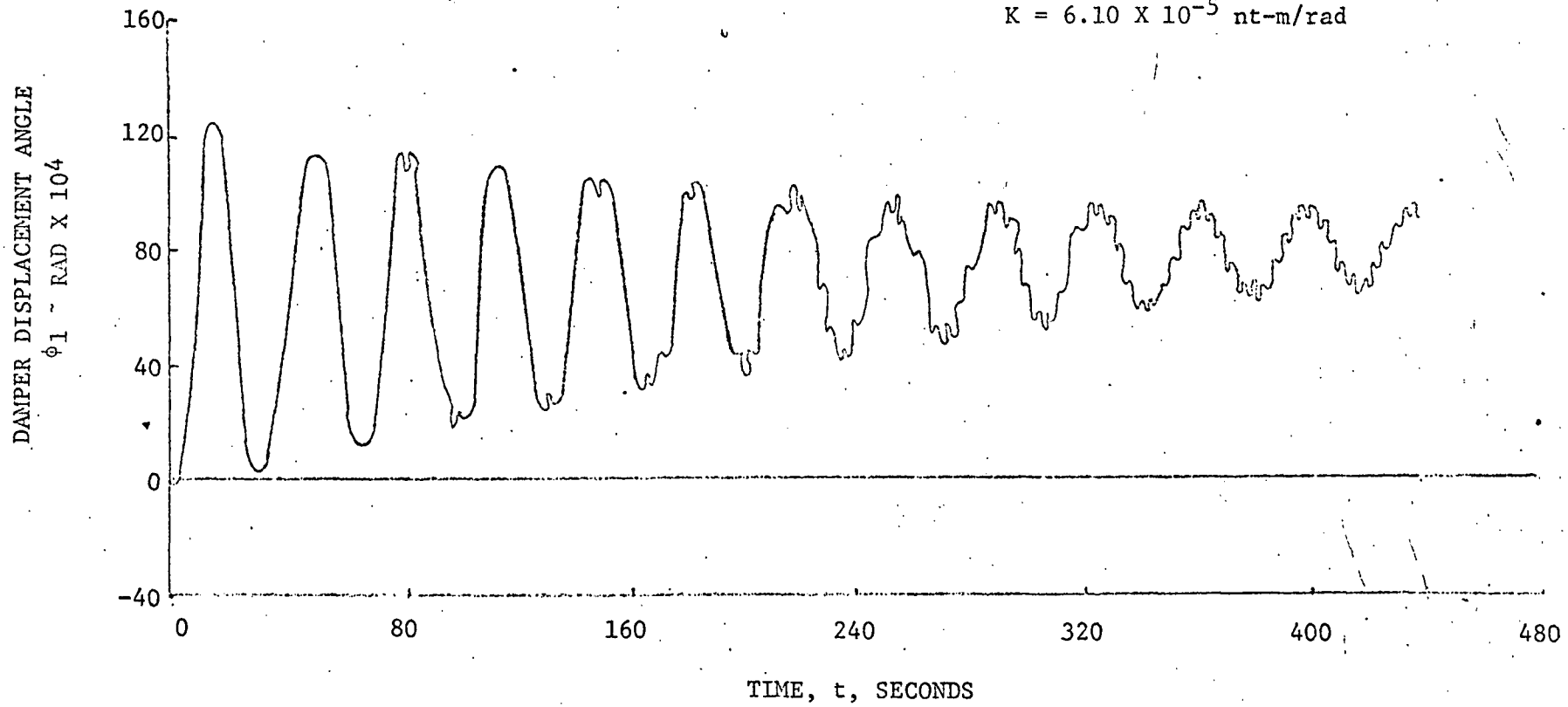

Figure 8a. Time History of the Transverse Components of Main Body Angular Velocity
Symmetrical Satellite and No Damping (Variable Torque Law)
$A = C = 27.00$ Kg-m^2
$B = 28.54$ Kg-m^2

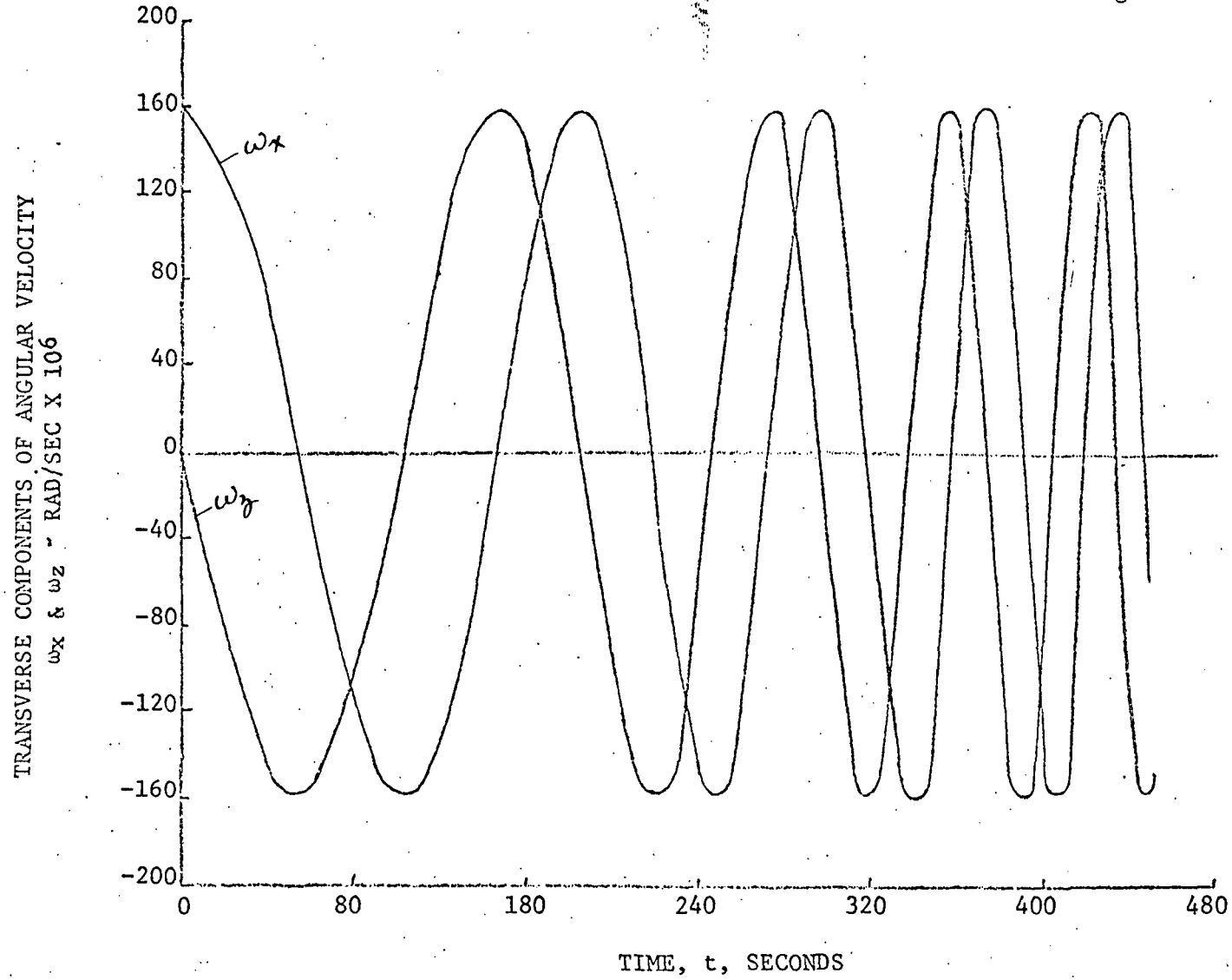

Figure 8b. Rotor Spin Rate During Spin-Up
Symmetrical Satellite and No Damping (Variable Torque Law)
$A = C = 27.00$ Kg-m^2
$B = 28.54$ Kg-m^2

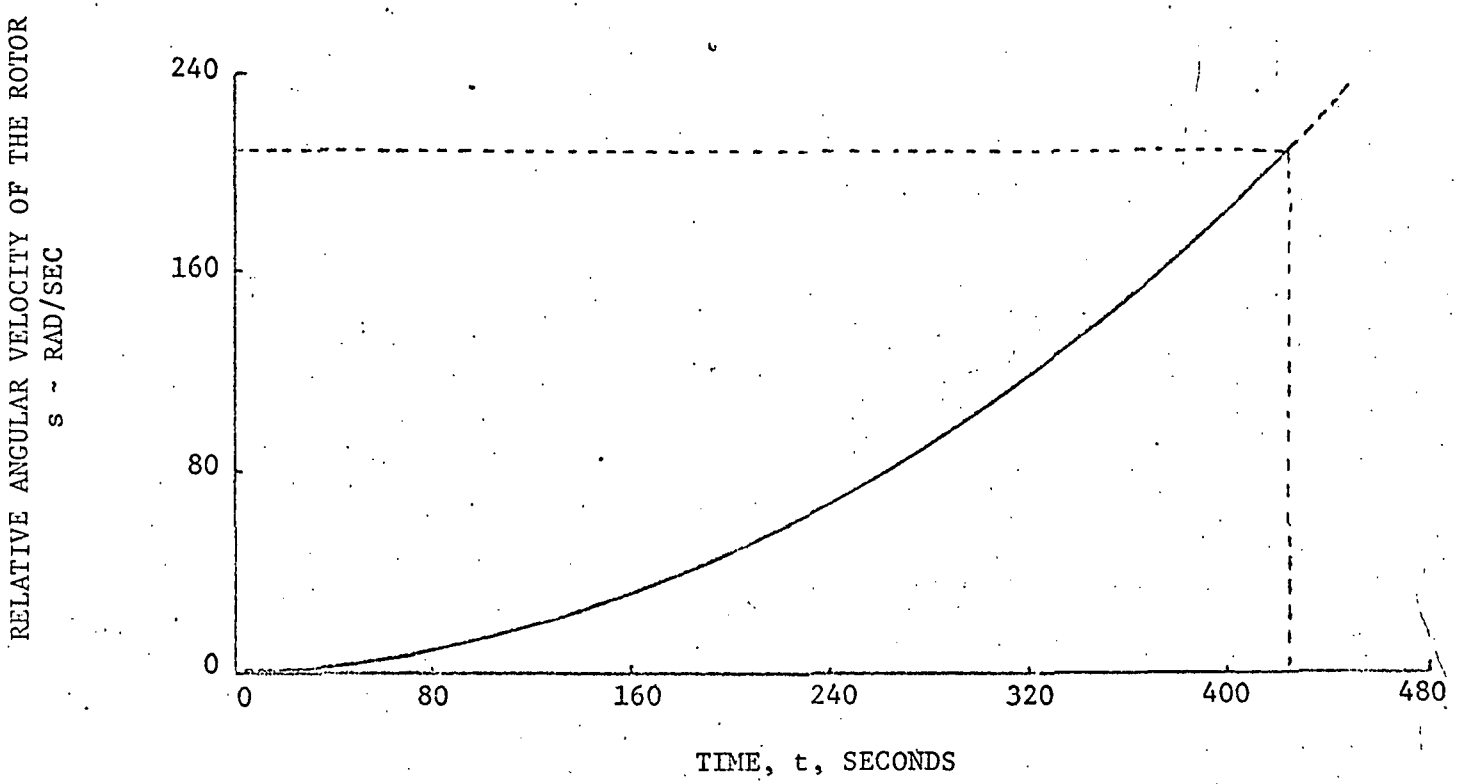

Figure 8c. Main Body Spin Rate During Spin-Up
Symmetrical Satellite and No Damping (Variable Torque Law)
$A = C = 27.00$ Kg-m^2
$B = 28.54$ Kg-m^2

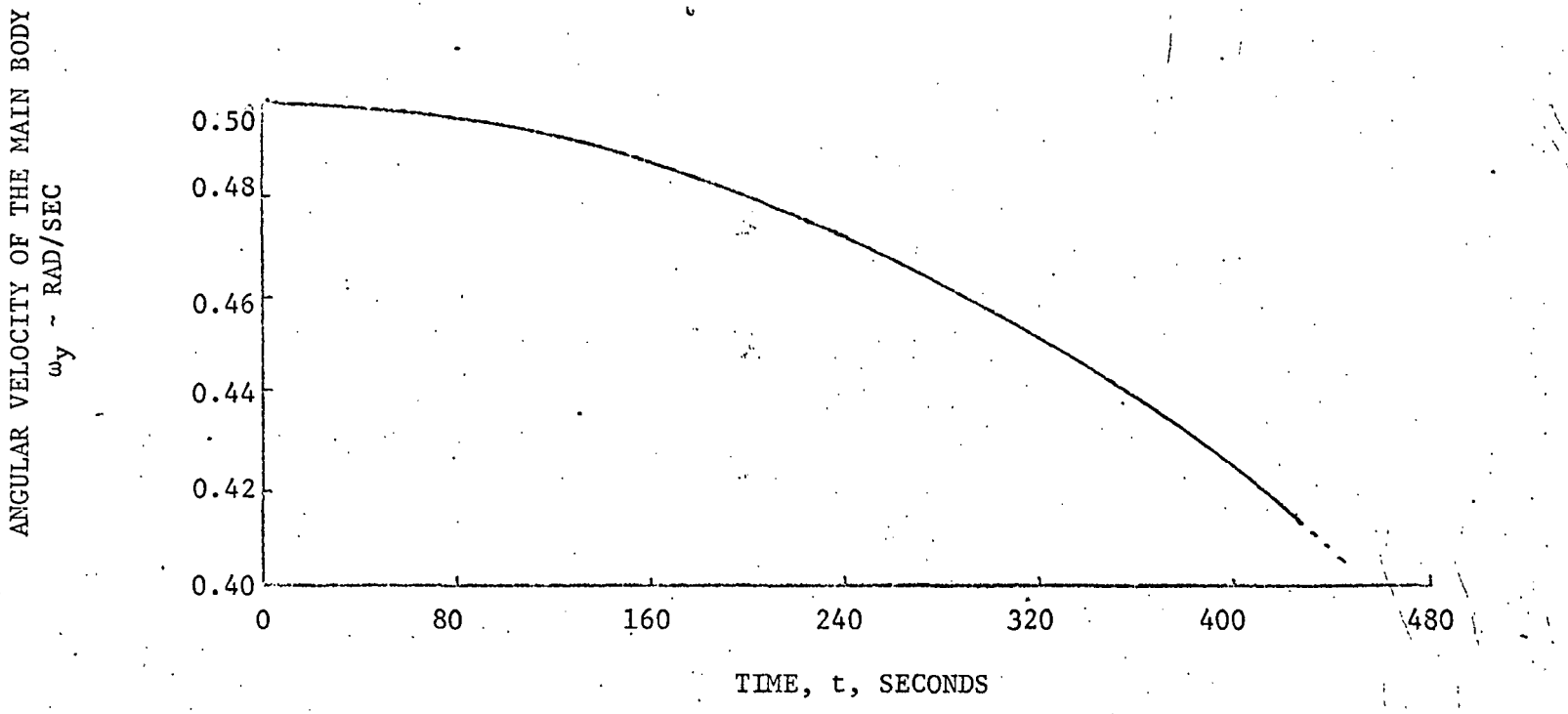

Figure 9a. Time History of the Transverse Components of Main Body Angular Velocity
Symmetrical Satellite with Damping (Variable Torque Law)

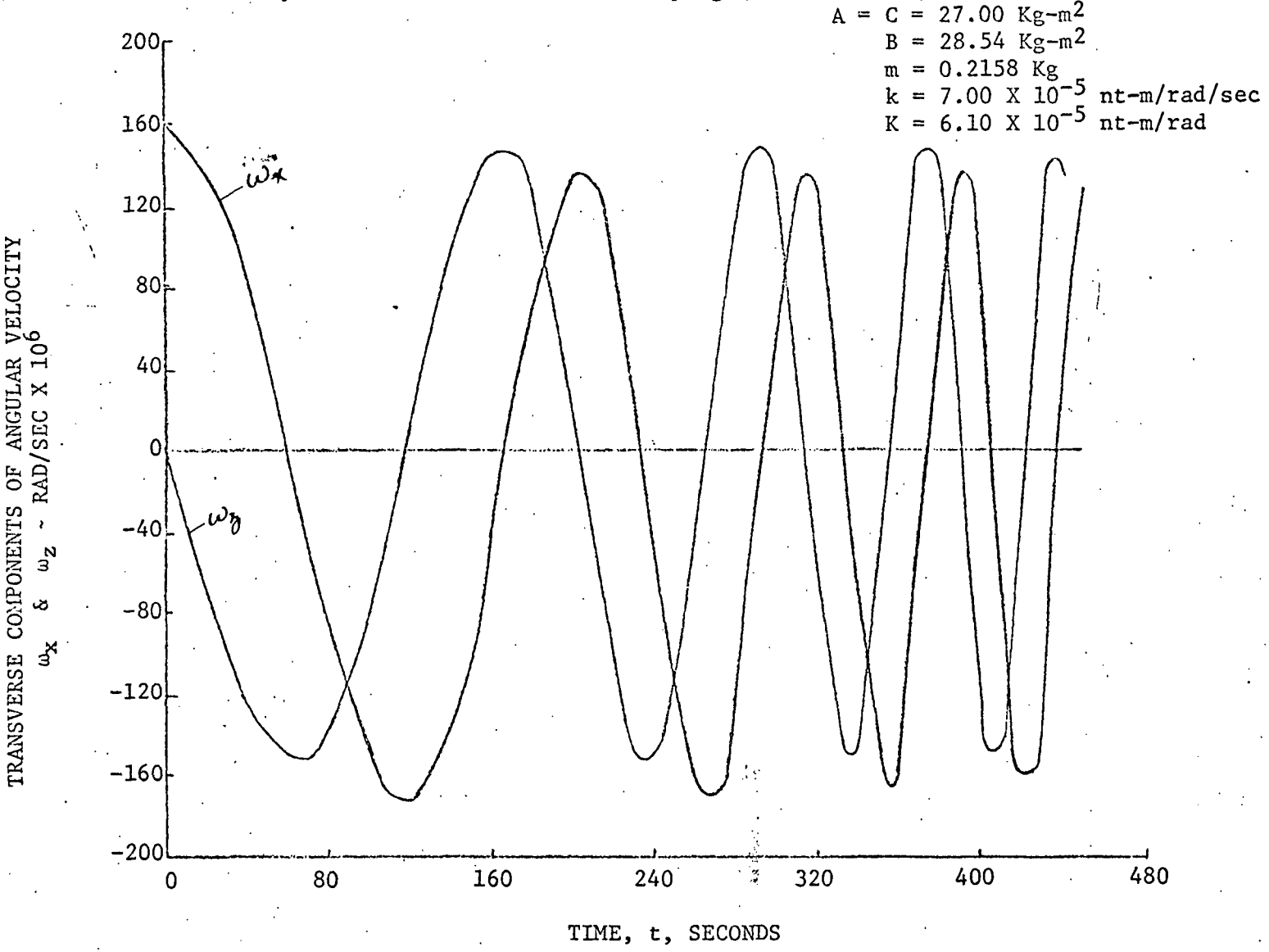

Figure 9b. Rotor Spin Rate During Spin-Up
Symmetrical Satellite with Damping (Variable Torque Law)
$A = C = 27.00$ Kg-m^2
$B = 28.54$ Kg-m^2
$m = 0.2158$ Kg
$k = 7.00 \times 10^{-5}$ nt-m/rad/sec
$K = 6.10 \times 10^{-5}$ nt-m/rad

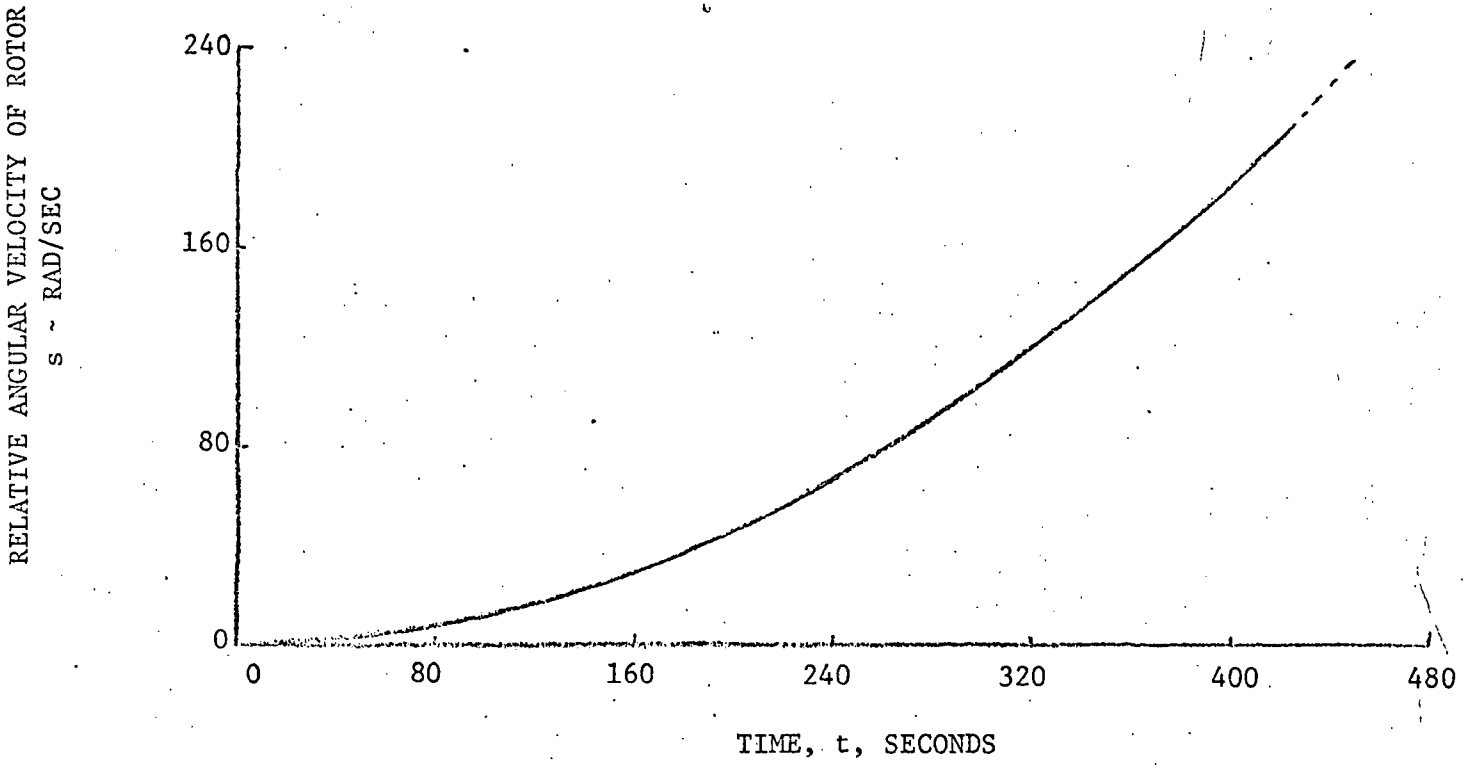

Figure 9c. Main Body Spin Rate During Spin-Up
Symmetrical Satellite with Damping (Variable Torque Law)

$A = C = 27.00$ Kg-m^2
$B = 28.54$ Kg-m^2
$m = 0.2158$ Kg
$k = 7.00 \times 10^{-5}$ nt-m/rad/sec
$K = 6.10 \times 10^{-5}$ nt-m/rad

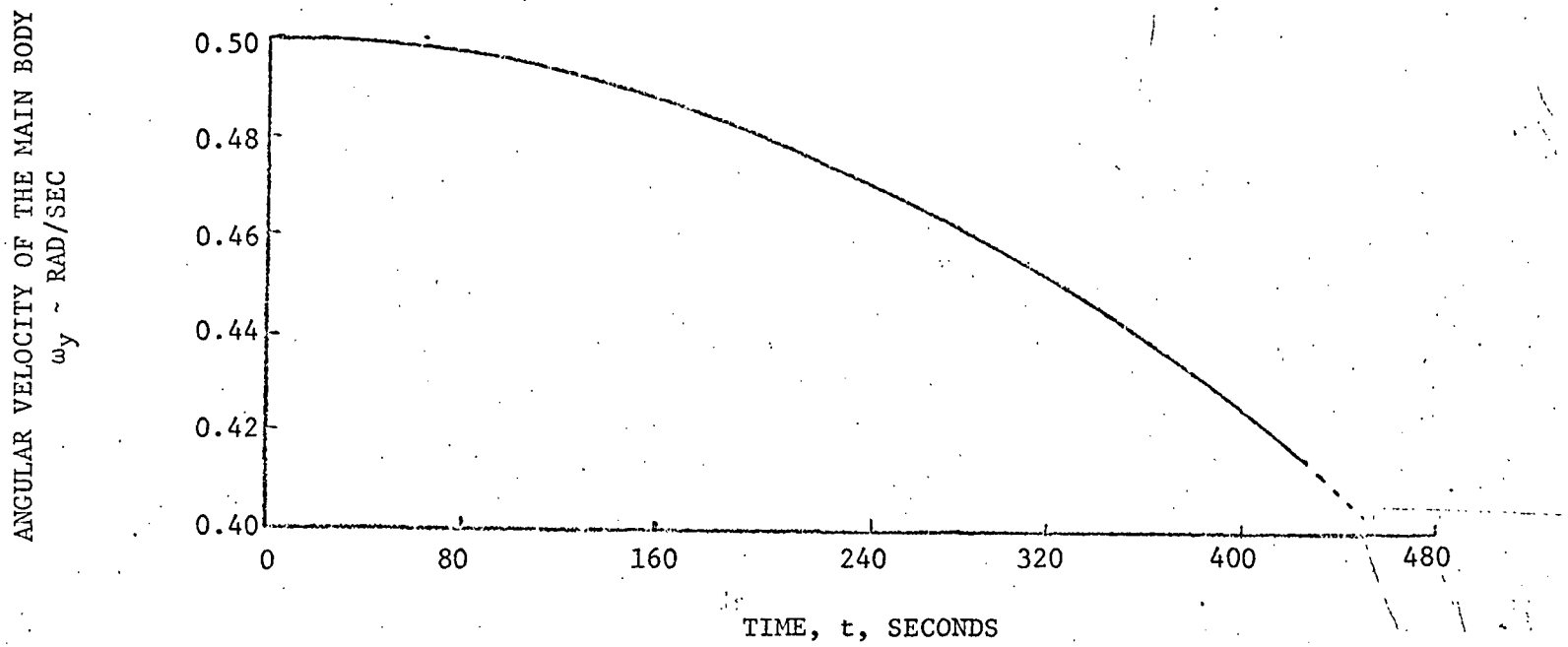

Figure 9d. Nutation Damper Response During Spin-Up
Symmetrical Satellite with Damping (Variable Torque Law)

$A = C = 27.00$ Kg-m^2
$B = 28.54$ Kg-m^2
$m = 0.2158$ Kg
$k = 7.00 \times 10^{-5}$ nt-m/rad/sec
$K = 6.10 \times 10^{-5}$ nt-m/rad

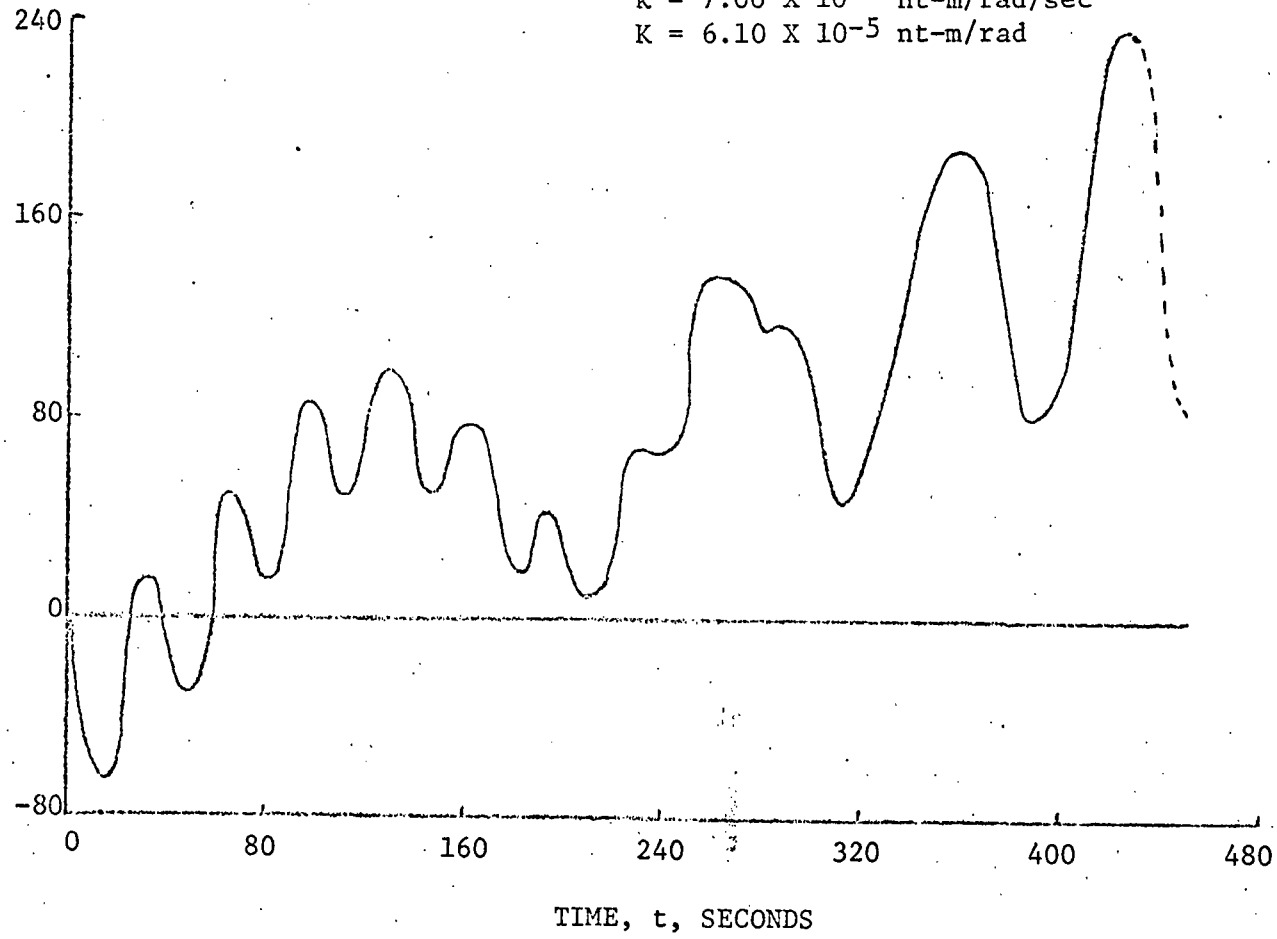

Fig. 10a. Time History of the Transverse Components of Main Body Angular Velocity (SAS-A No Damping)
All Moments of Inertia Parameters are in Kg-m^2.
I_{xx} = 27.015; I_{yy} = 28.54; I_{zz} = 26905; I_{xy} = 2.123 x 10^{-3}; I_{xz} = 0.1048; I_{yz} = 1.193 x 10^{-3};
$\omega_x(0)$ = 0.000159 rad/sec.

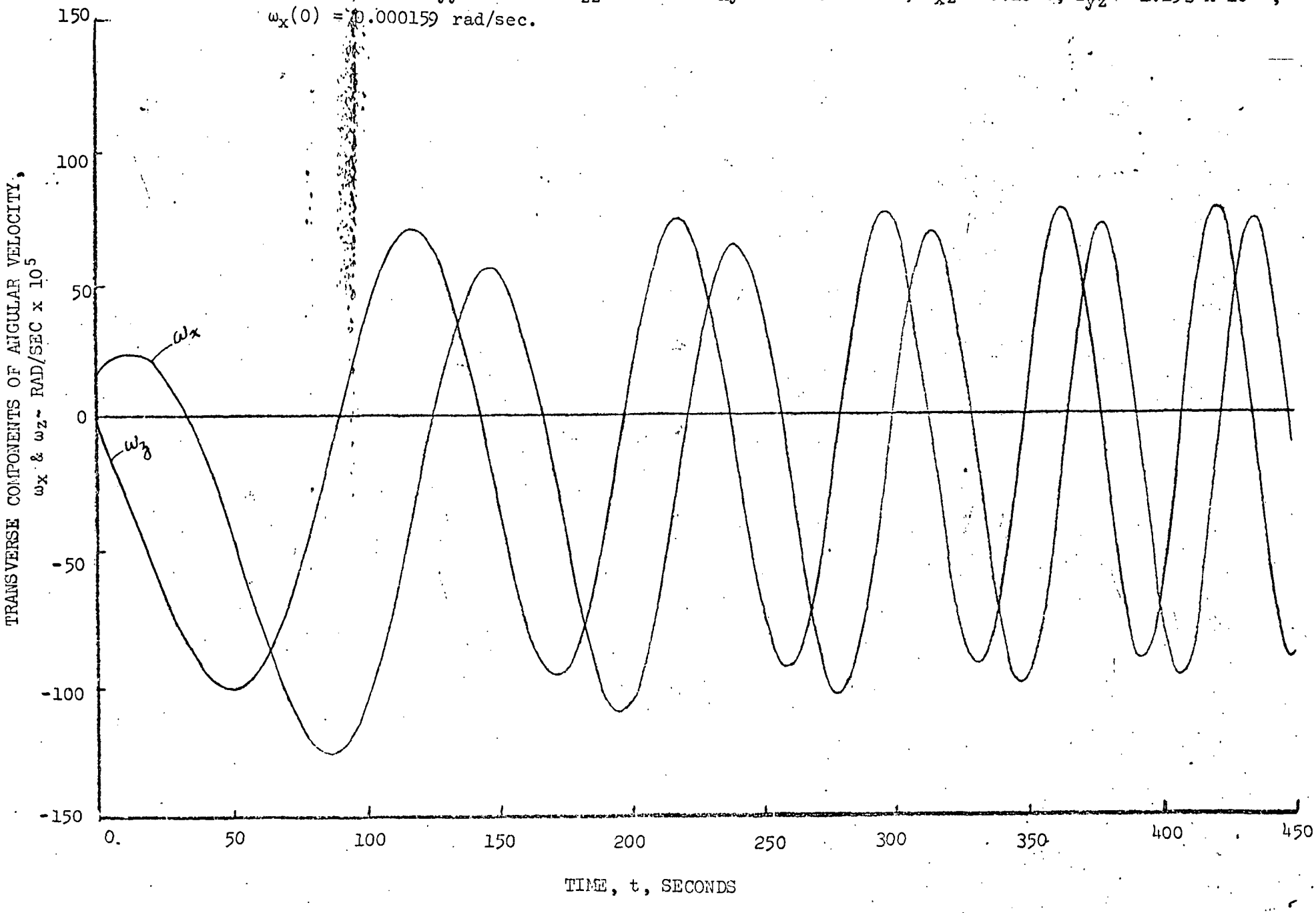

Fig. 10b. Main Body Spin Rate During Spin-Up (SAS-A No Damping)
I_{xx} = 27.015; I_{yy} = 28.54; I_{zz} = 26.905; I_{xy} = 2.123 x 10^{-3};
I_{xz} = 0.1048; I_{yz} = 1.193 x 10-3; $\omega_x(o)$ = 0.000159 rad/sec.

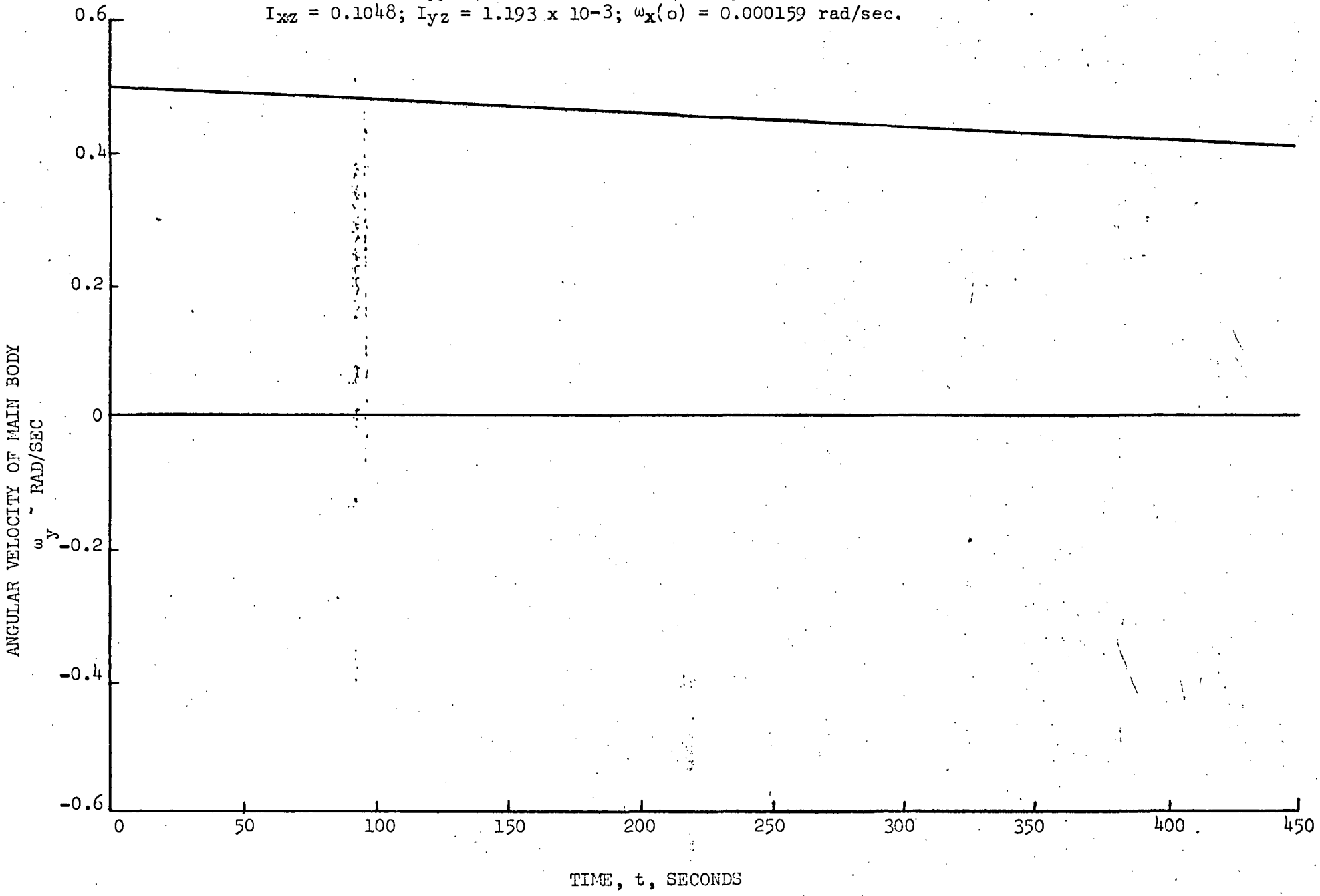

Fig. 10c. Rotor Spin Rate During Spin-Up (SAS-A No Damping)
I_{xx} = 27.015; I_{yy} = 28.54; I_{zz} = 26.905; I_{xy} = 2.123 x 10^{-3};
I_{xz} = 0.1048; I_{yz} = 1.193 x 10^{-3}; $\omega_x(o)$ = 0.000159 rad/sec.

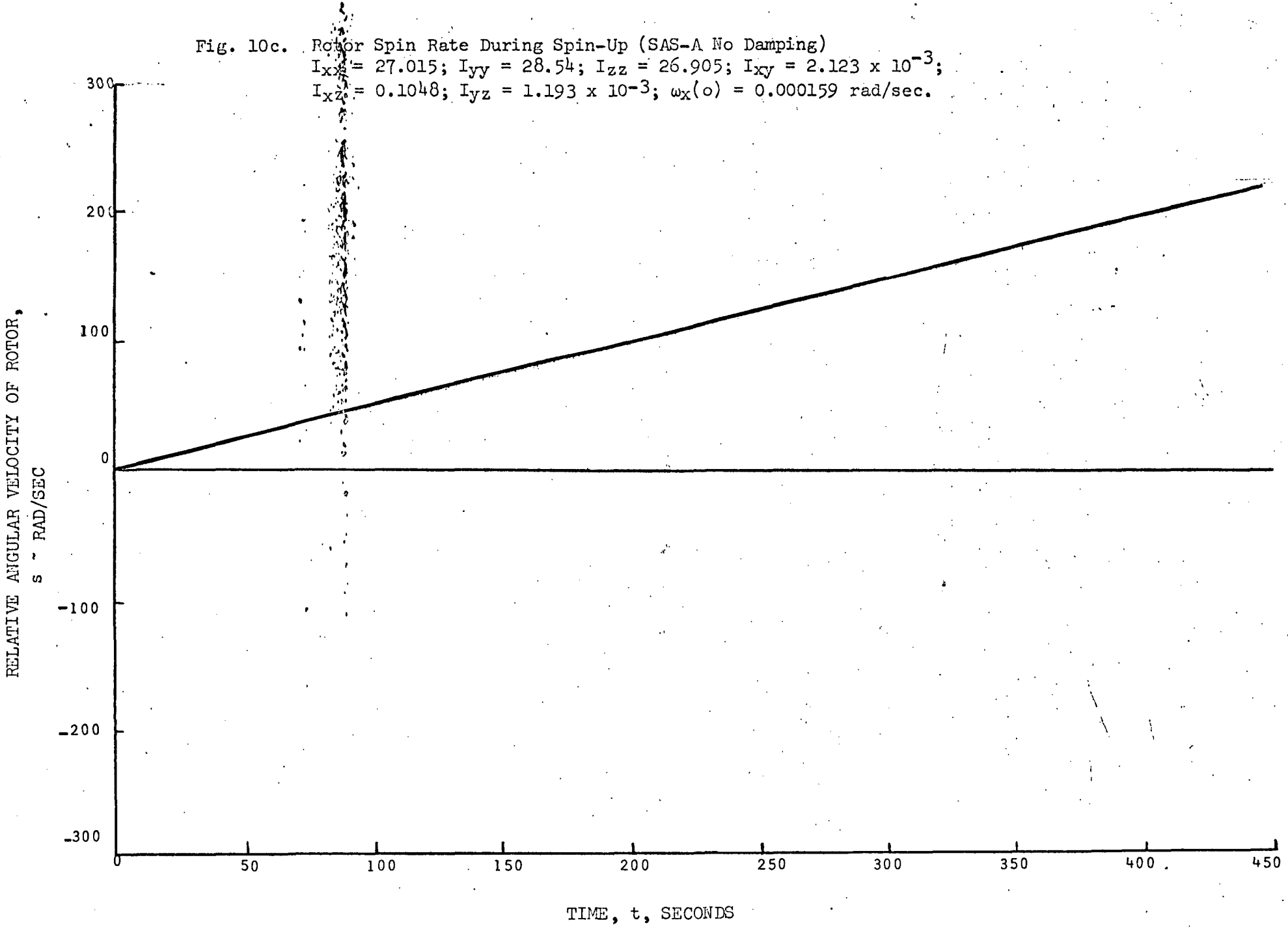

Fig. 11a. Time History of Transverse Components of Main Body Angular Velocity
(SAS-A with Damping)

$I_{xx} = 27.015$; $I_{yy} = 28.54$; $I_{zz} = 26.905$; $I_{xy} = 2.123 \times 10^{-3}$
$I_{xz} = 0.1048$; $I_{yz} = 1.193 \times 10^{-3}$
$m = 0.2158$ kg; $k = 7.05 \times 10^{-5}$, $K = 6.10 \times 10^{-5}$, $\omega_x(0) = 0.000159$ rad/sec.

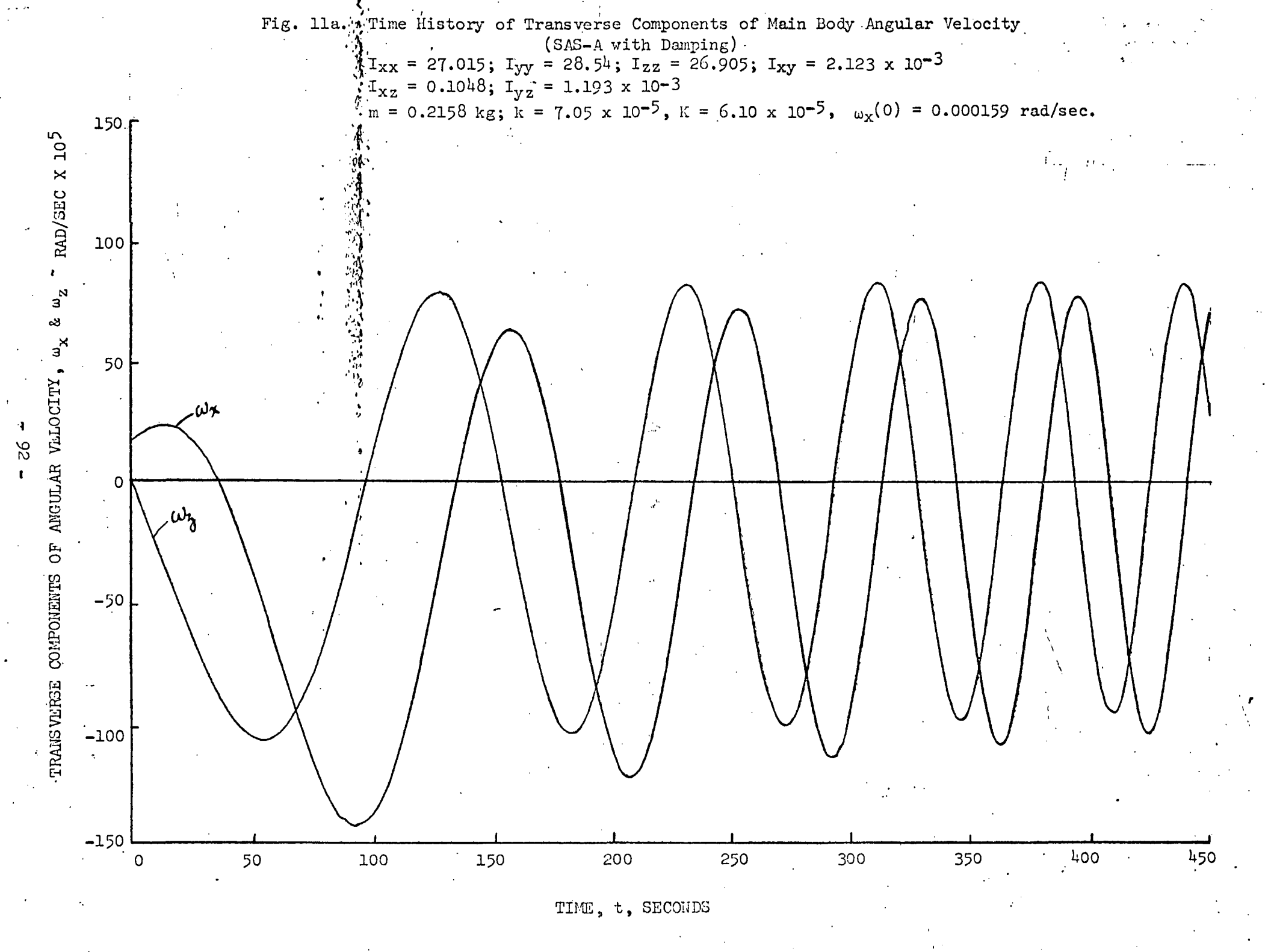

Fig. 11b. Nutation Damper Response During Spin-Up (SAS-A with Damping

I_{xx} = 27.015; I_{yy} = 28.54; I_{zz} = 26.905; I_{xy} = 2.123 x 10^{-3}

I_{xz} = 0.1048 I_{yz} = 1.193 x 10^{-3}

m = 0.2158 kg; k = 7.05 x 10^{-5}; K = 6.10 x 10^{-5} $\omega_x(o)$ = 0.000159 rad/sec.

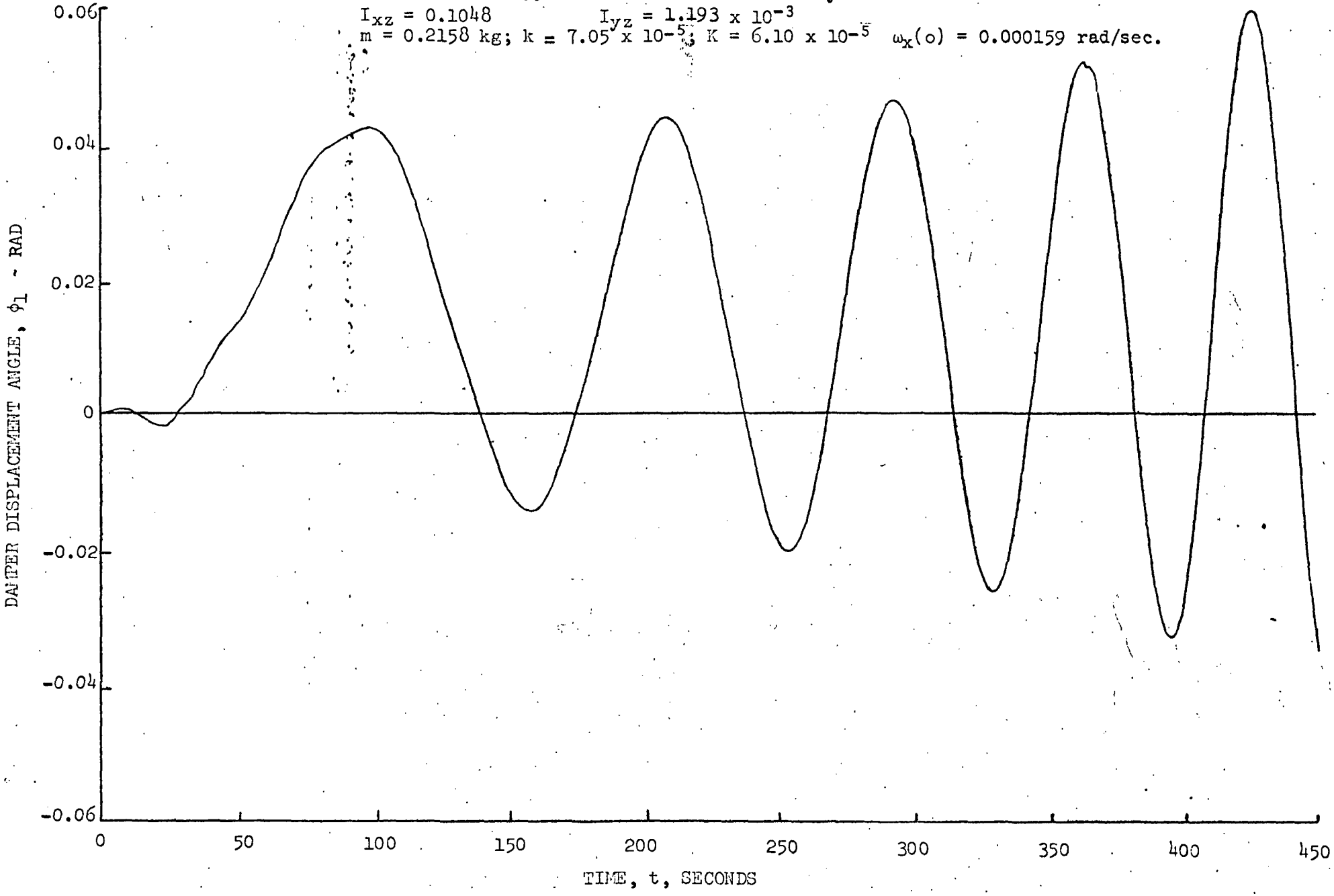

Fig. 12. Time History of the Transverse Components of Main Body Angular Velocity
(SAS-A No Damping)

I_{xx} = 27.015; I_{yy} = 28.54; I_{zz} = 26.905; I_{xy} = 2.123 x 10^{-3}; I_{xz} = 0.1048

I_{yz} = 1.193 x 10^{-3}; $\omega_x(o)$ = 0.00159 rad/sec.

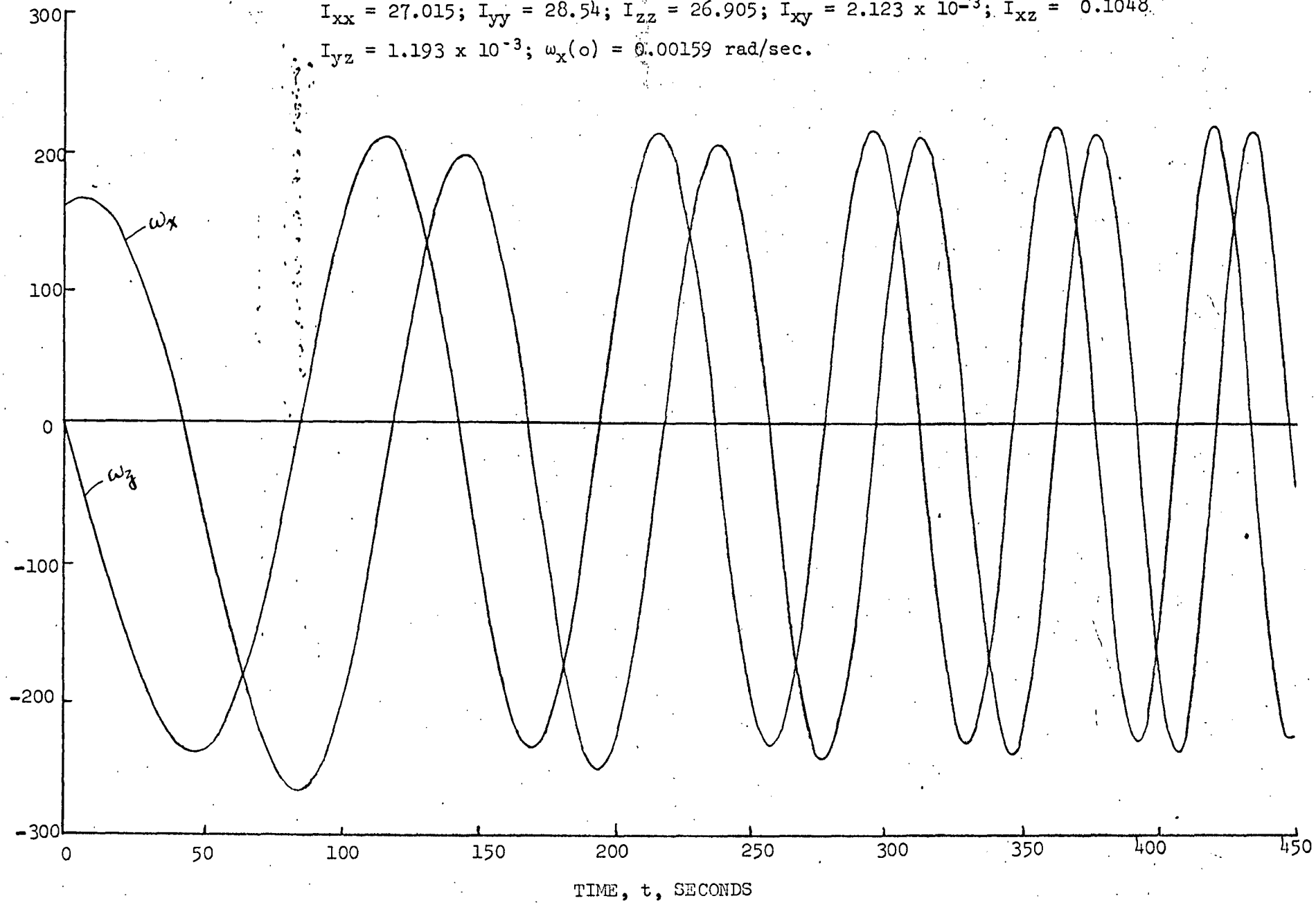

Fig. 13a. Time History of the Transverse Components of Main Body Angular Velocity
(SAS-A with Damping)

I_{xx} = 27.015; I_{yy} = 28.54; I_{zz} = 2.123 x 10^{-3}; I_{xy} = 0.1048; I_{xz} = 1.193 x 10^{-3}

m = 0.2158 kg; k = 7.05 x 10^{-5}; K = 6.10 x 10^{-5}; $\omega_x(o)$ = 0.00159 rad/sec.

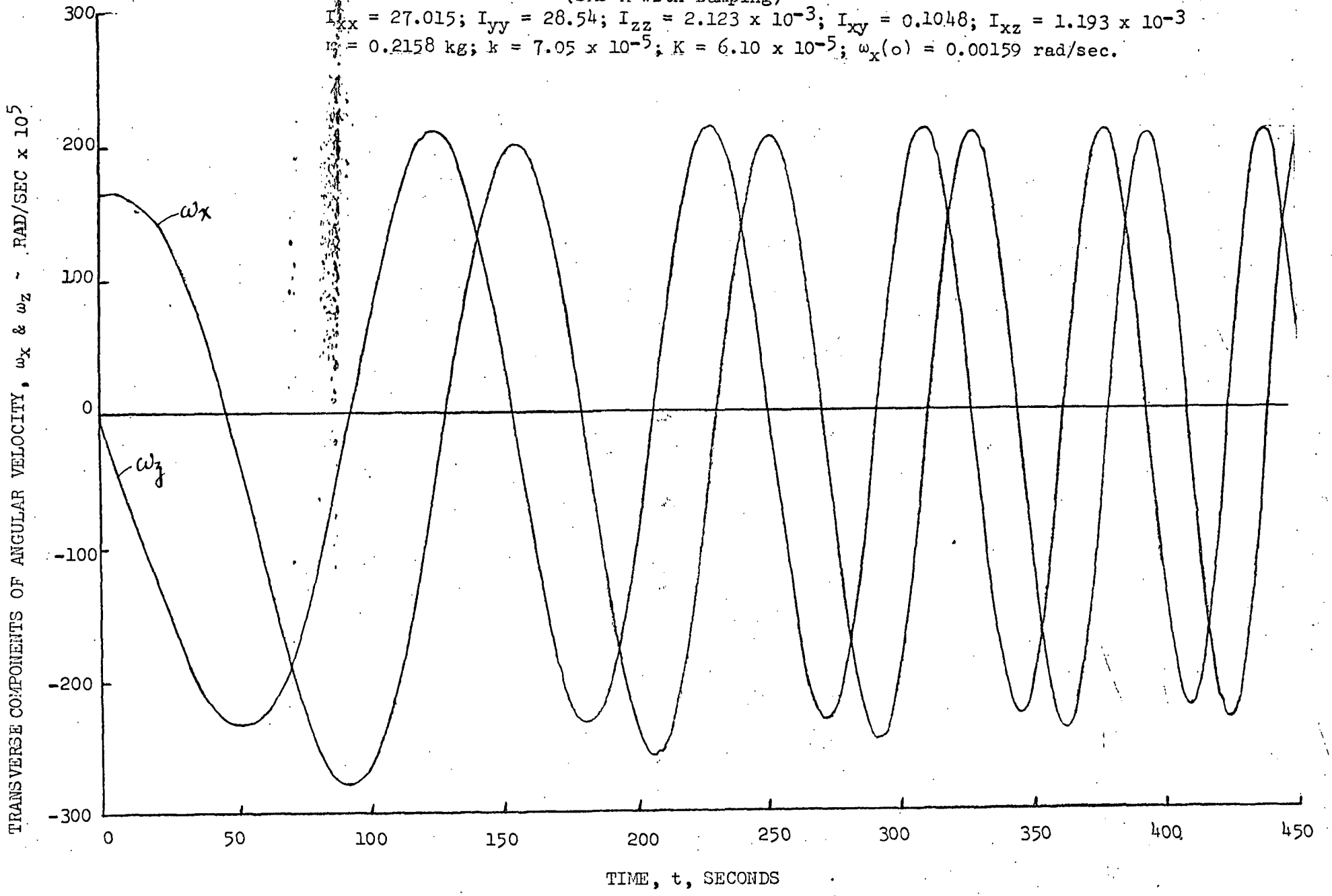

Fig. 13b. Nutation Damper Response During Spin-Up ((SAS-A with Damping)
I_{xx} = 27.015; I_{yy} = 28.54; I_{zz} = 26.905; I_{xy} = 2.123 x 10^{-3};
I_{xz} = 0.1048; I_{yz} = 1.193 x 10^{-3}
m = 0.2158 kg, k = 7.05 x 10^{-5}, K = 6.10 x 10^{-5}, $\omega_x(o)$ = 0.00159 rad/sec

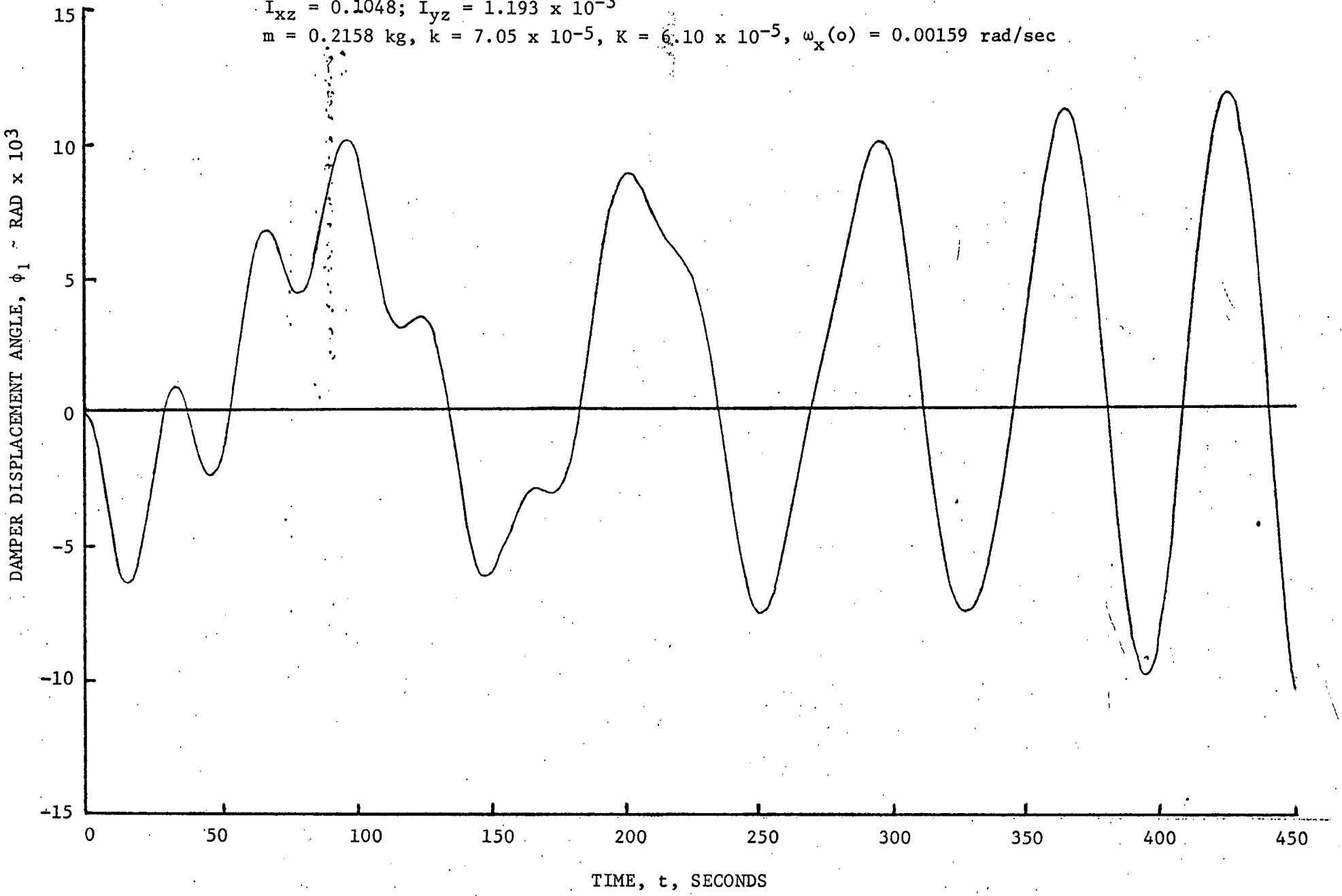

Fig. 14. Time History of the Transverse Components of Main Body Angular Velocity (SAS-A no damping)
I_{xx} = 27.015; I_{yy} = 28.54; I_{zz} = 26.905; I_{xy} = 2.123 x10-3; I_{xz} = 0.1048; I_{yz} = 1.193x10-3
$\omega_x(0)$ = 0.0159 rad/sec.

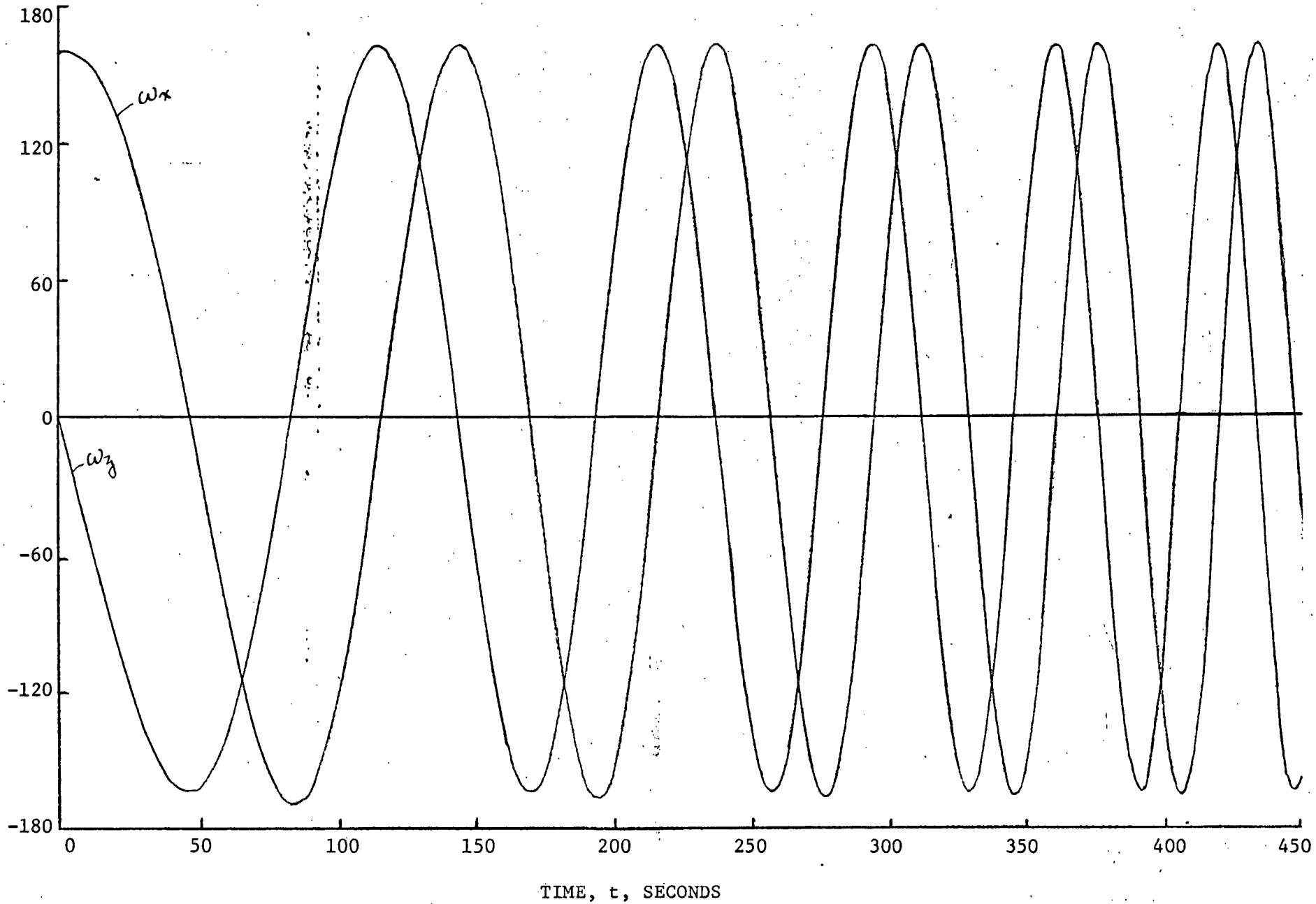

Fig. 15a. Time History of the Transverse Components of Main Body Angular Velocity
(SAS-A With Damping)

I_{xx} = 27.015; I_{yy} = 28.54; I_{zz} = 26.905

I_{xy} = 2.123 x 10^{-3}; I_{xz} = 0.1048; I_{yz} = 1.193 x 10^{-3}

m = 0.2158 Kg; k = 7.05 x 10^{-5}; K = 6.10 x 10^{-5}; $\omega_x(0)$ = 0.0159 rad/sec.

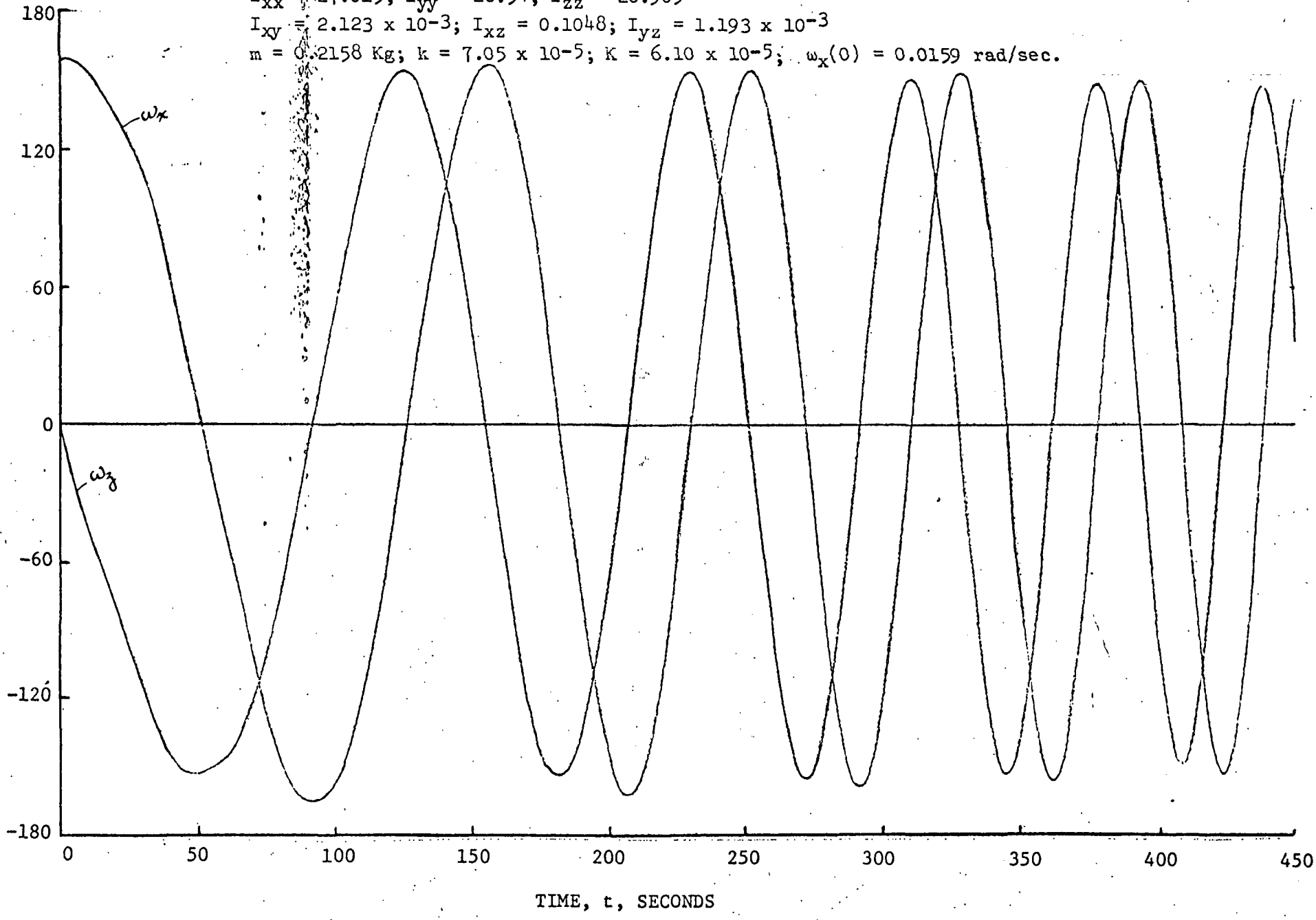

Fig. 15b. Nutation Damper Response During Spin-Up (SAS-A With Damping)
I_{xx} = 27.015; I_{yy} = 28.54; I_{zz} = 26.905
I_{xy} = 2.123 x 10-3; I_{xz} = 0.1048; I_{yz} = 1.193 x 10^{-3}
m = 0.2158 Kg; k = 7.05 x 10^{-5}; K = 6.10 x 10^{-5}; $\omega_x(0)$ = 0.0159 rad/sec.

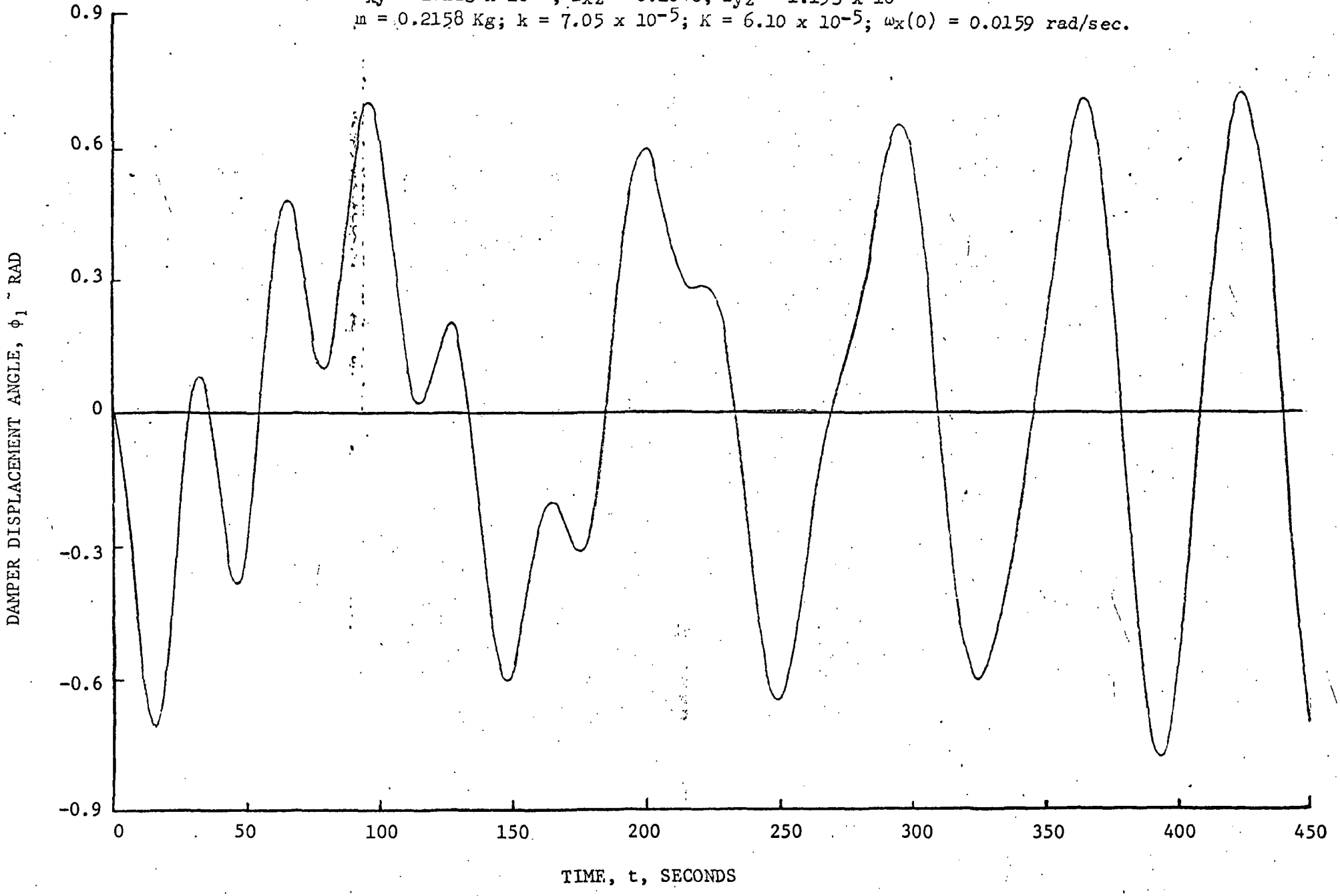

Fig. 16a. Time History of the Transverse Components of Main Body Angular Velocity (OSO Spacecraft)
All Moments of Inertia Parameters are in Slug - ft^2
I_{xx} = 131.00; I_{yy} = 34.00; I_{zz} = 136.00
I_{Rxx} = 199.00; I_{Ryy} = 378.00; I_{Rzz} = 208.00
$\gamma(o) = 0.1^o$; $\omega_x(o)$ = 0.003170 rad/sec.

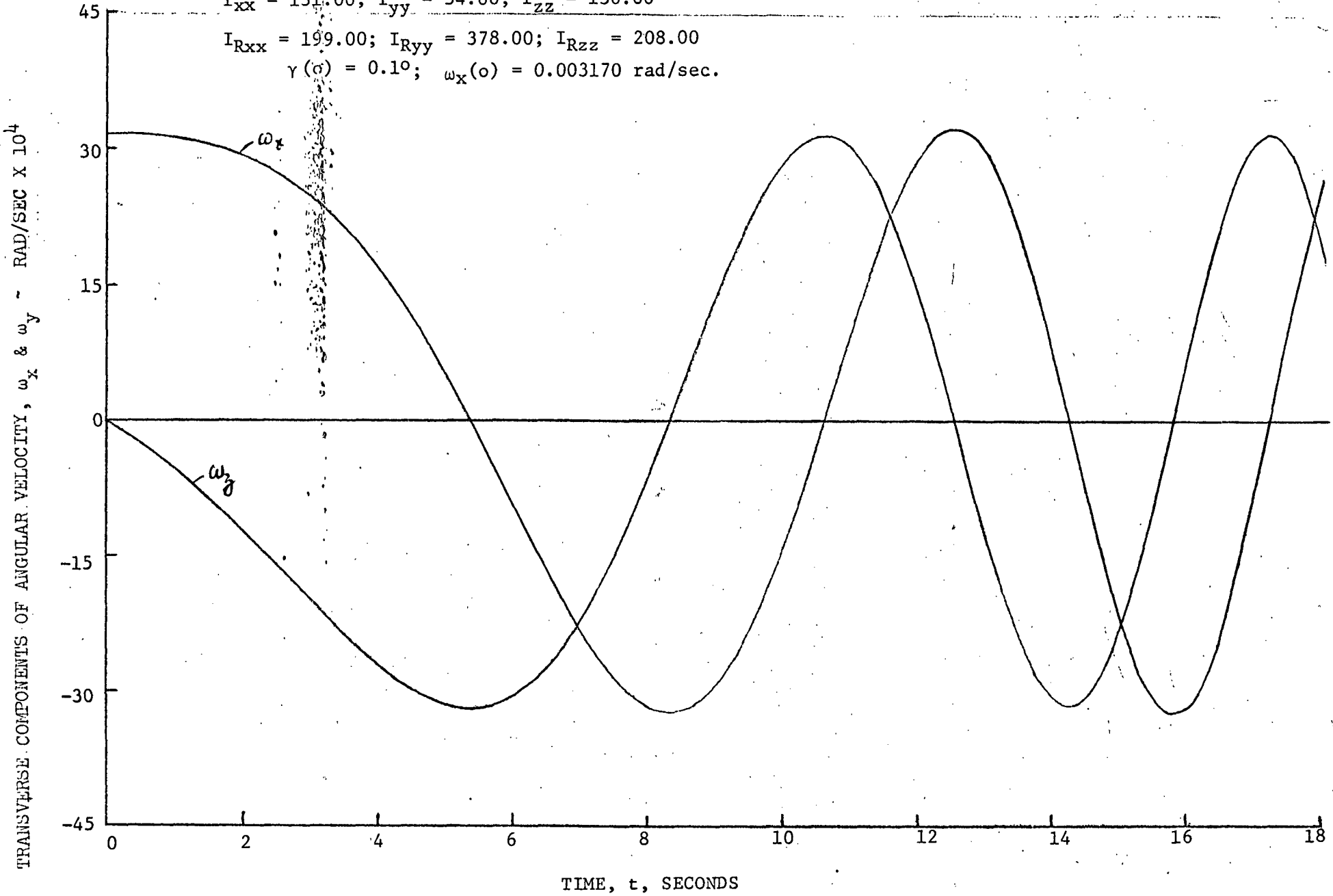

Fig. 16b. Main Body Spin Rate During Spin-Up (OSO Spacecraft)
I_{xx} = 131.00; I_{yy} = 34.00
I_{zz} = 136.00; $I_{R_{xx}}$ = 199.00
$I_{R_{yy}}$ = 378.00; $I_{R_{zz}}$ = 208.00
$\gamma(0)$ = 0.1°; $\omega_x(0)$ = 0.003170 rad/sec.

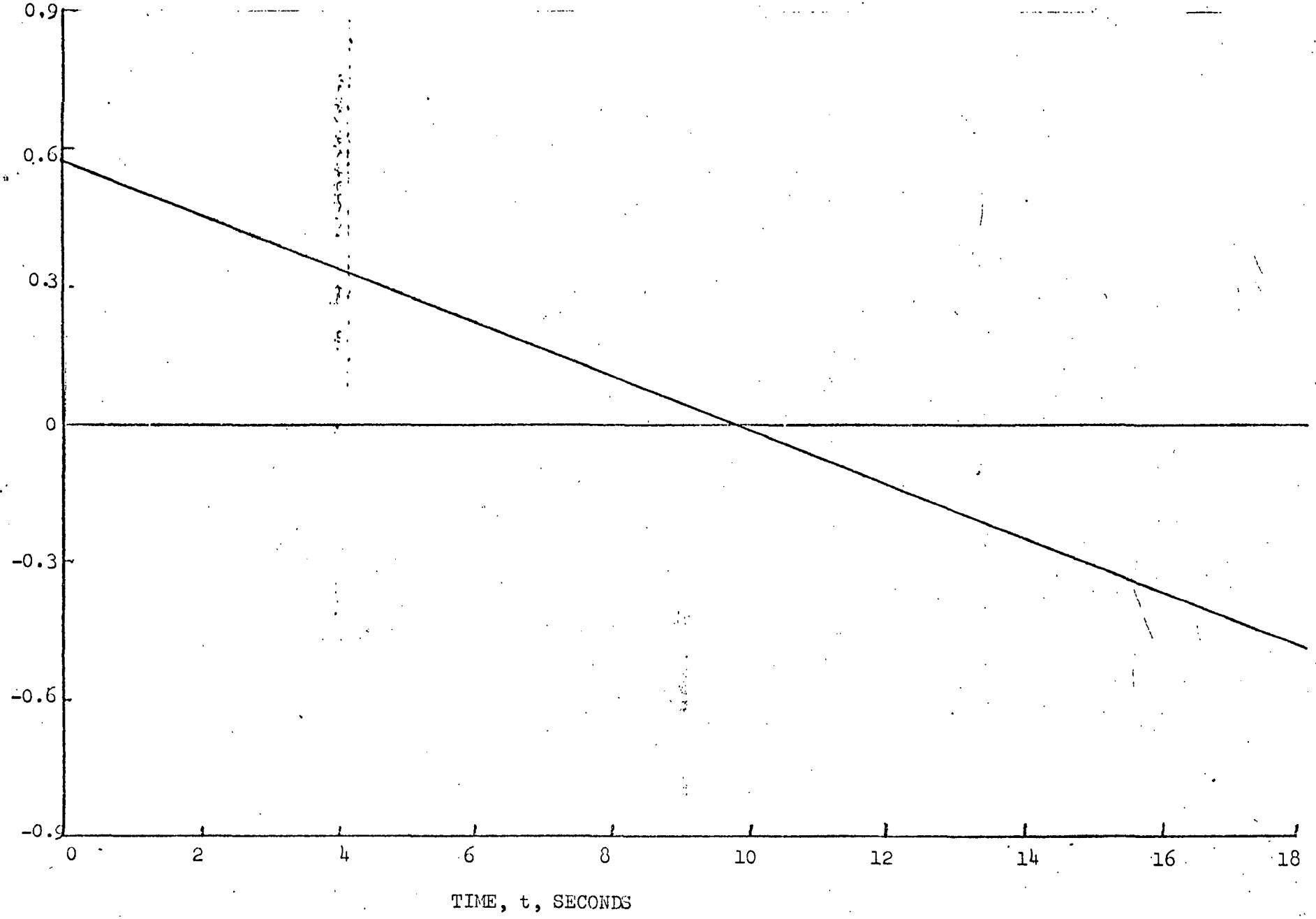

Fig. 10c. Rotor Spin Rate During Spin-up (OSO Spacecraft)

I_{xx} = 131.00; I_{yy} = 34.00; I_{zz} = 136.00

$I_{R_{xx}}$ = 199.00; $I_{R_{yy}}$ = 378.00; $I_{R_{zz}}$ = 208.00

$\gamma(0) = 0.1°$

$\omega_x(0)$ = 0.003170 rad/sec.

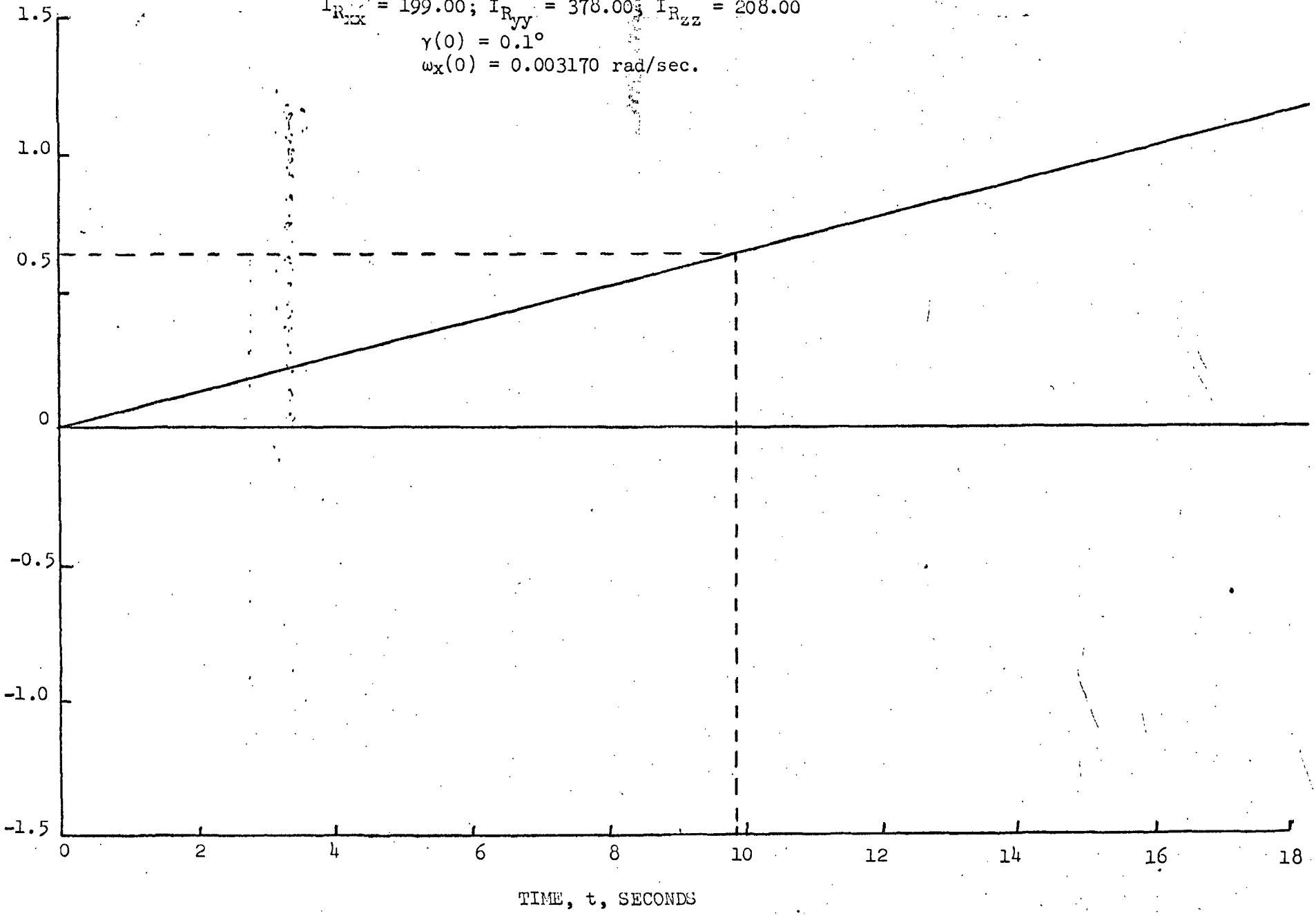

Fig. 17. Time History of the Transverse Components of Main Body Angular Velocity (OSO Spacecraft)

$I_{xx} = 131.00$; $I_{yy} = 34.00$; $I_{zz} = 136.00$

$I_{R_{xx}} = 199.00$; $I_{R_{yy}} = 378.00$; $I_{R_{zz}} = 208.00$

$\gamma(0) = 1°$, $\omega_x(0) = 0.03172$ rad/sec.

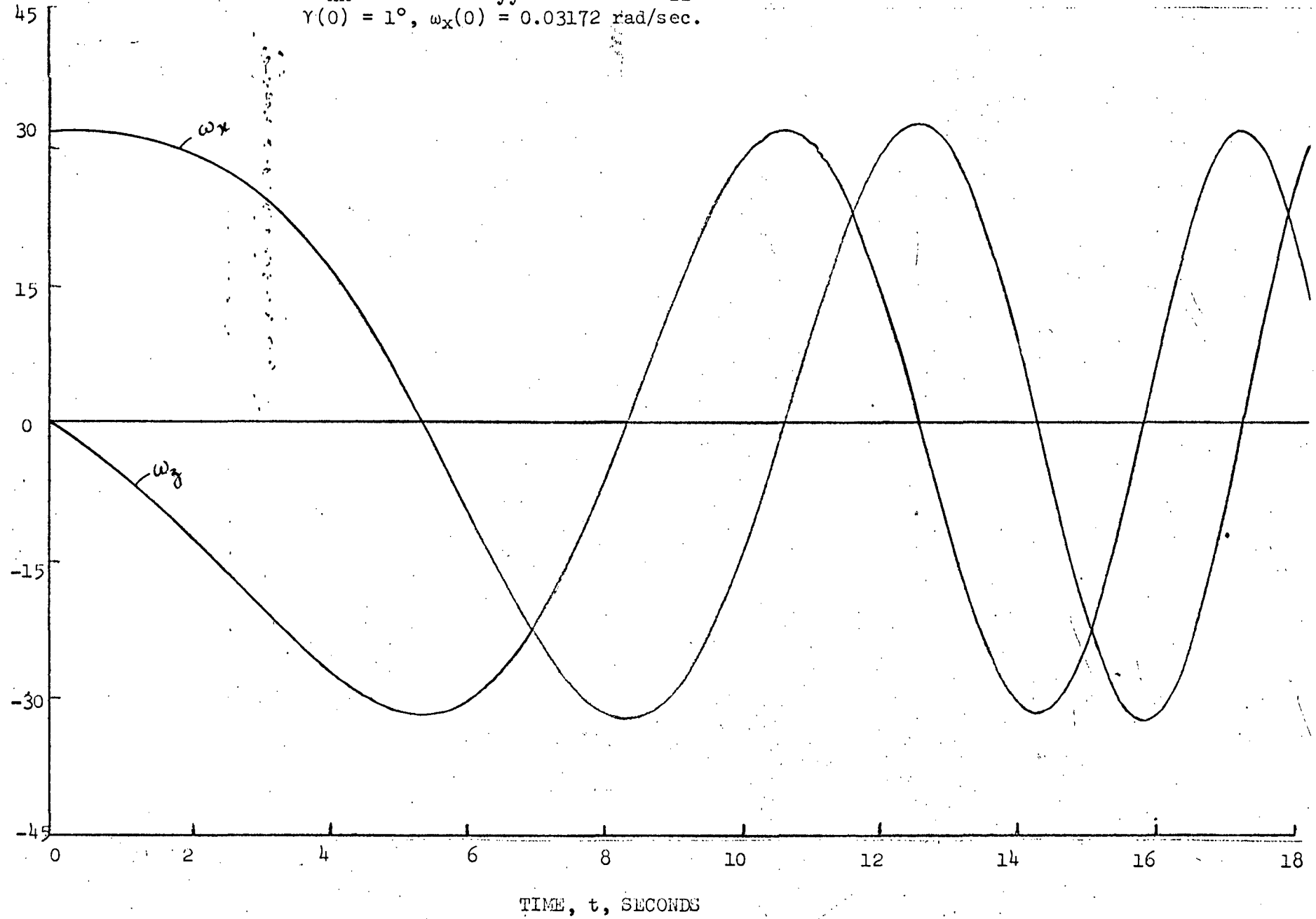

Fig. 18. Time History of the Transverse Components of Main Body Angular Velocity (OSO Spacecraft)

$I_{xx} = 131.00$; $I_{yy} = 34.00$; $I_{zz} = 136.00$

$I_{R_{xx}} = 199.00$; $I_{R_{yy}} = 378.00$; $I_{R_{zz}} = 208.00$

$\gamma(0) = 10°$, $\omega_x(0) = 0.3194$ rad/sec.

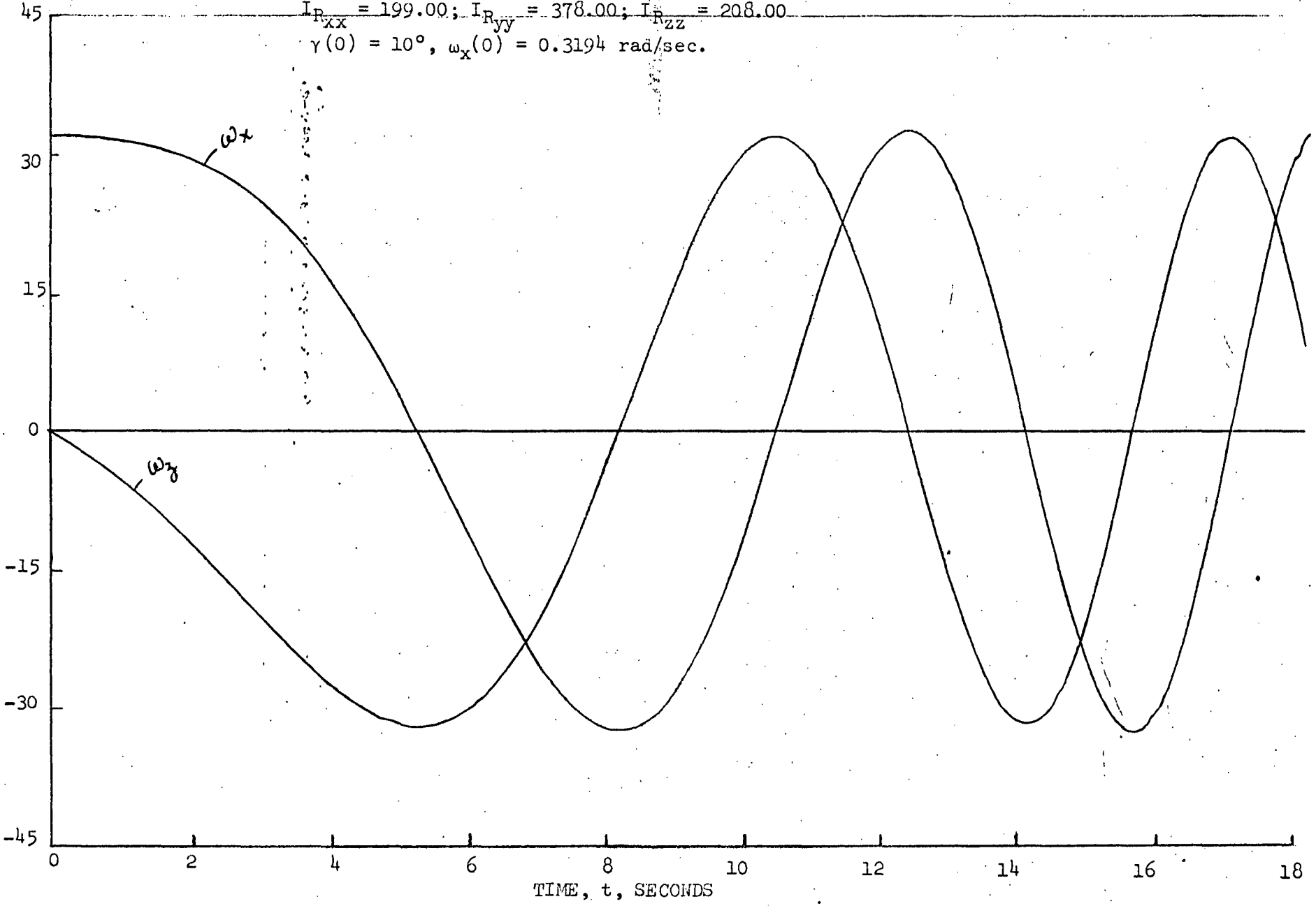

Fig. 19. Time History of the Transverse Components of Main Body Angular Velocity (OSO Spacecraft)

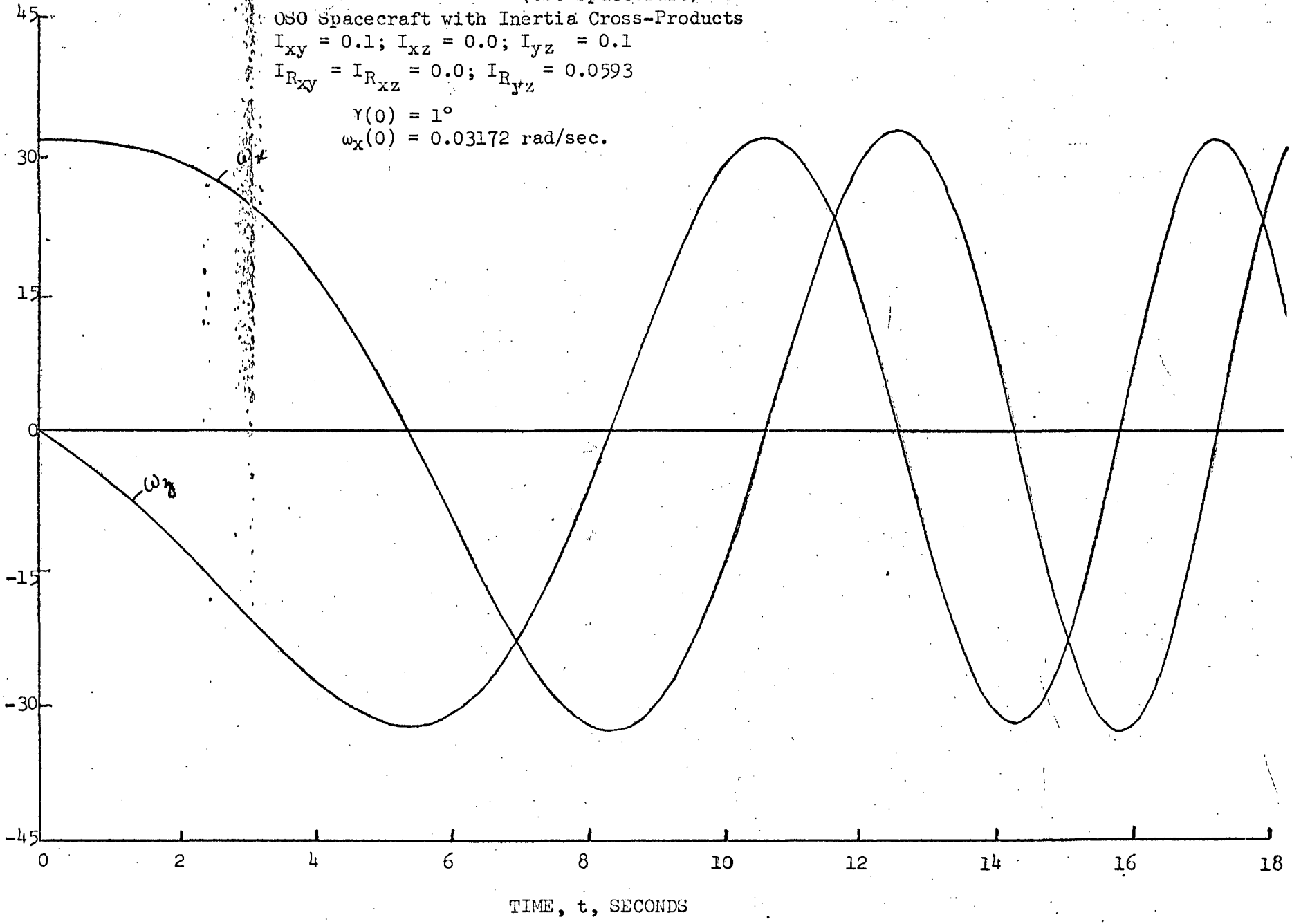

Fig. 20a. Time History of the Transverse Components of Main Body Angular Velocity (OSO Spacecraft)

$I_{xx} = 131.00$; $I_{yy} = 34.00$; $I_{zz} = 136.00$

$I_{R_{xx}} = 199.00$; $I_{R_{yy}} = 378.00$; $I_{R_{zz}} = 208.00$

$\omega_x(0) = 0.03172$ rad/sec; $\omega_y(0) = 6.985$ rad/sec.

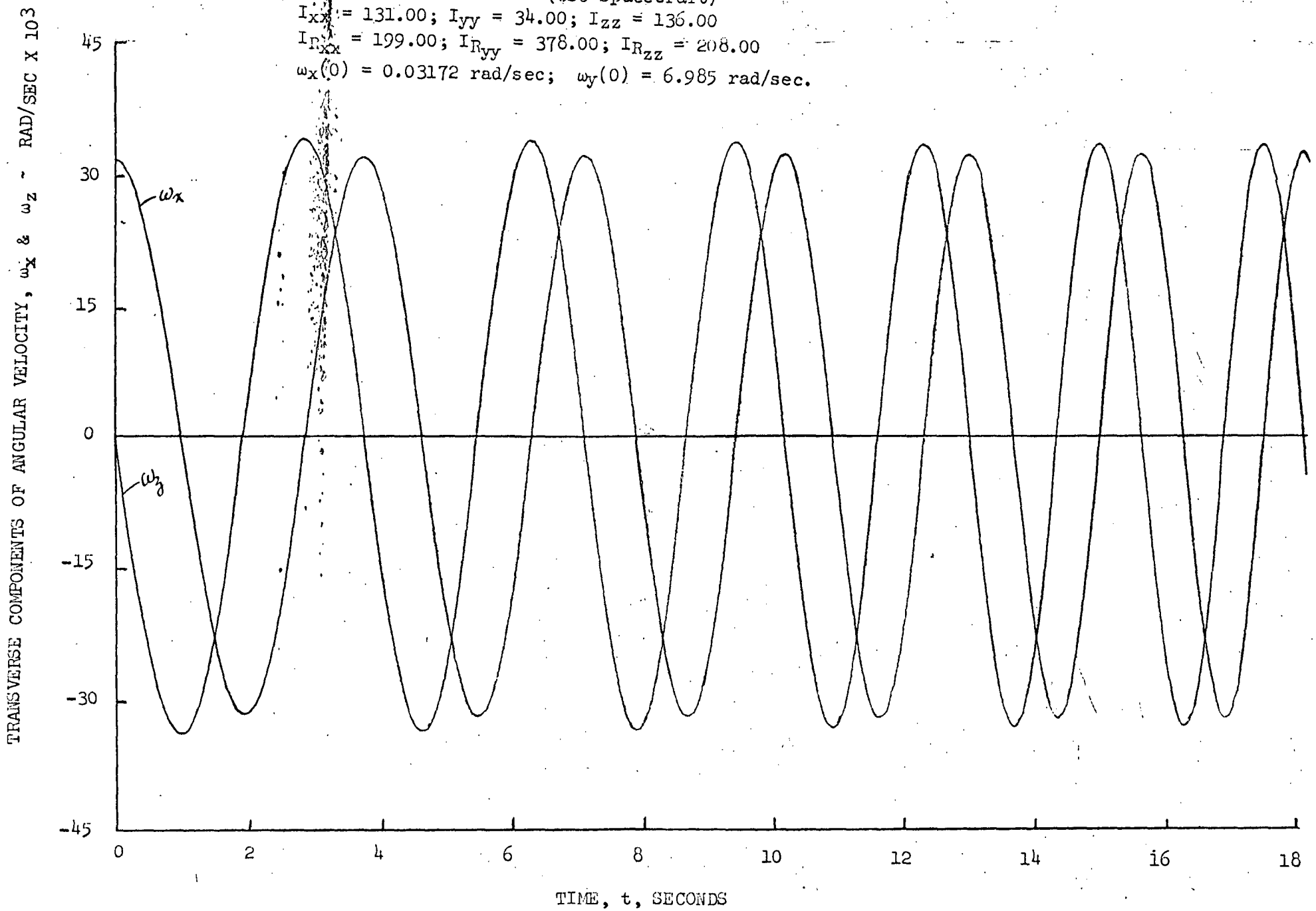

Fig. 20b. Main Body Spin Rate During Spin-Up (OSO Spacecraft)

I_{xx} = 131.00; I_{yy} = 34.00; I_{zz} = 136.00; $I_{R_{xx}}$ = 199.00

$I_{R_{yy}}$ = 378.00; $I_{R_{zz}}$ = 208.00; $\omega_x(0)$ = 0.03172 rad/sec.

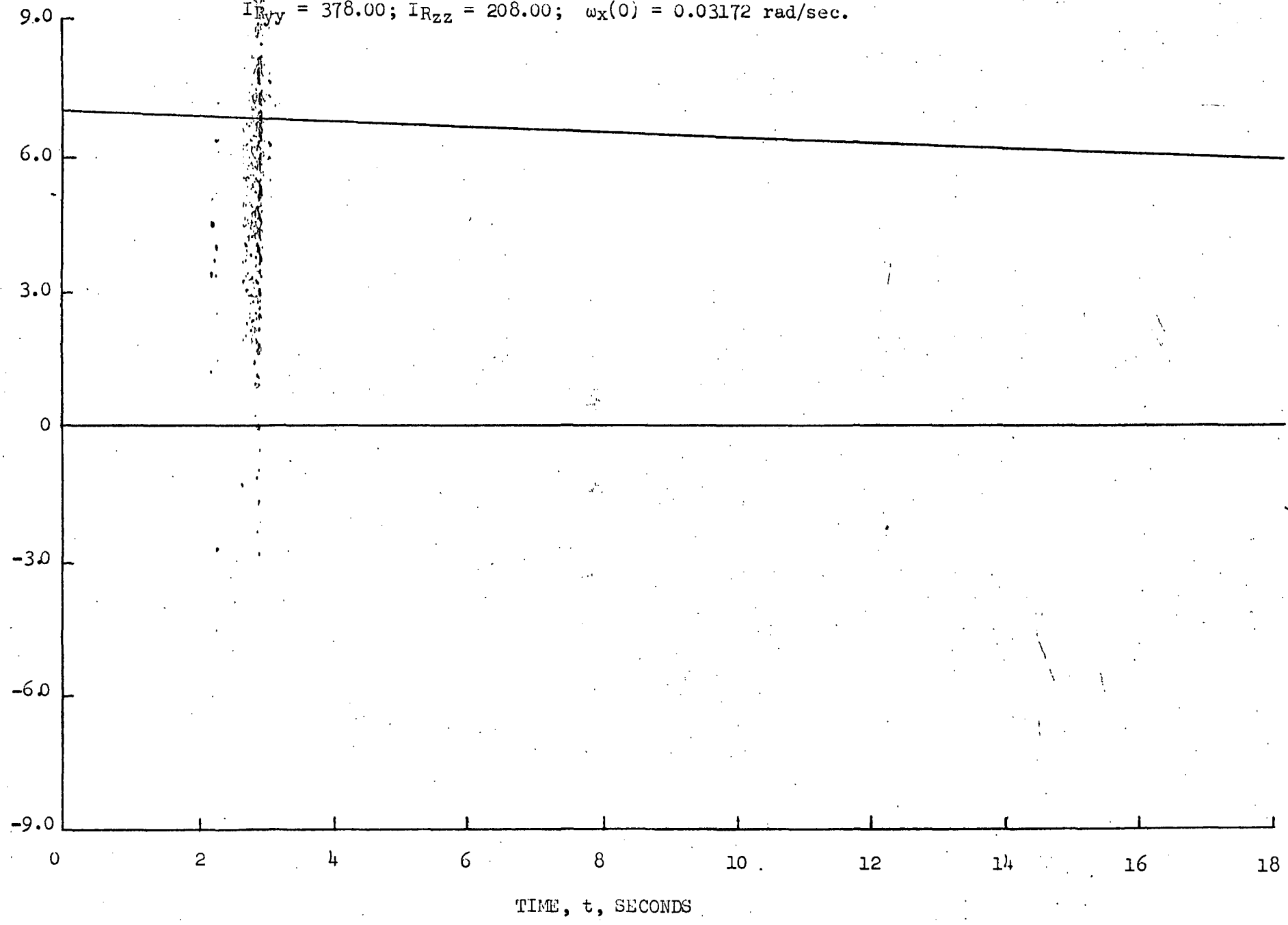

Fig. 20c. Rotor Spin Rate During Spin-Up (OSO Spacecraft)
I_{xx} = 131.00; I_{yy} = 34.00; I_{zz} = 136.00; $I_{R_{xx}}$ = 199.00
$I_{R_{yy}}$ = 378.00; $I_{R_{zz}}$ = 208.00; $\omega_x(0)$ = 0.03172 rad/sec.

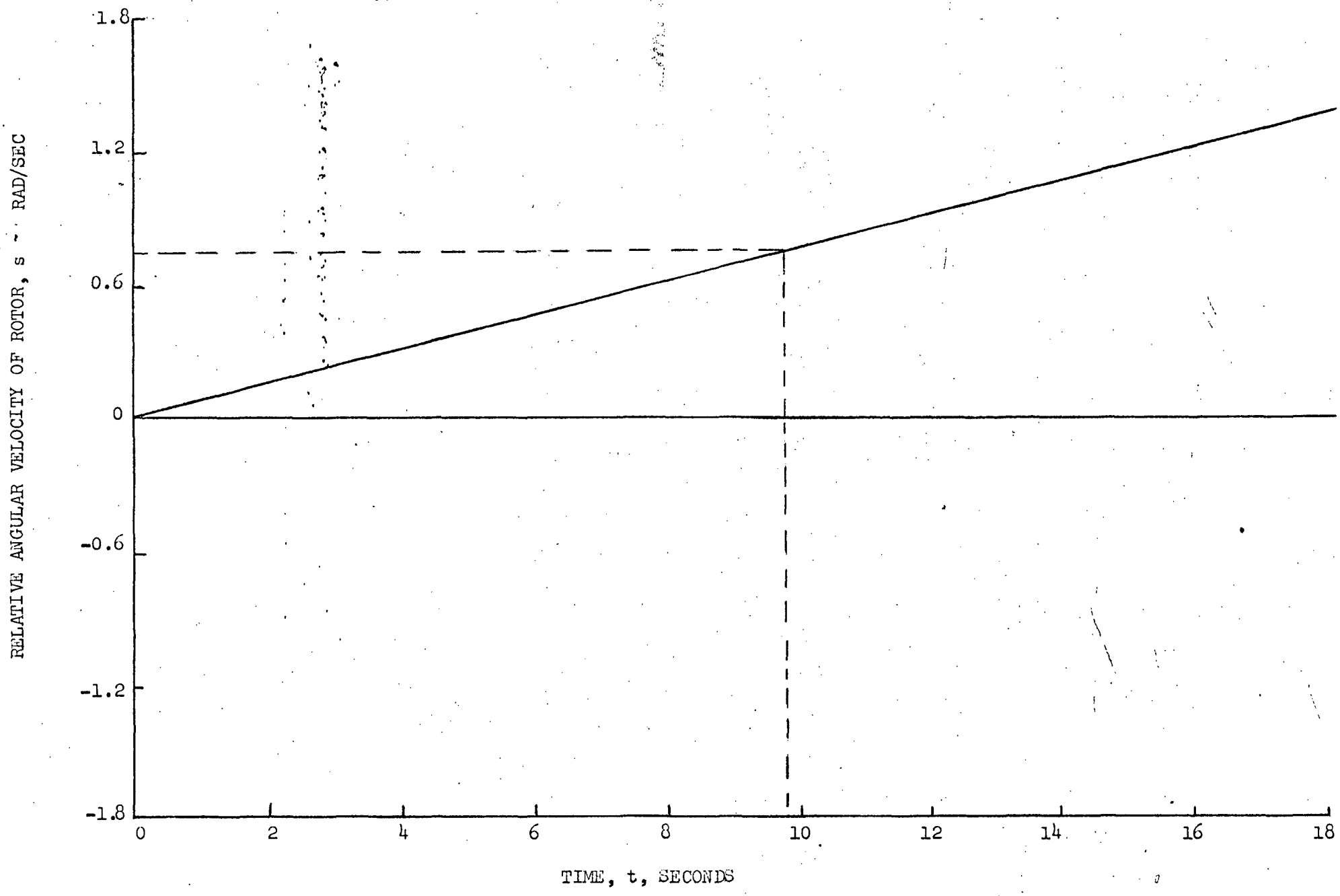

Fig. 21. Time History of Transverse Components of Main Body Angular Velocity (OSO Spacecraft)

$I_{xx} = 131.00$; $I_{yy} = 34.00$; $I_{zz} = 136.00$

$I_{R_{xx}} = 199.00$; $I_{R_{yy}} = 378.00$; $I_{R_{zz}} = 208.00$

$\omega_x(0) = 0.3172$ rad/sec.

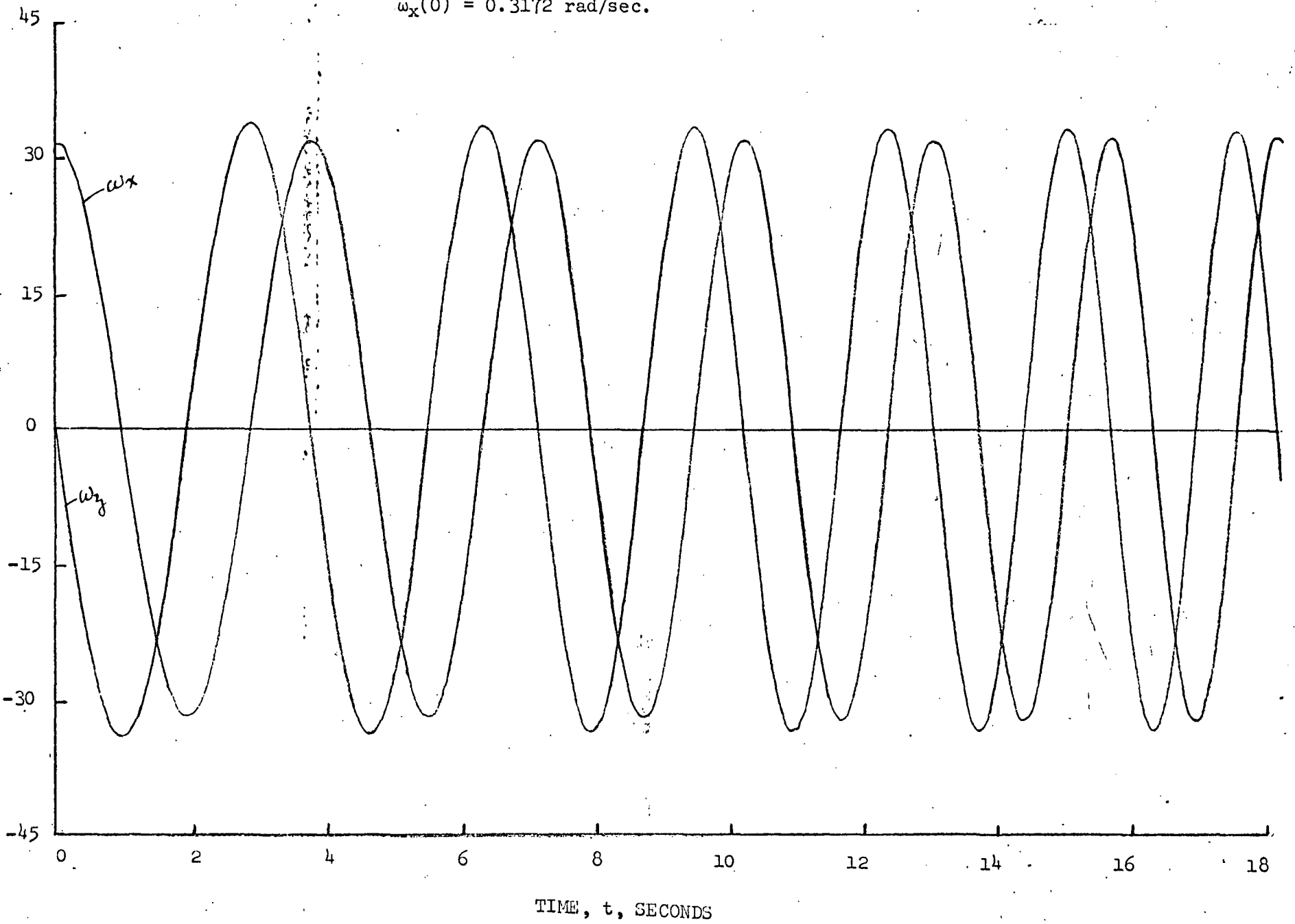

Fig. 22a. Time History of the Transverse Components of Main Body Angular Velocity (OSO Spacecraft)

I_{xx} = 131.00; I_{yy} = 34.00; I_{zz} = 136.00; $I_{R_{xx}}$ = 199.00

$I_{R_{yy}}$ = 378.00; $I_{R_{zz}}$ = 208.00, $\omega_x(0)$ = 3.172 rad/sec.

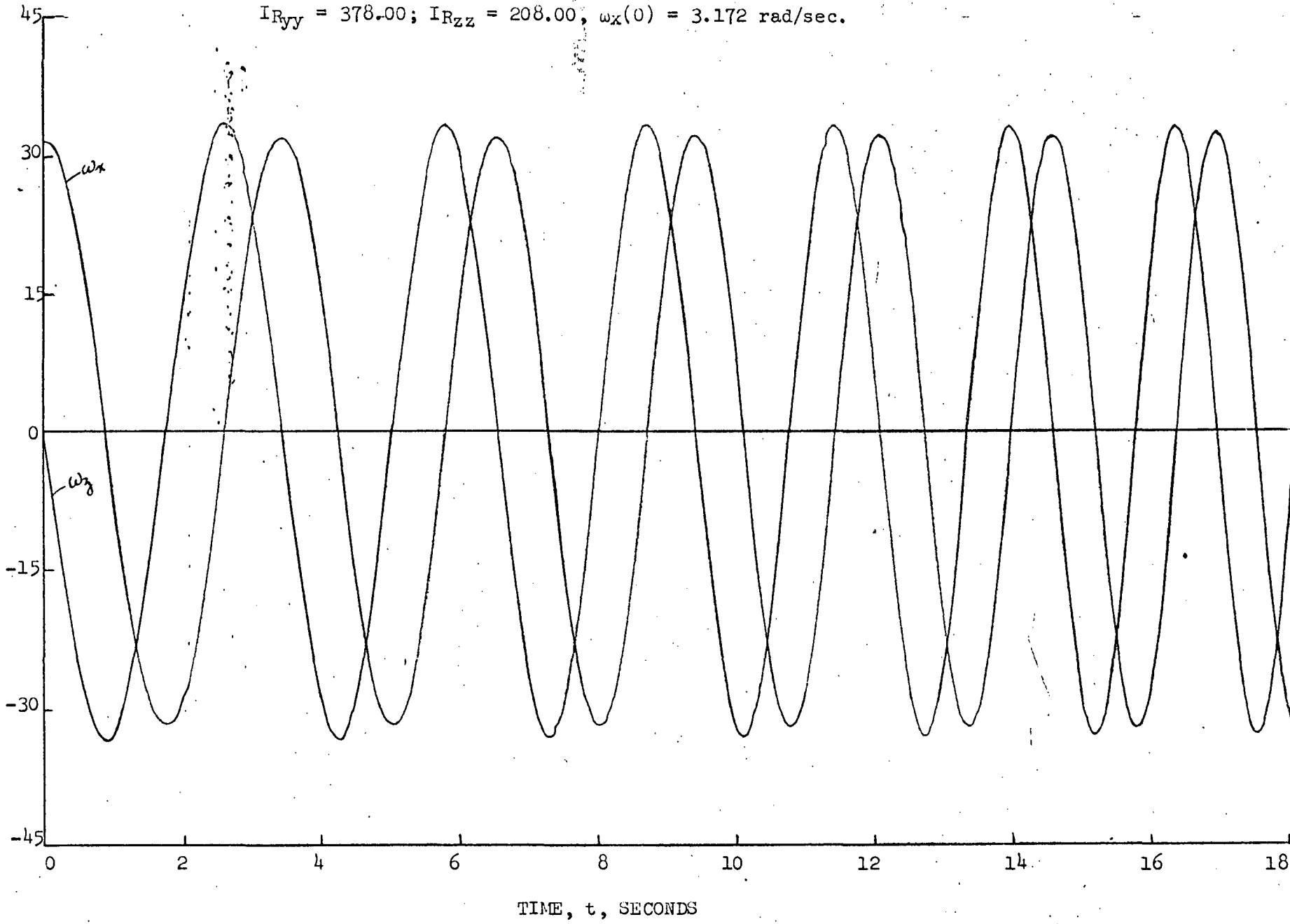

Fig. 22b. Main Body Spin Rate During Spin-Up (OSO Spacecraft)
I_{xx} = 131.00; I_{yy} = 34.00; I_{zz} = 136.00; $I_{R_{xx}}$ = 199.00; $I_{R_{yy}}$ = 378.00
$I_{R_{zz}}$ = 208.00, $\omega_x(0)$ = 3.172 rad/sec.

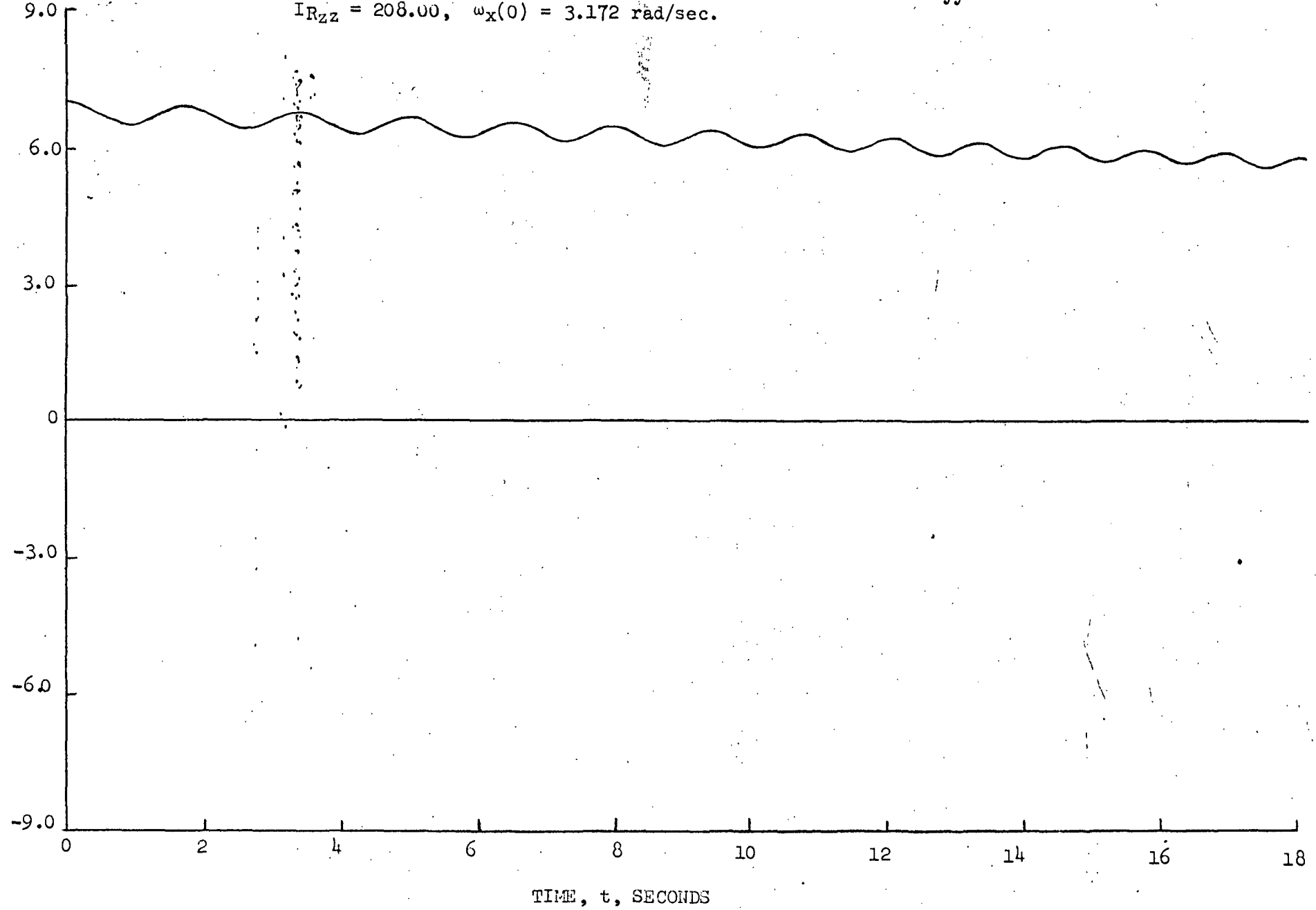

Fig. 22c. Rotor Spin Rate During Spin-Up (OSO Spacecraft)
I_{xx} = 131.00; I_{yy} = 34.00; I_{zz} = 136.00; $I_{R_{xx}}$ = 199.00
$I_{R_{yy}}$ = 378.00 $I_{R_{zz}}$ = 208.00, $\omega_x(0)$ = 3.172 rad/sec.

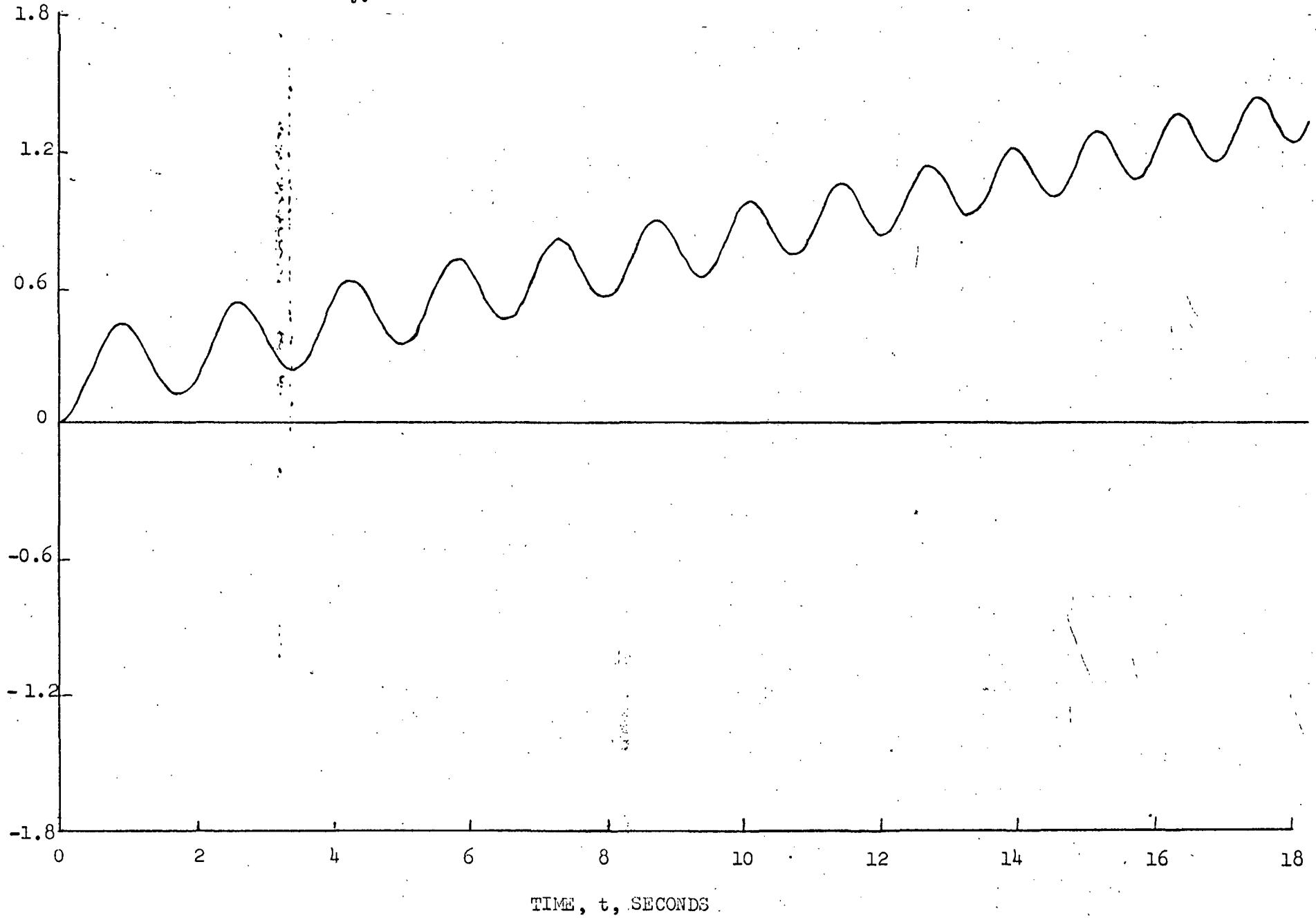

Fig, 23. Time History of the Transverse Components of Main Body Angular Velocity
(OSO Spacecraft)
I_{xy}= 0.1; I_{xz}= 0; I_{yz}= 0.1; $I_{R_{xy}}$ = 0.0; $I_{R_{xz}}$ = 0.0
$I_{R_{yz}}$ = 0.05930; $\omega_x(0)$ = 0.03172 rad/sec.

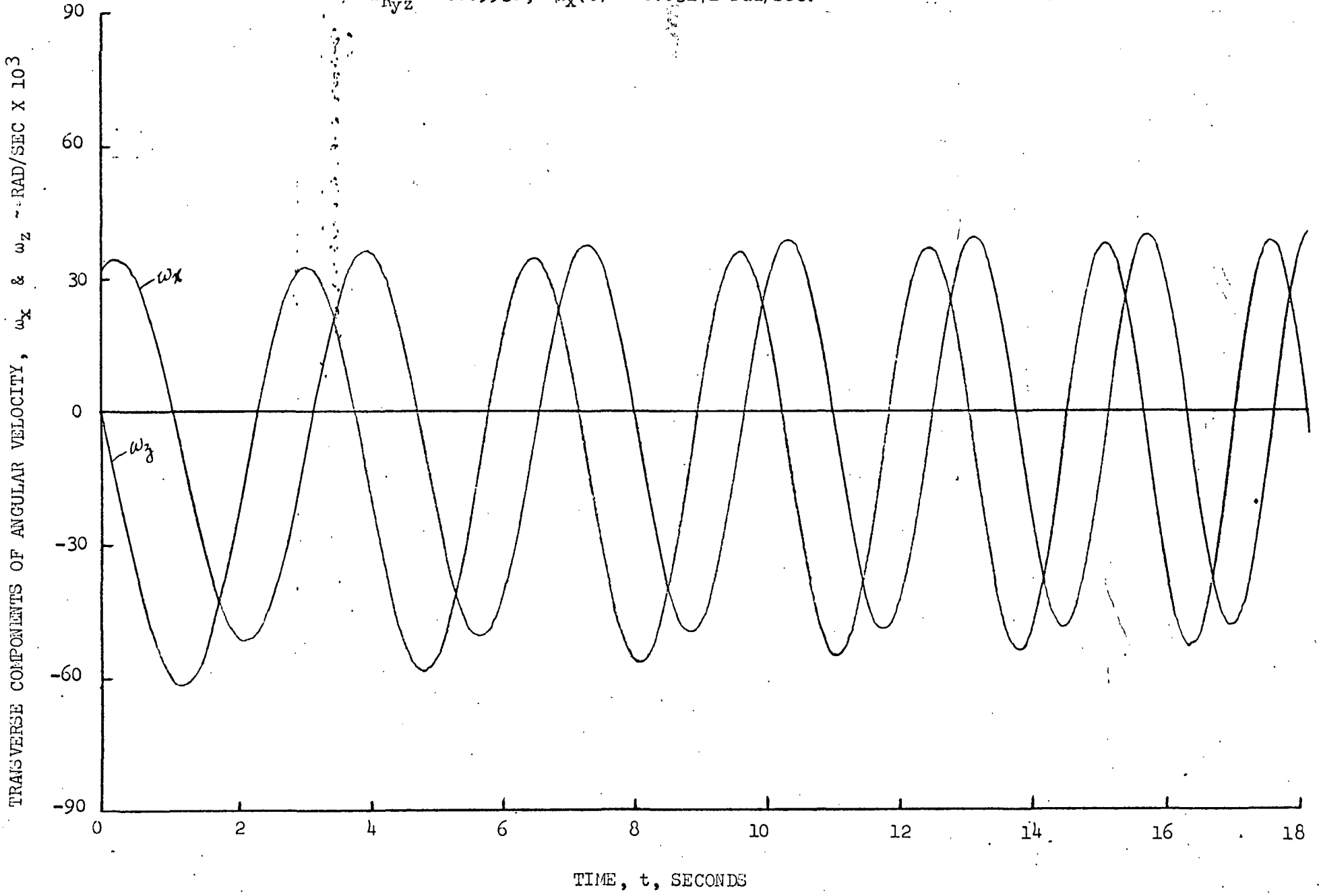

Fig. 24. Time History of the Transverse Components of Main Body Angular Velocity
(SAS-A no damping)
$I_{xx} = I_{zz} = 27.00$; $I_{yy} = 28.54$; $I_{xy} = I_{yz} = 0$; $I_{xz} = \gamma = 0.1048$, $\omega_x(0) = 0.000159$ rad/sec

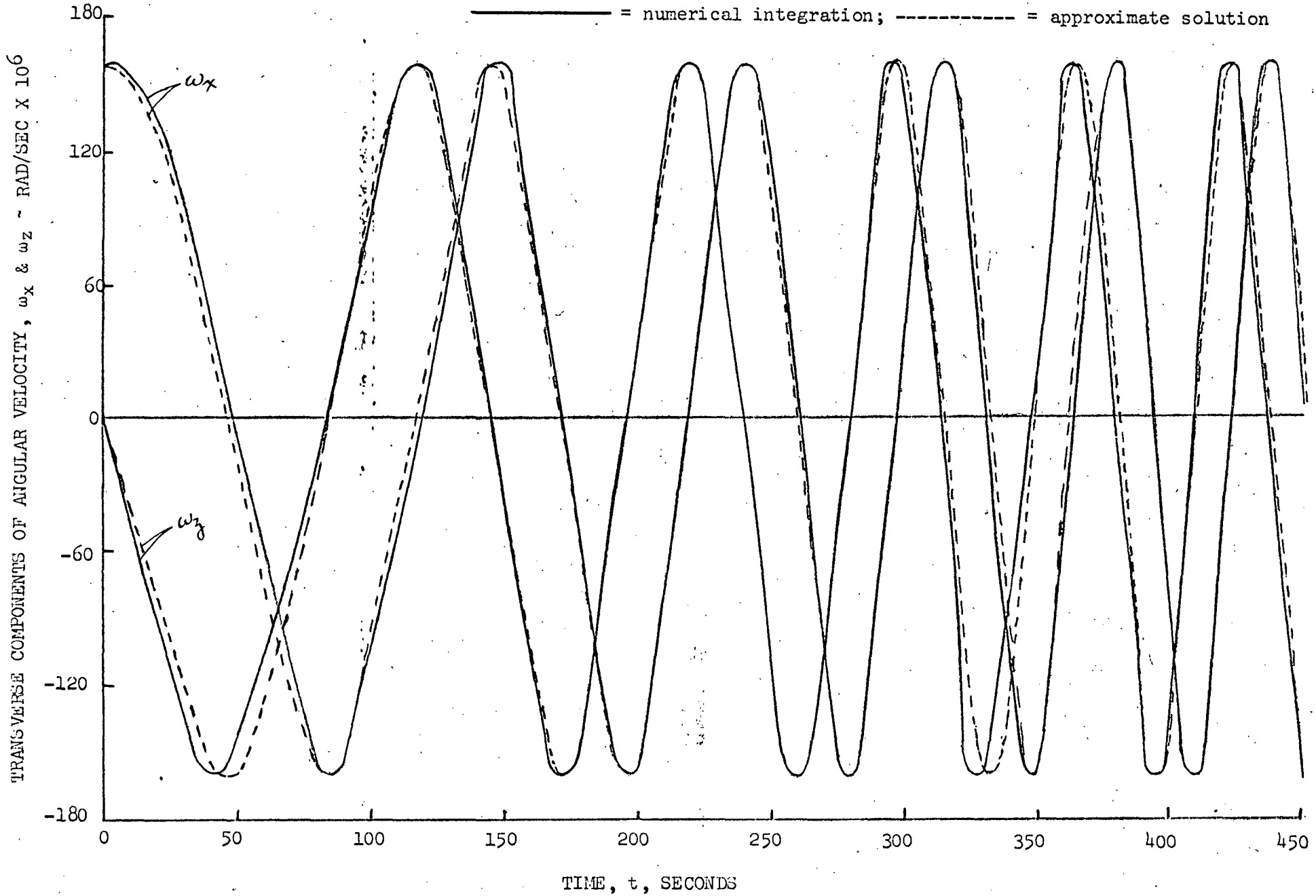

Fig. 25. Time History of the Transverse Components of Main Body Angular Velocity
(SAS-A No Damping)

$I_{xx} = I_{zz} = 27.00$; $I_{yy} = 28.54$; $I_{xy} = I_{yz} = 0$; $I_{xz} = \gamma = 0.50$; $\omega_x(0) = 0.000159$ rad/sec.

———— = numerical integration; - - - - - - - - - - - - = approximate solution

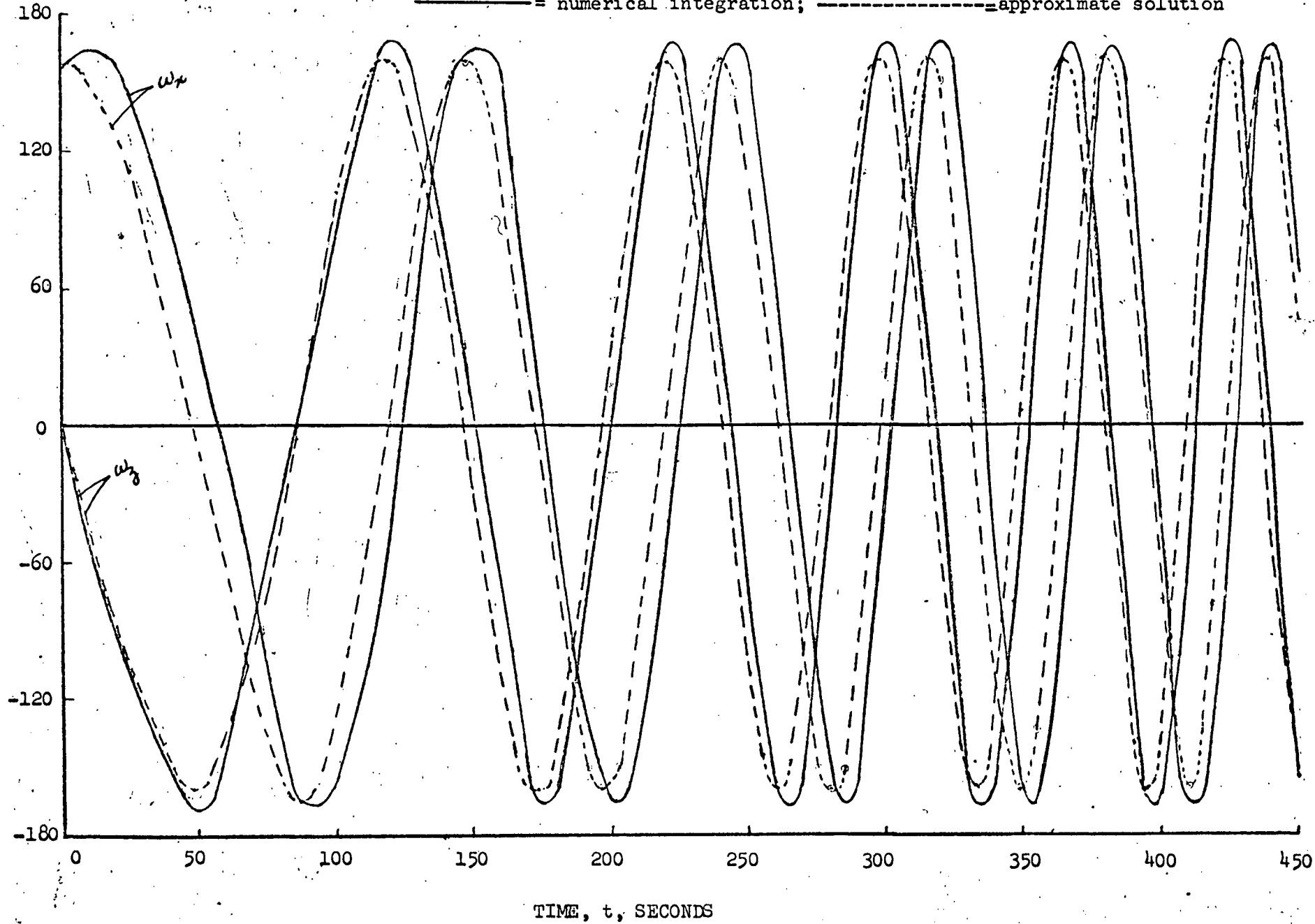

APPENDIX

A. Kinetic Energy Expression:

$$2T = 2(T_M + T_R)$$

$$2T = A\omega_x^2 + B\omega_y^2 + C\omega_z^2 + m\{r_1^2(\dot{\phi}_1^2 + \dot{\phi}_2^2 + \dot{\phi}_3^2 + \dot{\phi}_4^2) + \omega_y^2[4(r_1 + r_o)^2 - 2r_o r_1(4 - \cos\phi_1 - \cos\phi_2 - \cos\phi_3 - \cos\phi_4)] + \omega_z^2[4\ell^2 + r_1^2(\sin^2\phi_1 + \sin^2\phi_2) + (r_o + r_1\cos\phi_3)^2 + (r_o + r_1\cos\phi_4)^2] + \omega_x^2[4\ell^2 + (r_o + r_1\cos\phi_1)^2 + (r_o + r_1\cos\phi_2)^2 + r_1^2(\sin^2\phi_3 + \sin^2\phi_4)] - 2\omega_x\omega_y\ell r_1 f_1 - 2\omega_y\omega_z\ell r_1 f_2 + 2\omega_y\dot{\phi}_1(r_o r_1\cos\phi_1 + r_1^2) + 2\omega_y\dot{\phi}_2(r_o r_1\cos\phi_2 + r_1^2) + 2\omega_y\dot{\phi}_3(r_o r_1\cos\phi_3 + r_1^2) + 2\omega_y\dot{\phi}_4(r_o r_1\cos\phi_4 + r_1^2) - 2\omega_z\omega_x[r_1\sin\phi_1(r_1\cos\phi_1 + r_o) + r_1\sin\phi_2(r_1\cos\phi_2 + r_o) - r_1\sin\phi_3(r_1\cos\phi_3 + r_o) - r_1\sin\phi_4(r_1\cos\phi_4 + r_o)] - 2\ell\omega_z\dot{\phi}_1 r_1\cos\dot{\phi}_1 + 2\omega_z\dot{\phi}_2 r_1\ell\cos\phi_2 + 2\omega_z\dot{\phi}_3 r_1\ell\sin\phi_3 - 2\omega_z\dot{\phi}_4 r_1\ell\sin\dot{\phi}_4 - 2\omega_x\dot{\phi}_1 r_1\ell\sin\phi_1 + 2\omega_x\dot{\phi}_2 r_1\ell\sin\phi_2 - 2\omega_x\dot{\phi}_3 r_1\ell\cos\phi_3 + 2\omega_x\dot{\phi}_4 r_1\ell\cos\phi_4\} - \frac{m^2}{M}[\omega_y^2 r_1^2(f_1^2 + f_2^2) + \omega_z^2(16\ell^2 + r_1^2 f_1^2) + \omega_x^2(16\ell^2 + r_1^2 f_2^2) - 2\omega_z\omega_x r_1^2 f_1 f_2 - 8\omega_y\omega_z r_1\ell f_2 - 8\omega_x\omega_y r_1\ell f_1$$

$$+ r_1^2 g_1^2 + r_1^2 g_2^2 - 2\omega_y r_1^2 g_1 f_1 + 2\omega_y r_1^2 g_2 f_2 - 8\omega_z r_1 \ell g_2 + 8\omega_x r_1 \ell g_1\}$$

$$+ I_{R_y}(\omega_y + s)^2 + I_{R_x}\omega_x^2 + I_{R_z}\omega_z^2$$

where

$$f_1 = \sin\phi_1 - \sin\phi_2 + \cos\phi_3 - \cos\phi_4; \quad f_2 = \cos\phi_1 - \cos\phi_2 - \sin\phi_3 + \sin\phi_4$$

$$g_1 = -\dot{\phi}_1\sin\phi_1 + \dot{\phi}_2\sin\phi_2 - \dot{\phi}_3\cos\phi_3 + \dot{\phi}_4\cos\phi_4$$

$$g_2 = \dot{\phi}_1\cos\phi_1 - \dot{\phi}_2\cos\phi_2 - \dot{\phi}_3\sin\phi_3 + \dot{\phi}_4\sin\phi_4$$

B. Fortran Listing of Computer Programming:

```
// FORTRAN
*ONE WORD INTEGERS
*LIST SOURCE PROGRAM
      SUBROUTINE SEN 1 (T,Y,DY)
      DIMENSION Y(6), DY(6), C(5,5), CX(5,5)
      COMMON  WX,WY,WZ,S,W1,PHI,AIXX,AIYY,AIZZ,AIXY,AIXZ,AIYZ,AIRXX,
     $  AIRYY,AIRZZ,AIRXY,AIRXZ,AIRYZ,AL,AM,RO,R1,AKK,AK,ALBAR,ALRY,
     $ RRY,AMBAR,N,M
      COMMON C,CPA,CPB,A16,A17,A18,A19,A110,A111,A112,
     $A113,A114,A115,A116,A27,A28,A29,A210,A211,
     $A212,A213,A214,A37,A38,A39,A310,A311,A312,A313,
     $A314,A315,A316,A45,A46,A47,A48,A49,A410,A411,
     $A412,A54,A55,A56,A57
C
C
      DO 11 I=1,M
      DO 11 J=1,M
   11 CX(I,J)=C(I,J)
      CX(1,2)= CX(1,2)-CPA*PHI
      CX(2,1) =CX(2,1)-CPA*PHI
      CX(3,1) =CX(3,1)-CPB*PHI
      DY(1) = (A16+A17*PHI)*WX*WY-A18*WY*WZ+A19*WY**2+(A110*WZ+
     $A111*WY)*S-A112*WZ**2-A113*WZ*WX+A114*W1**2+A115*W1*WY+
     $A116*W1*WZ
      DY(2) = (A27+A28*PHI)*WY*WZ-A29*WZ*WX-A210*WX*WY-
     $A211*(WX**2-WZ**2)-(A212*WX-A213*WZ)*S+A214*PHI*W1*WY
      DY(3) =A37*WX*WZ+A38*WX**2-A39*WX*WY-(A310+A311*PHI)*WY*WZ-
     $(A312+A313*PHI)*WY**2-(A314*WY+A315*WX)*S-A316*PHI*W1*WY
      DY(4) = A45-A46*WZ*WX+A47*WY*WZ+A48*WZ*S+A49*WZ**2-A410*WX**2-
     $A411*WX*WY-A412*WX*S
      DY(5) =A54*PHI*WY**2-A55*WX*WY-A56*W1-A57*PHI
      DY(6) =W1
      CALL SIMQ(CX,DY,M,KS)
      IF(KS) 3,2,3
    2 RETURN
    3 WRITE(5,4)
 4    FORMAT(//' SINGULAR EQUATIONS')
      RETURN
      END

FEATURES SUPPORTED
 ONE WORD INTEGERS

CORE REQUIREMENTS FOR SEN1
 COMMON     194  VARIABLES    78  PROGRAM     512
```

```
PAGE    2      4/28/72

RELATIVE ENTRY POINT ADDRESS IS 005F (HEX)

END OF COMPILATION

// DUP

*STORE        WS  UA  SEN1
CART ID 000A   DB ADDR  5880   DB CNT   002A

// EJECT
```

```
PAGE    3      4/28/72

// FORTRAN
*ONE WORD INTEGERS
*LIST SOURCE PROGRAM
      SUBROUTINE  SEN 2 (T, Y, DY, IHLF, NDUMY, P)
      DIMENSION Y(6), DY (6), P (5)
      COMMON  WX,WY,WZ,S,W1,PHI,AIXX,AIYY,AIZZ,AIXY,AIXZ,AIYZ,AIRXX,
     $  AIRYY,AIRZZ,AIRXY,AIRXZ,AIRYZ,AL,AM,RO,R1,AKK,AK,ALBAR,ALRY,
     $ RRY,AMBAR,N,M
      DATA SY/0.0/
      DATA WYL/0.0/
      DATA TL/0.0/
C
C
C
      SY=SY+0.5*(T-TL)*(WY+WYL)
      TL =T
      WYL =WY
      TOUT = T+0.0005
      CHECK =0.5*(AIXX+AIRXX)*WX*WX+0.5*AIYY*WY*WY+0.5*
     $(AIZZ+AIRZZ)*WZ*WZ+ALRY*SY
      WRITE (5,4)  TOUT,Y,IHLF,CHECK
    4 FORMAT (1X,F7.3,6E13.5,I3,E13.5)
      P(5) = INBIT(0)
      RETURN
      END

FEATURES SUPPORTED
 ONE WORD INTEGERS

CORE REQUIREMENTS FOR SEN2
 COMMON      58  VARIABLES      18  PROGRAM     130

RELATIVE ENTRY POINT ADDRESS IS 001F (HEX)

END OF COMPILATION

// DUP

*STORE       WS  UA  SEN2
CART ID 000A   DB ADDR  58AA   DB CNT   000C

// EJECT
```

```
PAGE    4     4/28/72

// FORTRAN
*ONE WORD INTEGERS
*LIST SOURCE PROGRAM
*IOCS(1403 PRINTER)
      EXTERNAL  SEN1,  SEN2
      DIMENSION C(5,5), Y(6), DY(6), AUX (8,6), V(6)
      DIMENSION P(5)
      COMMON  WX,WY,WZ,S,W1,PHI,AIXX,AIYY,AIZZ,AIXY,AIXZ,AIYZ,AIRXX,
     $  AIRYY,AIRZZ,AIRXY,AIRXZ,AIRYZ,AL,AM,RO,R1,AKK,AK,ALBAR,ALRY,
     $ RRY,AMBAR,N,M
      COMMON C,CPA,CPB,A16,A17,A18,A19,A110,A111,A112,
     $A113,A114,A115,A116,A27,A28,A29,A210,A211,
     $A212,A213,A214,A37,A38,A39,A310,A311,A312,A313,
     $A314, A315, A316, A45, A46, A47, A48, A49, A410, A411,
     $A412, A54, A55, A56, A57
      EQUIVALENCE (P(1),TO), (P(2),TM), (P(3),DT), (P(4),ERR)
      EQUIVALENCE (Y(1),WX), (Y(2),WY),(Y(3),WZ),(Y(4),S)
      EQUIVALENCE (Y(5),W1), (Y(6),PHI)
      DATA DT/0.1/
      DATA TO/400.00/
      DATA TM/420.00/
      DATA V/0.1E-3,0.5,0.1E-3,0.2E3,0.3E-3,0.3E-2/
      DATA TOL/1.0E-4/
C
C     INITIALIZE 'COMMON'
C
      WX = 0.94519E-04
      WY = 0.41851E 00
```

```
      WZ = 0.24974E-03
      S = 0.19691E03
      PHI =0.0
      W1 =0.0
      AIXX =15.00
      AIYY = 28.00
      AIZZ =2.00.
      AIXY = 0.0
      AIXZ = 0.0
      AIYZ = 0.0
      AIRXX = 5.575E-3
      AIRYY = 11.519E-3
      AIRZZ = 5.575E-3
      AIRXY = 0.0
      AIRXZ = 0.0
      AIRYZ = 0.0
      AL = 0.35
      RO = 0.025
      R1 =.203
      AM =0.0
      AK =0.0
      AKK =0.0
      AMBAR =132.33
      ALBAR = 0.3499
      ALRY = 0.567E-2
      RRY = 0.0
      N = 6
      M = 5
C
C     COMPUTE COEFFECIENTS FOR SUBRCUTINE 'SEN1'
```

```
PAGE    5      4/28/72

C
      C(1,1) = AIXX+AIRXX+4.0*AM*AL**2+2.0*AM*(RO+R1)**2
      C(1,2) = -(AIXY+AIRXY)
      C(1,3) = -(AIXZ + AIRXZ)
      C(1,4) = -AIRXY
      C(1,5) = 0.0
      C(2,1) = -(AIXY+ AIRXY)
      C(2,2) =AIYY +AIRYY +4.0*AM*(RO +R1)**2
      C(2,3) = -(AIYZ+AIRYZ)
      C(2,4) = AIRYY
      C(2,5) = AM*R1*(RO+R1)
      C(3,1) = -(AIXZ+AIRXZ)
      C(3,2) = -(AIYZ+AIRYZ)
      C(3,3) = AIZZ +AIRZZ +4.0*AM*AL**2 +2.0*AM*(RO+R1)**2
      C(3,4) = -AIRYZ
      C(3,5) = -(AM*R1*ALBAR)
      C(4,1) = -AIRXY
      C(4,2) = AIRYY
      C(4,3) = -AIRYZ
      C(4,4) = AIRYY
      C(4,5) = 0.0
      C(5,1) = 0.0
      C(5,2) = AM*R1*(RO+R1)
      C(5,3) = -(AM*R1*ALBAR)
      C(5,4) = 0.0
      C(5,5) = AM*R1**2*(1.0-AM/AMBAR)
      CPA = AM*AL*R1
      CPB = AM*R1*(RO+R1)
```

```
      A 16 = AIXZ +AIRXZ
      A 17 =AM*R1*(RO+R1)
      A 18 =AIZZ + AIRZZ-AIYY-AIRYY + 4.0*AM*AL**2-2.0*AM*(RO+R1)**2
      A 19 =  AIYZ +AIRYZ
      A 110 = AIRYY
      A 111 = AIRYZ
      A 112 = AIYZ +AIRYZ
      A 113 = AIXY +AIRXY
      A 114 =AM*AL*R1
      A 115 = 2.0*AM*R1*ALBAR
      A 116 =2.0 *AM*R1*(RO+R1)
      A 27 =AIXY + AIRXY
      A 28 = AM*AL*R1
      A 29 =AIXX +AIRXX -AIZZ -AIRZZ
      A 210 = AIYZ + AIRYZ
      A 211 =AIXZ +AIRXZ
      A 212 = AIRYZ
      A 213 = AIRXY
      A 214 = 2.0*AM*RO*R1
      A 37 = AIYZ + AIRYZ
      A 38 =AIXY +AIRXY
      A 39 =AIYY +AIRYY -AIXX -AIRXX -4.0*AM*AL**2
      A 310 = AIXZ + AIRXZ
      A 311 =AM*R1*(RO+R1)
      A 312 =AIXY +AIRXY
      A 313 = AM*R1*ALBAR
      A 314 =AIRXY
      A 315 =AIRYY
      A 316 =2.0*AM*AL*R1
      A 45 =ALRY +RRY
```

```
PAGE    6      4/28/72

      A 46 = AIRXX -AIRZZ
      A 47 = AIRXY
      A 48 =AIRXY
      A 49 = AIRXZ
      A 410 =AIRXZ
      A 411 =AIRYZ
      A 412 = AIRYZ
      A 54 = -AM*R1* (RO+ AM*R1/AMBAR)
      A 55 = AM*R1*ALBAR
      A 56 = AK
      A 57 = AKK
      NVAR = N
      IF (AM) 105,10,105
 10   NVAR = N-2
      C(5,5) = 1.0
 105  VT = 0.0
      DO 11 I=1,NVAR
   11 VT =VT +1.0/V(I)
      DO 12 I=1,NVAR
 12   DY(I) =1.0/(VT*V(I))
      ERR = (NVAR/(15.0*VT))*TOL
      WRITE(5,21)
 21   FORMAT ('1', T6, 'T', T15, 'WX', T28, 'WY', T41, 'WZ', T55, 'S',
     $  T67, 'W1', T80, 'PHI', T87, 'IHLF', T95, 'CHECK' / 1X)
      CALL RKGS (P, Y, DY, NVAR, IHLF, SEN1, SEN2, AUX)
      WRITE(5,40)IHLF
   40 FORMAT (//' IHLF =',I3)
      CALL EXIT
      END
```

```
C       THE FOLLOWING IS THE PROGRAM TO COMPARE
C       THE NUMERICAL INTEGRATION AND APPROXIMATE
C       SOLUTIONS (EQS. (135) & (136))
C       ARIME & BRIME ARE THE TRANSVERSE AND
C       POLAR MOMENTS OF INERTIA OF THE MAIN BODY RESPECTIVELY
C       AK1 & AK2 ARE THE CONSTANTS WHICH CAN BE RELATED
C       WITH THE INITIAL CONDITION
```

```
      DIMENSION DAT(451,3)
      WRITE(6,21)
   21 FORMAT(1X,T6,'T',T15,'WX',T28,'WZ')
      TT = 0
      NDAT=0
    9 T = TT
C
C   LISTING OF DATA
      AK1 = 0.000159
      AK2 = 2.0303110
      A = 143.07850
      GAMMA=0.1048
      AIRYY = 0.011519
      WY = 0.5
      P = -0.7654720
      Q = -.0109014
      C = 0.4916578
      ARIME = 27.005575
      BRIME = 28.551519
      AK3 = (GAMMA/ARIME)*(WY+(P*AIRYY)/(Q*BRIME))
      ABS1 = ((Q*C)/ARIME)/2.0
      ABS2 = DABS(ABS1)
      AROOT = 0.5*(1/ABS2)**0.5
      AK4 = ((AK3*AK1)/2.0)*AROOT
C
      T = TT
      AI1 = -1.0/(2.0**0.5)
      CALL SER1(T,SUM1)
      SSUM1 = SUM1
      T = 0.0
      CALL SER1(T,SUM1)
      AI1 = AI1*((2.506-SSUM1)-(2.506-SUM1))
C
C
```

```
      T = TT
      AI2 = -1.0/(2.0*0.5)
      CALL SER2(T,SUM2)
      SSUM2 = SUM2
      T = 0.0
      CALL SER2(T,SUM2)
      AI2=AI2*((-2.506-SSUM2)-(-2.506-SUM2))
C
C
      XX = -1.0/2.0
      TA = (TT+A)**2
      TAA = A**2
      AI3 = -1.0/4.0*((ABS2*TA)**XX-(ABS2*TAA)**XX)
C
C
      F1=AK4*((DCOS(AK2)*AI1)-(DSIN(AK2)*AI3)+(DSIN(AK2)*AI2))
      F2=AK4*(-(DCOS(AK2)*AI3)-(DCOS(AK2)*AI2)+(DSIN(AK2)*AI1))
      F3=AK4*(-(DSIN(AK2)*AI1)-(DCOS(AK2)*AI3)+(DCOS(AK2)*AI2))
      F4=AK4*((DSIN(AK2)*AI3)+(DSIN(AK2)*AI2)+(DCOS(AK2)*AI1))
      WX=AK1*DCOS((ABS1*TA)+AK2)+F1*DCOS(ABS1*TA)+F2*DSIN(ABS1*TA)
      WZ=AK1*DSIN((ABS1*TA)+AK2)+F3*DCOS(ABS1*TA)+F4*DSIN(ABS1*TA)
      WRITE (6,100) TT,WX,WZ
  100 FORMAT(1X,F7.3,E13.5,E13.5)
```

```
      NDAT=NDAT+1
      DAT(NDAT,1)=TT
      DAT(NDAT,2)=WX
      DAT(NDAT,3)=WZ
      TT = TT+1.
      IF(TT-450.5) 9,7,7
    7 WRITE(7,101)((DAT(I,J),J=1,3),I=1,NDAT)
  101 FORMAT(20A4)
      CALL EXIT
      END
```

```
      SUBROUTINE SER1(T,SUM1)
      IMPLICIT REAL*8(A-H,O-Z)
      SUM1 = 0.0
      ARIME = 27.005575
      C = 0.4916578
      Q = .0109014
      FF = (Q*C)/ARIME
      A = 143.07850
      YY =-1.0
      DO 10 M = 1,27
      FACT = 1.0
      MM = M-1
      IF (MM.EQ.0) GO TO 11
      AA = (YY)**MM
      GO TO 4
   11 AA = 1
    4 AJ = (2*MM)+0.5
      AJJ=MM+0.5
      Y = FF*((T+A)**2)
      S1 = Y**AJJ
      S11= Y**MM
      S2 = AA*S1
      S3 = S2/AJ
      MM = (2*MM)+1
      DO 1 J = 1,MM
      FACT = FACT*J
    1 CONTINUE
      S4=S3/FACT
      S5=S4*S11
      SUM2=SUM2+S5
   10 CONTINUE
      RETURN
      END
```

```
      SUBROUTINE SER2(T,SUM2)
      IMPLICIT REAL*8(A-H,O-Z)
      SUM2 =0.0
      C = 0.4916578
      ARIME = 27.005575
      Q = .0109014
      FF = (Q*C)/ARIME
      A = 143.07850
      YY = -1.0
      DO 10 M = 1,27
      FACT = 1.0
      MM = M-1
      IF (MM.EQ.0) GO TO 11
      AA= (YY)**MM
      GO TO 4
   11 AA = 1
    4 AJ= (2*MM)-.5
      AJ1= MM-0.5
      Y = FF*((T+A)**2)
      S1= Y**AJ1
      S11= Y**MM
      S2 = AA*S1
      S3 = S2/AJ
      IF (MM.EQ.0) MM=1
      MM = MM*2.0
      DO 1 J = 1,MM
      FACT = FACT*J
    1 CONTINUE
      S4=S3/FACT
      S5=S4*S11
      SUM1=SUM1+S5
   10 CONTINUE
      RETURN
      END
//GO.SYSIN DD *
/*
```

APPENDIX C

Nutation Damper Bias Angle due to the Offset of the Spacecraft Mass Center in the Transverse Plane

During the despin operation of the SAS-A spacecraft the nutation damper was observed to be biased by a small amount off its expected equilibrium position.[6,16] This bias angle was observed to diminish as the main body spin rate decreased. This phenomenon resulted from the actual offset of the spacecraft mass center in the transverse plane due to small errors in the final mass balancing prior to launch.

This same bias in damper angle has been observed in the current numerical study (e.g. Figs. 5b, 6b, 7c) and can be explained by the fact that during the development of the equations of motion the lateral center of mass shift due to the damper motion was not included. In this appendix, the forces and moments acting on the damper mass in the transverse plane will be examined together with the bias angle from Fig. 5b and the center of mass offset displacement then calculated.

Analysis

(a) Offset of Center of Mass Due to Centrifugal Force:

For static equilibrium of the damper pendulum, the

torque caused by the centrifugal force is balanced by the restoring spring action. Referring to Fig. C-1 and following Ref. 16, the torque equation can be expressed:

$$\Sigma N = mr\omega_y^2 \sin \alpha \, r_1 - K\phi_1 = 0 \quad \ldots\ldots\ldots\ldots \quad (C.1)$$

where m = mass of damper pendulum

K = torsion wire spring constant

r = displacement of damper mass from actual mass center

r_1 = damper pendulum length

ω_y = spacecraft spin rate

(In Eq. (C-1), the effect of the Coriolis force has been neglected; it will be considered subsequently and shown to be a higher order effect for the SAS-A system).

From Fig. C-1, $\sin \alpha = \frac{d}{r_1}$,

so that Eq. (C.1) becomes:

$$\Sigma N = mr\omega_y^2 r_1 \left(\frac{d}{r_1}\right) - K\phi_1 = 0 \quad \ldots\ldots\ldots\ldots \quad (C.2)$$

From the geometry of the figure,

$$r_1^2 = r_1^{*2} + d^2$$

$$r = r_1^* + r_o \cos \beta + f \sin \beta \quad \ldots\ldots\ldots\ldots \quad (C.3)$$

$$\beta = \phi_1 + \alpha$$

and

$$f \cos \beta = d + r_o \sin \beta \quad \ldots\ldots\ldots\ldots\ldots \quad (C.4)$$

The exact solution for the spacecraft center of mass displacement f as a function of r_o, r_1, ϕ_1 and ω_y is complicated for large ϕ_1. It is noted in Eq. (C.2) that ϕ_1 varies directly as ω_y^2 for constant r. The solution for f in the case of SAS-A can be obtained by using small bias angles in the linearized equations.

The following assumptions can thus be made:

$d, f << r_1$

$r_1^* \approx r_1$

α, β, ϕ_1 are small and $\beta \approx \phi_1$

$r \approx r_1 + r_o$

Thus from Eqs. (C.2), (C.3) and (C.4)

$$f \approx \left[\frac{K}{m(r_1+r_o)\omega_y^2} + r_o \right]\phi_1 \quad \ldots\ldots\ldots\ldots\ldots \quad (C.5)$$

Using the parameters given for the SAS-A satellite:

$m = 0.2158$ kg

$K = 6.10 \times 10^{-5} \quad \frac{\text{nt-m}}{\text{rad}}$

$r_o = 0.025$ meter

$r_1 = 0.203$ meter

ϕ_1 = 0.006 rad (obtained from Fig. 5b)

$\omega_y = \omega_y(0) = 0.5$ rad/sec

and substituting these values into Eq. (C.5),

f = 1.52 millimeter

For small angles Eq. (C.3) can be written:

$$r = r_1 + r_o \cos \phi_1 + f \sin \phi_1 \quad \ldots\ldots\ldots \quad (C.6)$$

Substituting the values of r_1, r_o, f and ϕ_1 into Eq. (C.6)

r = 0.228 meter

From Eq. (C.4)

$$d = f \cos \phi_1 - r_o \sin \phi_1$$

After substituting the numerical values of f, r_o and ϕ_1 the above equation yields,

d = 0.0013701 meter

The magnitude of the torque due to the centrifugal force about the damper hinge point is expressed:

$$N_{C.F.} = mr\omega_y^2 d$$

$$= 0.2158 \times 0.228 \times (.5)^2 \times 0.0013701$$

$$= 1.68 \times 10^{-5} \text{ Newton-meter}$$

(b) Calculation of the Coriolis Force and Torque:

The velocity of a particle relative to a space fixed reference can be expressed as:

$$\bar{V}_s = \bar{V}_r + \bar{\omega} \times \bar{r} \quad \ldots\ldots\ldots\ldots\ldots\ldots \quad (C.7)$$

where, $\bar{V}_s$ = velocity of the particle relative to a space fixed reference

$\bar{V}_r$ = velocity of the particle in a rotating frame with angular velocity $\bar{\omega}$ relative to the fixed plane

Again the acceleration of a particle relative to space can be obtained from the following equation,

$$\left.\frac{d\bar{V}_s}{dt}\right|_{space} = \left.\frac{d\bar{V}_s}{dt}\right|_{rot} + \bar{\omega}x\bar{V}_s \quad \ldots\ldots\ldots \quad (C.8)$$

Substituting the expression for $\bar{V}_s$ from Eq. (C.7) into Eq. (C.8)

$$\left.\frac{d\bar{V}_s}{dt}\right|_{space} = \frac{d}{dt}(\bar{V}_r + \bar{\omega}x\bar{r})_{rot} + \bar{\omega}x(\bar{V}_r + \bar{\omega}x\bar{r}) \quad \ldots \quad (C.9)$$

Using, $\bar{V}_r = \left.\frac{d\bar{r}}{dt}\right|_{rot}$ we obtain

$$\frac{d\bar{V}_s}{dt}\Big|_{space} = \bar{a}_r + \bar{\omega}x\bar{r} + 2\bar{\omega}x\bar{V}_r + \bar{\omega}x(\bar{\omega}x\bar{r}) \quad \ldots\ldots \quad (C.10)$$

where $\bar{V}_r$ is the velocity measured by an observer rotating with this system. The term $|2\bar{\omega}x\bar{V}_r|$ is the magnitude of the Coriolis acceleration.

From Fig. C-1

$$\bar{r} = (r_o + r_1 \cos\phi_1)\bar{i} + (f + r_1 \sin\phi_1)\bar{k} \quad \ldots\ldots \quad (C.11)$$

Differentiating Eq. (C.11) yields:

$$\frac{d\bar{r}}{dt} = \bar{V}_r = (-r_1 \sin\phi_1\dot{\phi}_1)\bar{i} + (\dot{f} + r_1 \cos\phi_1\dot{\phi}_1)\bar{k} \quad \ldots \quad (C.12)$$

The total angular velocity vector during despin can be approximated by its largest component, ω_y as

$$\bar{\omega} = \omega_y\bar{j} \quad \ldots\ldots\ldots\ldots\ldots\ldots \quad (C.13)$$

where ω_y is the angular velocity of the main body.

The Coriolis acceleration may be represented:

$$\bar{a}_{cor} = 2[\bar{\omega}x\bar{V}_r] \quad \ldots\ldots\ldots\ldots\ldots\ldots \quad (C.14)$$

Substituting the values of $\bar{\omega}$ and V_r into Eq. (C.14)

$$\bar{a}_{cor} = 2[\{\omega_y\bar{j}\} \times \{(-r_1 \sin\phi_1\dot{\phi}_1)\bar{i} + (\dot{f} + r_1 \cos\phi_1\dot{\phi}_1)\bar{k}\}] \quad (C.15)$$

and after expansion,

$$\bar{a}_{cor} = [\omega_y(\dot{f} + r_1 \cos\phi_1\dot{\phi}_1)]\bar{i} - [\omega_y(-r_1 \sin\phi_1\dot{\phi}_1)]\bar{k} \quad (C.16)$$

The magnitude of the Coriolis force

$$F_{cor} = |\bar{F}_{cor}| = 2m\sqrt{\omega_y^2[(\dot{f} + r_1\cos\phi_1\dot{\phi}_1)^2 + (-r_1 \sin\phi_1\dot{\phi}_1)^2} \quad (C.17)$$

For the static case $\dot{f}$ and $\dot{\phi}_1$ are both zero, so,

$$|\bar{F}_{cor}| = 0$$

Differentiating Eq. (C.5), for $\omega_y \approx$ constant

$$\dot{f} \approx \left[\frac{K}{m(r_1 + r_o)\omega_y^2} + r_o\right]\dot{\phi}_1 \quad (C.18)$$

Substituting Eq. (C.18) into Eq. (C.17) we obtain the result as,

$$F_{cor} = 2m\sqrt{\omega_y^2\left(\frac{K}{m(r_o + r_1)\omega_y^2} + r_o + r_1\cos\phi_1\right)^2\dot{\phi}_1^2 + r_1 \sin^2\phi_1\dot{\phi}_1^2} \quad (C.19)$$

From the time history of $\dot{\phi}_1$ for the case considered in Figs. 5 an approximate average value of $\dot{\phi}_1$ can be obtained as

$$|\dot{\phi}_{1\ ave}| = |0.15 \times 10^{-3} \text{ rad/sec}|$$

Substituting the SAS-A parameters and $\dot{\phi}_{1\ ave}$ into Eq. (C.19), yields -

$$F_{cor} = 7.54090 \times 10^{-5} \text{ Newton}$$

The magnitude of the torque produced by Coriolis force can be expressed by

$$N_{cor} = F_{cor} \cos \alpha \cdot r_1 \quad \ldots\ldots\ldots\ldots \quad (C.20)$$

Using SAS-A nominal parameters it can be shown that:

$$N_{cor} = 1.53080 \times 10^{-6} \text{ Newton-meter.}$$

The average torque produced by Coriolis forces is about an order of magnitude less than the torque produced by the centrifugal force, so the effect of Coriolis force can be neglected in an approximate first order analysis.

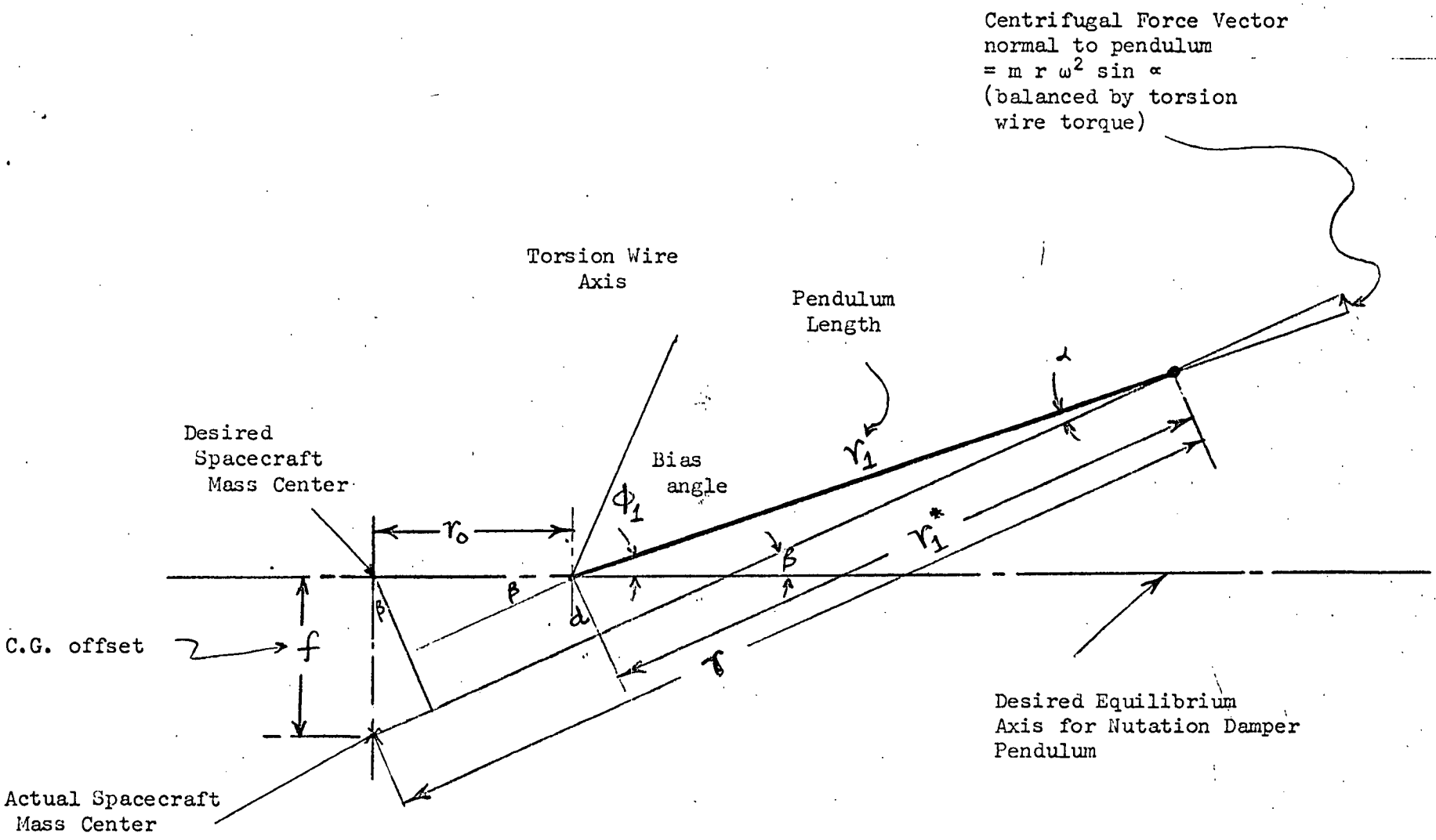

FIGURE C-1: Geometry of Nutation Damper Bias Analysis

APPENDIX D

Integrals Involved in the Solution of Equations (120) and (121)[11]

$$\int x^{\mu-1} \sin ax\, dx = -\frac{1}{2a^{\mu}} \{e^{\frac{\pi i}{2}(\mu-1)} \Gamma(\mu,-iax) + e^{\frac{\pi i}{2}(1-\mu)} \Gamma(\mu, iax)\}$$

$$\begin{aligned} \mathrm{Re}\,\mu &< 1 \\ a &> 0 \\ x &> 0 \end{aligned}$$

$$\int x^{\mu-1} \cos ax\, dx = -\frac{1}{2a^{\mu}} \{e^{i\frac{\mu\pi}{2}} \Gamma(\mu, -iax) + e^{-i\frac{\mu\pi}{2}} \Gamma(\mu, iax)\}$$